

©Copyright 2018

Chloe E. Hart

Thermodynamics of Acidophiles:  
Energetics of microbial growth, response to substrate availability,  
and interactions with heavy metals

Chloe E. Hart

A dissertation  
submitted in partial fulfillment of the  
requirements for the degree of

Doctor of Philosophy

University of Washington

2018

Reading Committee:

Drew Gorman-Lewis, Ph.D., Chair

Roger Buick, Ph.D.

John Baross, Ph.D.

Program Authorized to Offer Degree:  
Department of Earth and Space Sciences

University of Washington

## **Abstract**

Thermodynamics of Acidophiles:  
Energetics of microbial growth, response to substrate availability, and interactions with  
heavy metals

Chloe E. Hart

Chair of the Supervisory Committee:  
Drew Gorman-Lewis, Ph.D.  
Department of Earth and Space Sciences

Chemical and physical properties play a crucial role in the type and efficiency of microbial activity that can be supported within an ecosystem. In return, the presence of microbial activity affects the surrounding environment, driving biogeochemical cycles, altering chemical fluxes via metabolism and surface interactions, and affecting the lithosphere through mineral precipitation or dilution. Fluctuations in aqueous geochemistry, however, can alter growth efficiency and overall energetic demands of microorganisms. This dissertation uses a thermodynamic approach to explore energy requirements of acidophilic microorganisms in response to chemical changes and how their cell surfaces interact with heavy metals. Chapter 2 explores the effects of energy source availability on microbial energetics with the sulfur-oxidizing Archaea *Acidianus ambivalens* (*A. ambivalens*) in three decreasing concentrations of dissolved oxygen, from aerobic to microaerobic. The results show that growth proceeds most efficiently under low levels of oxygen while high levels of oxygen require the most energy, likely due to higher maintenance energy demands as a result of oxidative stress. Chapter 3 studies the energetic response to environmental redox conditions by quantifying bioenergetics of *A. ambivalens* during anaerobic growth with H<sub>2</sub> and sulfur. *A. ambivalens* growth was not affected by environmental oxidation state and shows similar growth efficiencies and energy budgets between anaerobic and microaerobic conditions. However, microaerobic growth

required less overall Gibbs energy, suggesting a slight preference for growth on sulfur and O<sub>2</sub> in low-oxygen environments. Chapter 4 characterizes the thermodynamics of growth for two mesophilic bacteria, *Acidithiobacillus ferrooxidans* and *Acidithiobacillus thiooxidans*. Energetics were determined during aerobic growth with Fe<sup>2+</sup> and oxygen for *A. ferrooxidans* and with sulfur and oxygen for both *A. ferrooxidans* and *A. thiooxidans*. *A. ferrooxidans* grew most efficiently with sulfur and O<sub>2</sub>, indicating a preference over growth with Fe<sup>2+</sup>. Energetics for all three sulfur oxidizers, *A. ambivalens*, *A. ferrooxidans*, and *A. thiooxidans*, are compared and show a significant correlation between Gibbs energy consumed, enthalpies of growth, and biomass yield, suggesting growth energetics are impacted more by chemistry changes via catabolism than biochemical differences between species. In Chapter 5, we measure cadmium adsorption to the thermoacidophile *Sulfolobus acidocaldarius* cell surfaces and provide the first thermodynamic description of surface adsorption of Cd by *S. acidocaldarius*. These results will not only help us understand interactions between natural environments and microbial activity, but will also help evaluate habitability of environments and energy available for life elsewhere.

## TABLE OF CONTENTS

	Page
List of Figures . . . . .	iv
List of Tables . . . . .	vi
Chapter 1: Introduction . . . . .	1
1.1 Organization of Dissertation . . . . .	1
1.2 Motivation . . . . .	1
Chapter 2: Energetics of <i>Acidianus ambivalens</i> in response to oxygen availability .	5
2.1 Introduction . . . . .	5
2.2 Materials and Methods . . . . .	8
2.2.1 Maintenance culture procedures . . . . .	8
2.2.2 Growth experiments . . . . .	9
2.2.3 Calorimetric procedures . . . . .	9
2.2.4 Chemical measurements . . . . .	10
2.2.5 Overall growth modeling . . . . .	10
2.2.6 Gibbs energy consumption . . . . .	12
2.3 Results . . . . .	13
2.3.1 Calorimetric results . . . . .	13
2.3.2 Culture growth results . . . . .	16
2.3.3 Thermodynamic components of growth . . . . .	17
2.3.4 Response to carbon and oxygen availability . . . . .	21
2.4 Discussion . . . . .	24
2.4.1 Energetic costs for life . . . . .	24
2.4.2 Energetic demands in aerobic and microaerobic conditions . . . . .	26
2.4.3 Thermodynamics of microbial growth . . . . .	27
2.5 Conclusion . . . . .	28

Chapter 3:	Energetics of <i>A. ambivalens</i> during anaerobic sulfur reduction and effects of oxidation state on growth . . . . .	30
3.1	Introduction . . . . .	30
3.2	Methods . . . . .	32
3.2.1	Culture maintenance . . . . .	32
3.2.2	Cell growth . . . . .	32
3.2.3	Calorimetric procedures . . . . .	32
3.2.4	Chemical measurements . . . . .	33
3.2.5	Overall growth modeling . . . . .	33
3.2.6	Gibbs energy consumption . . . . .	35
3.3	Results . . . . .	36
3.3.1	Calorimetry results . . . . .	36
3.3.2	Thermodynamic Description of Growth . . . . .	38
3.4	Discussion . . . . .	41
3.4.1	Anaerobic and Aerobic Growth Energetics . . . . .	41
3.4.2	Power Consumption and Energy Budgets . . . . .	45
3.4.3	Energetic Costs for <i>A. ambivalens</i> . . . . .	47
3.5	Conclusion . . . . .	48
Chapter 4:	Energetics of <i>Acidithiobacillus</i> spp. during sulfur and iron(II) oxidation	49
4.1	Introduction . . . . .	49
4.2	Methods . . . . .	51
4.2.1	Culture maintenance . . . . .	51
4.2.2	Calorimetric experiments . . . . .	51
4.2.3	Chemical measurements . . . . .	52
4.2.4	Overall growth modeling . . . . .	53
4.2.5	Gibbs energy consumption . . . . .	54
4.3	Results . . . . .	56
4.3.1	<i>A. ferrooxidans</i> – Fe(II) oxidation . . . . .	56
4.3.2	<i>A. ferrooxidans</i> – S <sup>0</sup> oxidation . . . . .	60
4.3.3	<i>A. thiooxidans</i> – S <sup>0</sup> oxidation . . . . .	63
4.4	Discussion . . . . .	67
4.4.1	Iron oxidation by <i>A. ferrooxidans</i> . . . . .	67

4.4.2	Substrate utilization— <i>A. ferrooxidans</i> . . . . .	67
4.4.3	Open and closed system growth . . . . .	71
4.4.4	Sulfur oxidation energetics . . . . .	72
4.5	Conclusion . . . . .	74
Chapter 5:	Thermodynamic characterization of cadmium adsorption onto cells of the thermoacidophile <i>Sulfolobus acidocaldarius</i> . . . . .	75
5.1	Introduction . . . . .	75
5.2	Materials and Methods . . . . .	77
5.2.1	Cell Growth . . . . .	77
5.2.2	Adsorption Experiments . . . . .	77
5.2.3	Desorption Experiments . . . . .	78
5.2.4	Calorimetric Experiments . . . . .	78
5.2.5	Derivation of model parameters . . . . .	79
5.3	Results and Discussion . . . . .	82
5.3.1	Cd Adsorption . . . . .	82
5.3.2	Surface Complexation Modeling . . . . .	82
5.3.3	Enthalpies of Cd Adsorption . . . . .	85
5.3.4	Temperature Dependence . . . . .	87
5.4	Conclusions . . . . .	90
Chapter 6:	Conclusions . . . . .	91
6.0.1	Summary of work . . . . .	91
Bibliography	. . . . .	94
Appendix A:	Supplementary Materials . . . . .	112
A.1	Chapter 2 . . . . .	112
A.2	Chapter 4 . . . . .	116
A.3	Chapter 5 . . . . .	119
Appendix B:	Curriculum vitae . . . . .	123

## LIST OF FIGURES

Figure Number	Page
2.1 Example heat curves for each of the three growth conditions. . . . .	14
2.2 Typical heat flow curve for <i>A. ambivalens</i> and growth curve . . . . .	15
2.3 Measured enthalpies of growth and calculated Gibbs energy consumed. . . .	19
2.4 Calculated Gibbs energy consumption and heat produced during growth compared to standard state Gibbs energy and enthalpy of the overall growth reaction.	20
2.5 Gibbs energy consumed compared to initial dissolved oxygen availability. . .	22
2.6 Gibbs energy consumed compared to initial dissolved CO <sub>2</sub> availability. . . . .	23
3.1 Calorimetric heat flow curves for all <i>Acidianus ambivalens</i> replicates during microbial growth with H <sub>2</sub> /S. . . . .	37
3.2 Gibbs energy consumed and enthalpies of growth for <i>A. ambivalens</i> growth with H <sub>2</sub> /S compared to standard state. . . . .	40
3.3 Energetics of aerobic, microaerobic, and anaerobic growth normalized to moles of electrons transferred. . . . .	44
3.4 Biomass produced and power consumed during microbial growth for <i>A. ambivalens</i> under anaerobic, microaerobic, and aerobic conditions. . . . .	46
4.1 Example heat flow curve and growth curve of <i>Acidithiobacillus ferrooxidans</i> during iron oxidation. . . . .	57
4.2 Energetics of <i>Acidithiobacillus ferrooxidans</i> during iron(II) oxidation. . . . .	59
4.3 Energetics of <i>Acidithiobacillus ferrooxidans</i> during growth on sulfur. . . . .	62
4.4 Energetics of growth for <i>Acidithiobacillus thiooxidans</i> during sulfur oxidation	66
4.5 Combined energetics data from <i>Acidithiobacillus ferrooxidans</i> and <i>Acidithiobacillus thiooxidans</i> normalized per electron mole. . . . .	69
4.6 Total cells produced and power consumed for all growth results. . . . .	70
4.7 Combined sulfur oxidation energetics from mesophilic Bacteria <i>Acidithiobacillus ferrooxidans</i> and <i>Acidithiobacillus thiooxidans</i> and thermoacidophilic Archaea <i>Acidianus ambivalens</i> . . . . .	73



5.1	Cd adsorption by <i>Sulfolobus acidocaldarius</i> as a function of pH with surface complexation model results. . . . .	83
5.2	Raw data from isothermal calorimetry and corrected heat with surface complexation modeling fits. . . . .	88
5.3	Cd partitioning onto <i>S. acidocaldarius</i> at 25°C and 75°C. . . . .	89
A.1	Summary of heat flow curves produced by <i>Acidianus ambivalens</i> during sulfur oxidation under recommended growth conditions. . . . .	113
A.2	Summary of heat flow curves produced by <i>Acidianus ambivalens</i> during sulfur oxidation under oxygen-limited growth conditions. . . . .	114
A.3	Summary of heat flow curves produced by <i>Acidianus ambivalens</i> during sulfur oxidation under oxygen- and carbon-limited growth conditions. . . . .	115
A.4	Summary of heat flows produced by <i>Acidithiobacillus ferrooxidans</i> during iron oxidation . . . . .	116
A.5	Calorimetric heat flow for replicates of <i>Acidithiobacillus ferrooxidans</i> during sulfur oxidation. . . . .	117
A.6	Heat flow recorded by calorimetry for <i>Acidithiobacillus thiooxidans</i> during sulfur oxidation. . . . .	118

## LIST OF TABLES

Table Number		Page
2.1	Summary of data collected calculated for each replicate of the three tested oxygen regimes for <i>Acidianus ambivalens</i> . . . . .	18
3.1	<i>Acidianus ambivalens</i> growth with $H_2 / S^\circ$ . . . . .	39
3.2	Average growth data and energetic results for <i>Acidianus ambivalens</i> under aerobic and microaerobic conditions with $S^\circ / O_2$ . . . . .	42
4.1	<i>Acidithiobacillus ferrooxidans</i> growth on $Fe(II) / O_2$ . . . . .	58
4.2	<i>Acidithiobacillus ferrooxidans</i> growth on $S / O_2$ . . . . .	61
4.3	<i>Acidithiobacillus thiooxidans</i> growth on $S / O_2$ . . . . .	64
5.1	<i>Sulfolobus acidocaldarius</i> . . . . .	79
5.2	Model Parameters . . . . .	84

## ACKNOWLEDGMENTS

I would like to thank all the faculty and staff in the Department of Earth and Space Sciences and the Astrobiology program. Without your dedication and support, this degree would not have been possible. The faculty I had the pleasure of interacting with helped me look at my research from fresh perspectives and expand my love for science. I would also like to thank my brilliant committee members, Drew Gorman-Lewis, Roger Buick, John Leigh, and John Baross, for your stimulating lectures, helpful guidance, and feedback along the way.

I especially would like to thank my advisor, Drew Gorman-Lewis. Thank you for taking me on as a graduate student and allowing me to pursue my research interests. Through the chaos, whirlwind of worry, and broken electrodes, I greatly appreciated the calm and balance you brought to every situation. I am beyond grateful for the teaching, outreach, mentoring, and research opportunities you've provided or encouraged and helping me grow as a scientist.

Additionally, I have to thank my friends and family. To my friends in ESS and Astrobiology, you became a fantastic support system, both in your academic and intellectual support and reminding me to leave the lab every once in a while. I am also tremendously grateful to my family back home. I appreciate your support and love through this entire journey. Thank you for believing in me and for all the laughter we share every time we are together.

To my parents, thank you for all your inspiration. To both, you have taught me to find humor and happiness in good times and in bad, though I am still need reminding not to sweat the small stuff. To my mother Tammy, you have taught me tenacity, independence, and strength. To my father Joe, I can't thank you enough for fueling my first spark of interest in microbiology and environmental science. Along the way, you have also taught me

how to work hard, play hard, and tell all the worst jokes.

And to Zachary. Thank you for your never-ending support over the years. I don't know what I would do without your friendship and love. Thank you for putting a smile on my face when I need it most and pushing me to be my best self. You are the best cheerleader, even 2400 miles away. I look forward to our future adventures together!

## DEDICATION

*To my wonderful parents, Joe & Tammy, for their love, support, and endless laughter*

## Chapter 1

# INTRODUCTION

### **1.1 Organization of Dissertation**

The introduction chapter provides a brief overview of the motivation for this dissertation work. Chapters 2-5 have been written as stand-alone papers. Chapter 2, **Energetics of *Acidianus ambivalens*** in response to oxygen availability” was submitted to the journal *Geobiology* in October 2017, declined with encouragement to resubmit, and will be resubmitted in June 2018. Chapter 3, **Energetics of *A. ambivalens* during anaerobic sulfur reduction and effects of oxidation state on growth** will be submitted to the journal *Geomicrobiology*, Chapter 4, ***Acidithiobacillus* spp. growth energetics during iron(II) and sulfur oxidation** will be submitted to *Geochimica et Cosmochimica Acta*, and Chapter 5, **Surface complexation of cadmium by thermoacidophile *Sulfolobus acidocaldarius*** will be submitted to the journal *Chemical Geology*. A compiled bibliography for all chapters is located at the end of the dissertation.

### **1.2 Motivation**

In geothermal and acidic environments, geochemistry plays a vital role in determining the type and abundance of microbial activity. Extreme chemolithoautotrophs grow and thrive in these harsh conditions through energy-yielding reduction-oxidation reactions with inorganic substrates (i.e. sulfur, iron, hydrogen). All life requires energy to drive reactions such as growth and cell maintenance; therefore, fluctuations in the geochemistry can alter microbial activity by affecting the availability of energy sources, nutrients, oxidation state of the environment, or introducing harmful contaminants. As microorganisms are ubiquitous on Earth and are key players in biogeochemical cycles, it is important to understand the energy

requirements of microbial growth and the factors that can alter overall energetics and growth efficiency. Previous energetic research has focused primarily on the amount of Gibbs energy required and/or growth efficiency for heterotrophs and methanogens. Therefore, there is a gap in our knowledge concerning the energetics of extreme chemolithoautotrophs and their response to environmental factors.

Quantifying the energy necessary for microbial growth in extreme environments helps establish the chemical and physical limits to life. Chemolithoautotrophic extremophiles are considered the most relevant analogs for life elsewhere in the Solar System. One strategy to evaluate habitability of other planets and moons is to “Follow the energy”. Following the energy is driven by the notion that all life requires energy; thus, the objective is to search for environments with chemical disequilibrium that could sustain life. Information from extraterrestrial environments can be acquired through remote sensing, *in situ* measurements with rovers/landers, or, in the future, sample return missions. This can help us determine the physical and chemical conditions (e.g. temperature, oxidation state, energy sources) and could allow us to estimate the amount of energy available and type of metabolisms that could be supported there.

The gap in our knowledge concerning energetics of thermophiles and acidophiles and their astrobiological significance make these species ideal subjects for energetics research. This dissertation takes a geochemical and thermodynamic approach to understanding microbial energetics of acidophilic chemolithoautotrophs and their surface interactions with heavy metals. In the following chapters, I characterize microbial growth for different acidophilic Archaea and Bacteria to determine how growth varies based on chemical properties of the environment, catabolic reactions used to drive growth, species-specific traits that affect maintenance energy requirements, and how microbial surfaces interact with metals found in acidic waters.

In Chapter 2, I quantified growth energetics in terms of Gibbs energy consumed ( $\Delta G$ ) and enthalpy produced ( $\Delta H$ ) for the thermoacidophile *Acidianus ambivalens* (*A. ambivalens*) during aerobic sulfur oxidation. Microbial growth, modeled using macrochemical equations

to describe overall metabolism, required the most Gibbs energy under high oxygen concentrations. The large energetic demand was accompanied by low growth efficiencies in terms of biomass yield. Energetic demand decreased and growth efficiency increased as oxygen became more limited. These findings suggest high oxygen concentrations increase maintenance energy requirements and, as a result, overall energetic demand for *A. ambivalens* growth through oxidative stresses.

In Chapter 3, energetics of *A. ambivalens* was characterized under anaerobic conditions, the oxidation of hydrogen with sulfur serving as the energy-yielding catabolic reaction. Overall metabolic efficiency during growth under anaerobic conditions was compared to growth by sulfur oxidation in aerobic and microaerobic conditions (Chapter 2) to investigate the effects of environmental redox state on energetics. Despite the lower energy requirements to synthesize biomolecules in anaerobic environments, anaerobic growth metabolizing  $\text{H}_2 / \text{S}$  yielded similar efficiencies as microaerobic growth metabolizing  $\text{S} / \text{O}_2$ . However, normalized to moles of electrons transferred, microaerobic growth consumed less Gibbs energy than anaerobic and fully aerobic growth, suggesting a slight preference for growth with  $\text{O}_2$  and sulfur in low-oxygen environments.

Chapter 4 characterized the thermodynamics of growth of two mesophilic bacteria, *Acidithiobacillus ferrooxidans* and *Acidithiobacillus thiooxidans*. Energetics were determined during aerobic growth with  $\text{Fe}^{2+}$  and oxygen for *A. ferrooxidans* and with sulfur and oxygen for both *A. ferrooxidans* and *A. thiooxidans* over a range of growth efficiencies. *A. ferrooxidans* required less Gibbs energy during growth and produced high biomass yields when grown with sulfur compared to growth with  $\text{Fe}^{2+}$ , indicating a preference for the higher energy-yielding sulfur oxidation reaction. Microbial energetics for all three sulfur oxidizers, *A. ambivalens*, *A. ferrooxidans*, and *A. thiooxidans*, were compared, resulting in the potential to predict growth energetics for other sulfur-oxidizing microorganisms.

In Chapter 5, we studied the interactions between cell surfaces of the thermoacidophile *Sulfolobus acidocaldarius* and cadmium, a highly toxic heavy metal. Surface adsorption of Cd was determined as a function of pH and for different biomass concentrations, demonstrat-



ing Cd readily adsorbed to the cells. Using surface complexation modeling and calorimetry, I provided the first thermodynamic description of surface adsorption of Cd by *S. acidocaldarius*.

By characterizing microbial growth for a variety of organisms and metabolic strategies under different growth conditions, I hope to understand how and to what extent different environmental factors can affect overall energetics. This research will help us further understand the complex relationship between life and energy and help identify suitable habitable environments in the solar system and beyond.

## Chapter 2

**ENERGETICS OF *ACIDIANUS AMBIVALENS* IN  
RESPONSE TO OXYGEN AVAILABILITY**

*This manuscript will be submitted to the journal Geobiology.*

Co-authored by Chloe E. Hart, Drew Gorman-Lewis

**2.1 Introduction**

Microorganisms are ubiquitous on Earth and key players in biogeochemical cycles. Even in the harshest environments, we find microorganisms making a living on chemical disequilibrium (e.g. [84, 78, 155]). In geothermal regions such as Yellowstone National Park (YNP), we find life built to withstand elevated temperatures ( $> 70^{\circ}\text{C}$ ), low pH ( $< 3$ ), toxic gases (i.e.  $\text{H}_2\text{S}$ ), and harsh metal(loid)s [124]. Chemotrophic microorganisms dominate the hottest regions in YNP, above the temperature limit for photosynthetic life ( $\sim 73^{\circ}\text{C}$ , [87, 169, 2]). Their metabolic activity is fundamental for cycling essential elements such as sulfur and iron [24, 93].

Many case studies have been conducted in YNP to identify the inorganic energy sources and determine how much Gibbs energy ( $\Delta G$ ) is available to support chemolithotrophic life (e.g. [113, 148, 109, 79, 140]). Inorganic sulfur compounds are common in acidic geothermal regions [176, 16, 15] and thus play an essential role in microbial metabolisms [24, 102]. One of the highest energy yielding reactions available in acidic hot springs is aerobic sulfur oxidation, which produces sulfuric acid [140]. Oxygen availability can be naturally low in hot spring environments due to the decrease in solubility at elevated temperatures and chemical data has shown dissolved oxygen can vary both spatially within a geothermal setting (e.g. [176, 123, 35, 75]) and within a hot spring environment (mm- $\mu\text{m}$  scale, [23]). Changes in

oxygen availability consequently affects the amount of potential Gibbs energy available for microorganisms requiring oxygen as a terminal electron acceptor during metabolism. Because of this available Gibbs energy variability, laboratory-based studies are necessary to better understand microbial energetic demands and to what extent environmental conditions may affect them.

After temperature and pH (e.g. [47]), energy source availability is a major factor on both the abundance and distribution of life in an ecosystem [154, 3, 33]. Energy source limitation can impact microbial growth beyond the amount of biomass produced. For example, mesophilic heterotrophs have shown an increase in growth efficiency, in terms of cells produced per amount of substrate consumed, as a response to carbon limitations [133, 39, 52]. Fluctuations in growth efficiency impacts the environment by altering the extent of Gibbs energy consumption and chemical fluxes influenced by metabolism. While sulfur metabolisms have been widely investigated in many organisms (e.g. [24, 102]), we lack a thermodynamic understanding of energy usage under extreme conditions in response to fluctuations of energy sources. Toward this end, we investigated aerobic sulfur oxidation by *Acidianus ambivalens* (*A. ambivalens*) under various oxygen levels and characterized Gibbs energy consumption ( $\Delta G$ ) and enthalpy of growth ( $\Delta H$ ).

*A. ambivalens* is an ideal microorganism to investigate aerobic sulfur oxidation. *A. ambivalens* is a crenarchaeon that grows optimally between 75-85°C in acidic (pH 2.5) environments [180, 181, 51]. *A. ambivalens* is metabolically versatile and can grow anaerobically by H<sub>2</sub> oxidation with sulfur, H<sub>2</sub> oxidation with Fe<sup>3+</sup>, and sulfur oxidation with Fe<sup>3+</sup> or, under aerobic conditions, with oxygen, as described by the reaction  $S^{\circ} + 1.5 O_2 + H_2O \longrightarrow 2 H^+ + SO_4^{2-}$  [180, 181, 51, 91, 4]. *A. ambivalens* can fix inorganic carbon through the 3-hydroxypropionate/4-hydroxybutyrate pathway [22], though yeast extract can also be used to stimulate growth [181]. Multiple investigators have studied molecular and genetic aspects of metabolism in *A. ambivalens* and the species is regarded as a well-studied crenarchaeon [180, 181, 51, 77, 97]. However, we lack comprehensive studies of its energetics under varying energy availability.

Researchers have taken various approaches to quantify microbial energy usage, both in laboratory settings and in natural environments. In a laboratory setting,  $\Delta G$  consumed during microbial growth can be measured, typically based on the catabolic reaction of the organism in question, to quantify energetic budgets for specific microbes (e.g. [147, 4]). Computationally, energetic demands can also be calculated in terms of  $\Delta G$  necessary for biosynthesis (e.g. [5, 7, 108, 6]). While several investigations focus on energetic demands of microbial growth in terms of  $\Delta G$  it does not completely describe the energetics of growth. As shown in Equation 2.1, Gibbs energy is dissipated as enthalpy ( $\Delta H$ ) and entropy ( $\Delta S$ ,  $T$  is absolute temperature).

$$\Delta G = \Delta H - T\Delta S \quad (2.1)$$

Regardless of metabolic pathway, a portion of Gibbs energy is dissipated as heat ( $\Delta H < 0$ ) or heat could be adsorbed ( $\Delta H > 0$ , Liu et al., 2001). Consequently, to thoroughly characterize energy usage of microbes, it is necessary to quantify  $\Delta G$  consumption during growth in addition to total enthalpy via calorimetry. Some research has included calorimetry as a tool to measure total microbial activity in terms of heat produced (e.g. [158, 18, 175, 25, 111, 131]), but few studies have fully characterized energetics of individual species in terms of both  $\Delta G$  and  $\Delta H$ . Calorimetry is the ideal means to measure the enthalpy of growth at constant temperature and pressure.

The focus of this work was to determine how oxygen availability affects Gibbs energy consumption by *A. ambivalens* and how that Gibbs energy is dissipated. We merged two approaches to quantify microbial growth energetics. The first approach, largely used in biotechnology fields, models both catabolic and anabolic reactions of metabolism to create an overall growth reaction [162, 164, 68, 20]. The production of biomass is treated as a basic chemical reaction, where the metabolic reactants progress irreversibly to the metabolic products and new cell material. The second approach, proposed by Smith and Shock [147], quantified Gibbs energy consumption through the change in catabolic chemical species in the medium. Both catabolic and biosynthetic reactions influence the change in chemical

composition of the medium. Therefore, it is assumed anabolic reactions were inherently taken into account with this approach even though they were not explicitly used in the calculations.

We used our combined model of overall microbial growth in addition to chemical composition data to determine Gibbs energy consumption of cultures. Calorimetric measurements of culture growth allowed us to determine the total enthalpy of growth. By working with a pure culture in controlled growth conditions, we can isolate the energetic effects due primarily to the availability of oxygen. The results show that  $\Delta G$  consumption and  $\Delta H$  produced per C-mole biomass are significantly reduced as oxygen availability decreases and accompany an increase in biomass yield. This characterization provides a fundamental energetic description of *A. ambivalens* growth that is essential for understanding how geochemical factors impact energy usage.

## **2.2 Materials and Methods**

### *2.2.1 Maintenance culture procedures*

Maintenance cultures of *A. ambivalens* (ATCC 49204) were grown according to growth conditions described by Zillig *et al.* [181], using Brocks basal salt medium [26] supplemented with additional  $\text{KH}_2\text{PO}_4$  (0.02 M final concentration), absence of yeast extract, and medium adjusted to pH 2.8 with  $\text{H}_2\text{SO}_4$  prior to autoclaving. Sulfur powder was sterilized through three sequential autoclave cycles at 100°C for 30 minutes. Maintenance cultures were prepared aseptically in 100 mL septa vials with 50 mL growth medium, 2 g/L sterile sulfur powder, and 2% (v/v) cell mixture inoculation. Once sealed with butyl rubber stoppers and crimped with aluminum seals, vials were injected with 100%  $\text{CO}_2$  gas for a final concentration of 10%  $\text{CO}_2$  in the headspace and incubated at 76°C for 6-7 days.

### 2.2.2 Growth experiments

Three distinct growth conditions were investigated, designated by the initial amount of oxygen provided. In the recommended growth (RG) experiments, culture procedures were based on published literature and were identical to the maintenance culture procedures described above. The aim was for initial oxygen concentrations in the medium to be near saturation ( $\sim 200\mu\text{M}$  at  $76^\circ\text{C}$ ). Oxygen-limited (OL) experiments were prepared following the maintenance culture protocol, but the headspace was purged with 100%  $\text{CO}_2$  gas to remove excess  $\text{O}_2$  in the headspace yet provide ample inorganic carbon for biomass production. The design aimed to provide an initial dissolved oxygen concentration of  $\sim 50\%$  saturation ( $\sim 100\mu\text{M}$ ). Lastly, the design for oxygen- and  $\text{CO}_2$ -limited (OCL) experiments was constructed to provide an initial dissolved oxygen concentration of  $\sim 25\%$  saturation ( $\sim 50\mu\text{M}$ ). The design was also aimed to test if growth efficiency in OL experiments were affected by the increased availability of inorganic carbon. The OCL experiments were prepared following the maintenance culture protocol, but the experiment vials were brought into an anaerobic chamber with a 99%  $\text{N}_2$  and 1%  $\text{H}_2$  atmosphere to seal the vials. The final headspace was  $\text{N}_2$  injected with  $\text{CO}_2$  for a final concentration of 10%  $\text{CO}_2$ . These steps were taken to further minimize  $\text{O}_2$  in the headspace and lose some additional  $\text{O}_2$  from the media during vacuuming and gas exchange in the airlock chamber. Control vials were also prepared in this manner and brought up to growth temperature ( $76^\circ\text{C}$ ) to verify there was minimal hydrogen gas contamination, as *A. ambivalens* can use  $\text{H}_2$  as an electron donor to reduce sulfur.

### 2.2.3 Calorimetric procedures

Enthalpies of growth ( $\Delta\text{H}$ ) were measured with a TA Instruments TAM III Nanocalorimeter that measures heat flow between a reaction cell and a reference cell [80, 165]. The calorimeter heat flow response was calibrated by an electrical heating procedure verified by measuring the heat of protonation of trishydroxymethylaminomethane [61].

All experiment cultures were grown in 4 mL Hastelloy calorimetric cells containing 2.5

mL total culture and 2 g/L sterile sulfur. Both reaction and reference Hastelloy cells were filled with identical media and headspace constituents. The reaction cell contained an aliquot of *A. ambivalens* to provide an initial cell density of  $10^5$  cells/mL and the reference cell was kept sterile and void of cells. The heat flow of the samples was monitored over time and integration of the heat flow signal after baseline correction resulted in the total heat produced during growth.

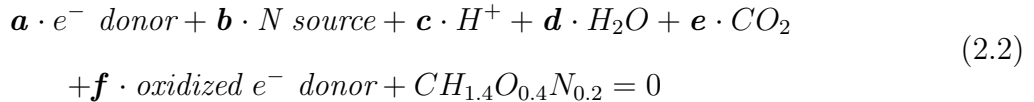
#### 2.2.4 Chemical measurements

At the beginning and end of growth, chemical data were collected to measure the change in components of the growth medium. Sulfate concentrations were determined through Hach TNTplus<sup>®</sup> spectrophotometric sulfate test vials, pH was measured with a combination microelectrode (Microelectrodes, Inc.) calibrated daily with four NIST standards, and dissolved oxygen was measured with a Unisense Clark-type dissolved oxygen microsensor. Both pH and dissolved oxygen measurements were taken at 76°C due to their sensitivity to temperature. Slides for cell counts were prepared using a polycarbonate 0.2  $\mu\text{m}$  filter membrane with SYBR Green I dye following the procedure of Lunau *et al.* [100] and examined with appropriate filters on a Zeiss Axiostar Plus microscope.

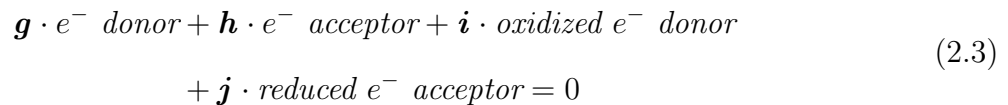
#### 2.2.5 Overall growth modeling

Equations reported by Heijnen and Kleerebezem [68] (Equations 2.2-2.7 below) were applied to model the overall energetics using simplified macrochemical equations. The equations are based on biosynthesis of one carbon-mole (C-mol) of generic biomass represented by the formula  $\text{CH}_{1.8}\text{O}_{0.5}\text{N}_{0.2}$  [34, 63, 94, 162, 68]. The biomass formula is comprised of the four major elements of cellular material and has a molar mass of 24.6 g/C-mol. Autotrophic organisms like *A. ambivalens* synthesize biomass during the anabolic reaction represented

by Equation 2.2.



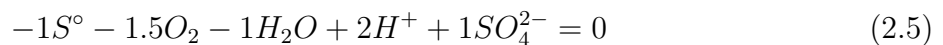
The Gibbs energy necessary to drive anabolism is generated through redox reactions during catabolism. A generic catabolic reaction is shown in Equation 2.3.



Metabolic coefficients  $\mathbf{a}$  through  $\mathbf{j}$  were determined by solving a series of linear equations to satisfy mass, charge, and degree of reduction balances (Supplementary material). Reactants consumed during growth result in negative coefficients while products result in positive coefficients. For aerobic growth on sulfur, the derived anabolic reaction to produce 1 C-mol of generic biomass for *A. ambivalens* becomes Equation 2.4:



The catabolic reaction for sulfur oxidation to sulfuric acid results in the following reaction displayed in Equation 2.5



The catabolic multiplicative factor ( $f_{cat}$ , Equation 2.6) represents the number of times the catabolic reaction is performed in relation to the anabolic reaction to produce 1 C-mol of biomass. The catabolic factor is calculated from experimental data, using the amount of biomass yield ( $Y_{X/D}$ , defined as C-mol of biomass produced per mole electron donor consumed) and the anabolic coefficient of the electron donor ( $Y_D^{an}$ , or coefficient  $g$  in Equation 2.2). Biomass produced in C-mol was calculated by converting the number of cells to moles of carbon using the value 2.5 fmol-C/cell, the average carbon content per cell for *A. ambivalens* performing sulfur reduction with hydrogen reported by Amenabar *et al.* [4] via  $^{13}C$  assimilation.

$$f_{cat} = \frac{-1}{Y_{X/D}} + Y_D^{an} \quad (2.6)$$



The overall growth reaction coefficients are determined by combining  $f_{cat}$  (Equation 2.6), anabolic coefficients (Equation 2.2), and the catabolic coefficients (Equation 2.3), as shown in Equation 2.7.

$$\text{Overall growth reaction} = \text{Anabolism} + f_{cat} \times \text{Catabolism} \quad (2.7)$$

The microbial growth model established by Heijnen and Kleerebezem [68] was applied to growth of *A. ambivalens*. Catabolic factors were calculated for each experiment by using the biomass yield and stoichiometric coefficient of sulfur in the anabolic reaction (Equations 2.6 and 2.4) to produce overall growth reactions (Equation 2.7) for each experimental replicate. The overall growth reactions were used for further thermodynamic calculations.

### 2.2.6 Gibbs energy consumption

Gibbs energy consumed during growth ( $\Delta G$ ) was calculated for each experiment based on the activities ( $\alpha$ ) of all the chemical species in the overall growth reaction and the stoichiometric coefficients of the overall growth reaction determined by the biomass yield in each replicate (see above). The standard state Gibbs energies of formation ( $\Delta G_f^\circ$ ) for the chemical species in the growth reaction were calculated at the experimental temperature with the revised Helgeson-Kirkham-Flowers (HKF) equations of state [72, 71] using SUPCRT92 [139, 83]. For biomass,  $\Delta G_f^\circ = -67$  kJ/mol was used for all growth experiments [69]. Standard state Gibbs energies of reactions ( $\Delta G_r^\circ$ ) of the overall growth reaction determined for each experiment were calculated using Equation 2.8, where  $\Delta G_{f,products}^\circ$  and  $\Delta G_{f,reactants}^\circ$  are the standard state Gibbs energies of formation for the products and reactants of the growth reaction, respectively.

$$\Delta G_r^\circ = \Sigma \Delta G_{f,products}^\circ - \Sigma \Delta G_{f,reactants}^\circ \quad (2.8)$$

Gibbs energy available for growth ( $\Delta G_r$ ) is defined by Equation 2.9, where  $\Delta G_r^\circ$  is modified with the concentration-dependent reaction quotient ( $Q$ ).

$$\Delta G_r = \Delta G_r^\circ + 2.3026 \times R \times T \times \log Q \quad (2.9)$$

The reaction quotient,  $Q$ , is calculated with the activities of the products and reactants involved in the overall growth equation and is shown in Equation 2.10, where  $a_i^{Y^{ogr}}$  denotes thermodynamic activity of the  $i^{th}$  chemical species and  $Y^{ogr}$  represents the stoichiometric reaction coefficient of the  $i^{th}$  species in the overall growth reaction (Equation 2.7).

$$Q = \prod a_i^{Y^{ogr}} \quad (2.10)$$

Activities of the aqueous species were calculated using PHREEQC [119] and sulfur was assumed to have an activity of 1. Activity of biomass in solution was converted from molality (C-mol/kg solvent) assuming an activity coefficient of 1. Overall Gibbs energy consumed ( $\Delta G$ ) during growth for each experiment was calculated with Equation 2.11 as the difference between initial  $\Delta G_r$  available, calculated from the initial chemical composition of the medium solution and biomass, and final  $\Delta G_r$  available, calculated from the final chemical composition of the medium solution and biomass.

$$\Delta G = \Delta G_{r,initial} - \Delta G_{r,final} \quad (2.11)$$

Microbial growth was ultimately evaluated in terms of  $\Delta G$  consumed and  $\Delta H$  produced, both in kJ/C-mol biomass.

## 2.3 Results

### 2.3.1 Calorimetric results

*A. ambivalens* produced clear heat flow signals during growth in all three oxygen conditions tested (see Supplementary Material). A typical heat flow signal over time for each oxygen regime is depicted in Figure 2.1. The heat flow signal paralleled the growth phase of the culture with lag, exponential, and stationary phase corresponding with the initial baseline, exponential increase and peak heat flow signal, and return to baseline respectively as shown in the example in Figure 2.2. RG produced the largest heat flow signals with a lag phase of approximately 67 hours before spending 53 hours in exponential phase. The peak heat flows reached 33-48  $\mu W$  after approximately 113 hours of growth and returned to baseline after

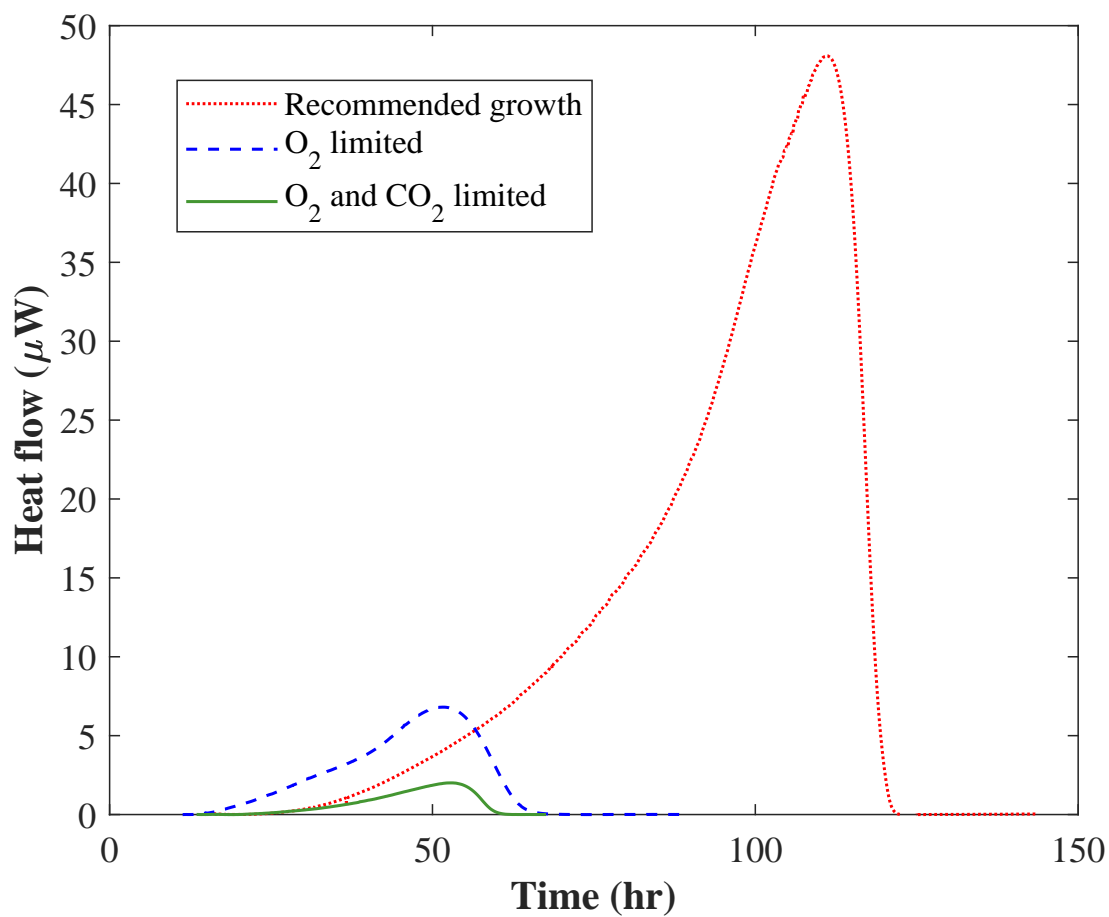


Figure 2.1: Example heat curves produced by the calorimeter during microbial growth for each of the three experimental conditions in terms of  $\mu\text{watts}$  of heat over time in hours. Total heat produced during growth, in joules, was calculated by integrating the area under each heat flow curve ( $\mu\text{Watts}$ ) over time (in seconds). Recommended growth conditions produced the largest heat signals (red dotted line), followed by oxygen-limited (blue dashed line), and the lowest heat signals were produced in the oxygen- and carbon-limited replicates (green solid line).

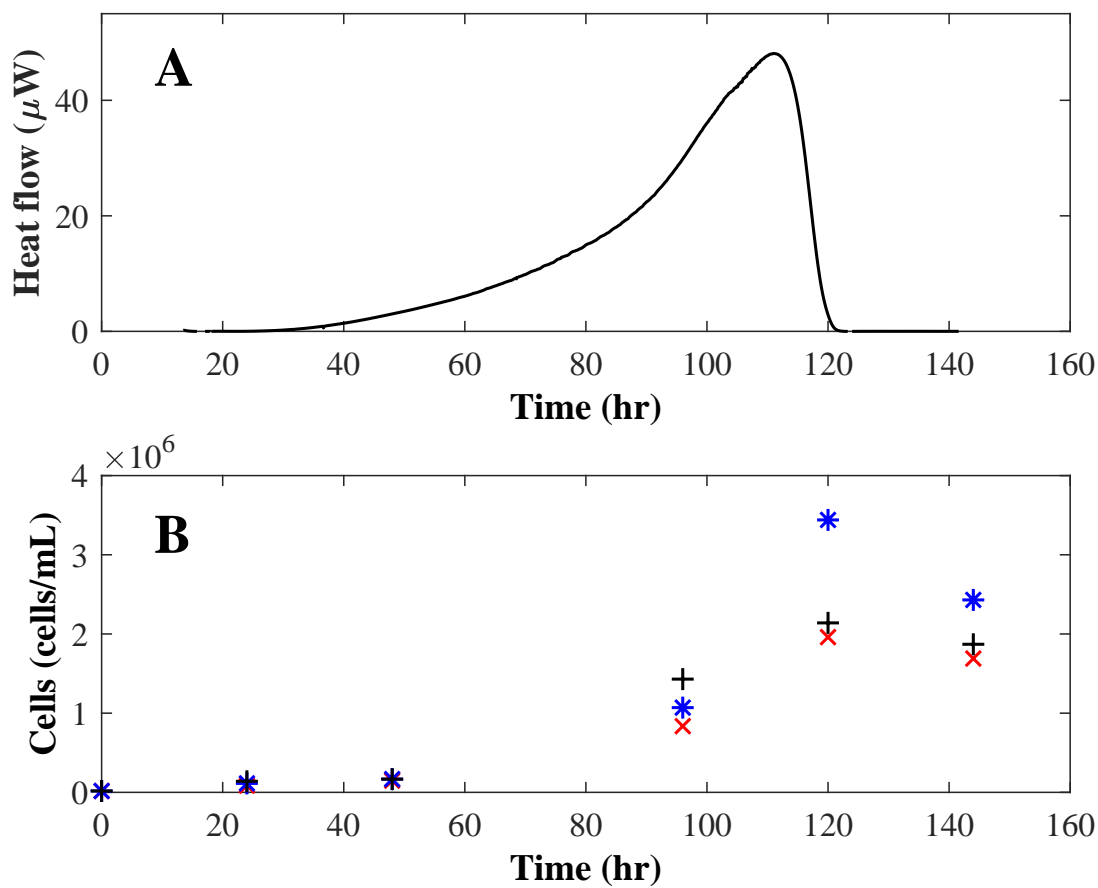


Figure 2.2: (A) Typical heat curve for *A. ambivalens* displaying heat ( $\mu\text{W}$ ) over growth time (hours) recorded by the calorimeter. (B) Growth curve from external cultures monitored in tandem to calorimeter culture example depicting concentration of cells (cells/mL) over the course of growth, in hours. Heat flow increases during exponential growth of the culture and returns to baseline as the culture reaches stationary phase. Different symbols in growth curve represent cell counts from different replicates.

119 hours. OL growth conditions produced the second largest average heat signal. The lag phase was shorter than RG, with an approximate duration of 30 hours, followed by 40 hours of exponential growth. Peak heat flows ranged from 4.3 to 15.5  $\mu\text{W}$  and occurred after about 52 hours of growth before returning to baseline after 70 hours. OCL experiments were the lowest heat signals but were similar to OL experiments in lag phase and total growth duration. Lag phase occurred for 30 hours, followed by 40 hours of exponential growth. After approximately 59 hours, peak heat flow occurred and reached 2-4.5  $\mu\text{W}$ . Heat flow returned to baseline after approximately 72 hours.

### 2.3.2 Culture growth results

Data from each replicate of the experimental conditions are summarized in Table 2.1. Cultures grown under RG conditions consumed an average of 10  $\mu\text{mol}$  of sulfur during growth. These conditions resulted in the most total biomass production, approximately 2-fold greater than either oxygen-limited conditions. The average biomass was calculated to be  $1.18 \times 10^{-8}$  C-mol and the biomass yield ranged from 0.0006 to 0.0017 C-mol/S-mol. OL growth conditions consumed much less sulfur, with an average of 1.5  $\mu\text{mol}$  consumed during growth. The average total biomass production was  $6.93 \times 10^{-9}$  C-mol and yields were higher than RG, with a range of 0.0023 to 0.0132 C-mol/S-mol. Similar sulfur consumption and total biomass values were produced in OCL experiments as OL conditions. The average sulfur consumption was 1.8  $\mu\text{mol}$  in OCL experiments and average total biomass produced was  $5.61 \times 10^{-9}$  C-mol. Biomass yields ranged from 0.0014 to 0.0099 C-mol/S-mol.

Cell morphology remained consistent between the different growth experiments; there was no apparent expression of appendages or other changes to the cell surface across all replicates. Cell diameters of the coccus cells were statistically similar across the different oxygen treatments ( $P > 0.1$  for all t-tests). The mean for RG (N=69) cells were  $1.06 \pm 0.26 \mu\text{m}$ , OL (N=52) cell diameters were  $1.01 \pm 0.19 \mu\text{m}$ , and OCL (N=52) cell diameter mean was  $1.04 \pm 0.18 \mu\text{m}$ .

### 2.3.3 Thermodynamic components of growth

Modeling overall growth to determine biomass yield,  $\Delta G$  consumed, and  $\Delta H$  produced allows one to interpret energy efficiency and usage by microbes in a thermodynamic framework. Biomass yield is a good indication of how closely the catabolic reaction is coupled to the anabolic reaction [133, 68]. A relatively higher biomass yield indicates more catabolic energy is conserved as new biomass as opposed to other cellular processes or non-growth reactions.  $\Delta G$  and  $\Delta H$ , both normalized to the amount of C-mol produced, can determine how much Gibbs energy is necessary for growth and the extent of Gibbs energy dissipation as enthalpy [64, 147]. By measuring both, we can see more detailed changes in energetics across the tested oxygen regimes.

Total heat produced during growth was determined for each replicate by integrating the heat flow curve obtained via calorimetry.  $-\Delta H$  of growth was calculated by taking the quotient of total heat and biomass produced for a final, normalized value in kJ/C-mol. The total heat produced during growth decreased across the tested oxygen regimes. RG, with the highest amount of dissolved oxygen available ( $\sim 190\mu\text{M}$ ), released the largest amount of enthalpy during growth ranging from  $3.59 \times 10^5$  to  $7.02 \times 10^5$  kJ/C-mol. OL conditions ( $\sim 110\mu\text{M O}_2$ ) produced less heat, with  $-\Delta H$  values between  $5.89 \times 10^4$  to  $1.62 \times 10^5$  kJ/C-mol. OCL conditions ( $\sim 56\mu\text{M O}_2$ ) produced the lowest amount of heat, with  $-\Delta H$  values ranging from  $3.02 \times 10^4$  to  $5.77 \times 10^4$  kJ/C-mol.

Gibbs energy consumed ( $-\Delta G$ ) followed the same trend as  $-\Delta H$  across the different oxygen conditions.  $-\Delta G$  calculations ranged from  $1 \times 10^4$  to  $3.04 \times 10^4$  for RG growth conditions,  $5.94 \times 10^2$  to  $2.66 \times 10^3$  for OL conditions, and  $2.25 \times 10^2$  to  $1.65 \times 10^3$  for OCL conditions. These results are portrayed in Figure 2.3 as a function of biomass yield for each individual experiment. Both  $-\Delta H$  and  $-\Delta G$  for RG conditions were very large but resulted in the lowest biomass yield. The two oxygen limited conditions generally followed the same negatively correlated trend between  $-\Delta H$ ,  $-\Delta G$ , and biomass yield but resulted in greater biomass yields than RG experiments.

Table 2.1: Summary of data collected calculated for each replicate of the three tested oxygen regimes for *Acidianus ambivalens*.

	Biomass (C-nmol)	S° ( $\mu$ moles)	Yield c-mol/S	Initial O <sub>2</sub> ( $\mu$ M)	Initial CO <sub>2</sub> (mM)	$-\Delta G$ (kJ/C-mol)	$-\Delta H$ (kJ/C-mol)	Energetic yield (fmol/ $\mu$ J)
<b><i>Recommended growth</i></b>								
	14	8.4	0.0017	182	0.9	$1.00 \times 10^4$	$3.65 \times 10^5$	100
	16	10.2	0.0015	182	0.9	$1.21 \times 10^4$	$3.62 \times 10^5$	83
	14	10.8	0.0013	192	0.9	$1.42 \times 10^4$	$3.59 \times 10^5$	71
	6	9.8	0.0006	192	0.9	$3.04 \times 10^4$	$7.02 \times 10^5$	33
	11	10.3	0.0011	198	0.9	$1.44 \times 10^4$	$5.03 \times 10^5$	69
	10	11.0	0.0009	198	0.9	$2.16 \times 10^4$	$5.35 \times 10^5$	46
<i>Avg</i>	12	10.1	0.0012	191	0.9	$1.71 \times 10^4$	$4.71 \times 10^5$	67
<b><i>Oxygen-limited</i></b>								
	6.4	1.6	0.0039	123	13.7	$1.70 \times 10^3$	$6.43 \times 10^4$	592
	6.8	1.4	0.0049	123	13.7	$6.79 \times 10^2$	$7.99 \times 10^4$	1493
	8.1	1.0	0.0081	107	13.7	$8.72 \times 10^2$	$1.62 \times 10^5$	1153
	4.0	1.8	0.0023	107	13.7	$2.16 \times 10^3$	$1.55 \times 10^5$	464
	6.5	2.3	0.0029	100	13.7	$2.66 \times 10^3$	$1.44 \times 10^5$	377
	9.9	0.8	0.0132	100	13.7	$5.94 \times 10^2$	$5.89 \times 10^4$	1709
<i>Avg</i>	6.9	1.5	0.0059	110	13.7	$1.44 \times 10^3$	$1.11 \times 10^5$	964
<b><i>Oxygen- and carbon-limited</i></b>								
	6.2	2.5	0.0025	28	0.9	$2.63 \times 10^2$	$3.02 \times 10^4$	3930
	2.5	1.8	0.0014	28	0.9	$2.25 \times 10^2$	$3.17 \times 10^4$	4564
	3.6	0.8	0.0048	63	0.9	$1.65 \times 10^3$	$3.49 \times 10^4$	605
	8.0	3.0	0.0027	63	0.9	$1.60 \times 10^3$	$5.77 \times 10^4$	625
	6.2	2.2	0.0028	78	0.9	$2.83 \times 10^2$	$5.59 \times 10^4$	513
	7.2	0.7	0.0099	78	0.9	$5.15 \times 10^2$	$5.51 \times 10^4$	1021
<i>Avg</i>	5.6	1.8	0.0040	56	0.9	$7.57 \times 10^2$	$4.43 \times 10^4$	1876

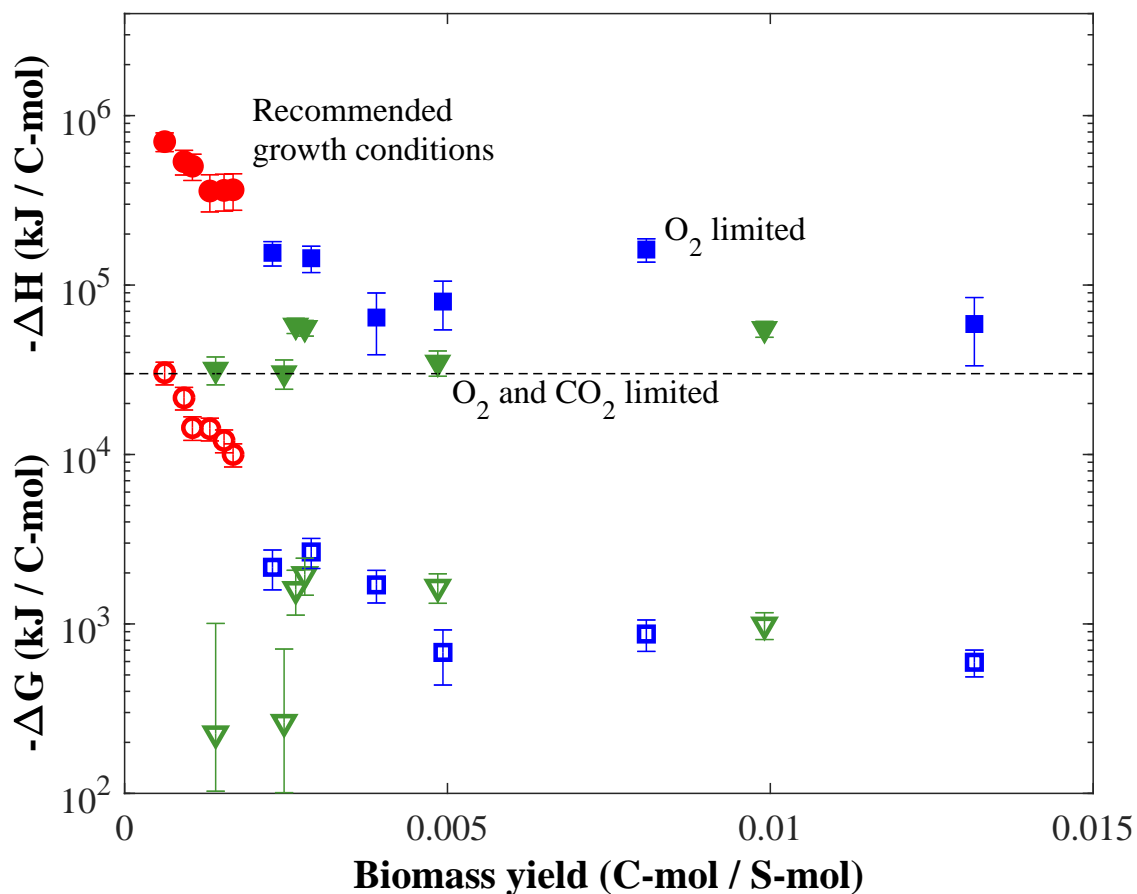


Figure 2.3: Measured enthalpies of growth ( $-\Delta H$ ) and calculated Gibbs energy consumed ( $-\Delta G$ ) for the replicates in the three experimental growth conditions on a log scale in relation to the corresponding biomass yield. Filled symbols represent measured enthalpy values (upper half) and corresponding open symbols show Gibbs energy consumed (lower half; Recommended growth = red circles; O<sub>2</sub>-limited = blue squares; O<sub>2</sub> and CO<sub>2</sub>-limited = green triangles). Each symbol represents one replicate in the designated growth condition and error bars are included for all measurements.



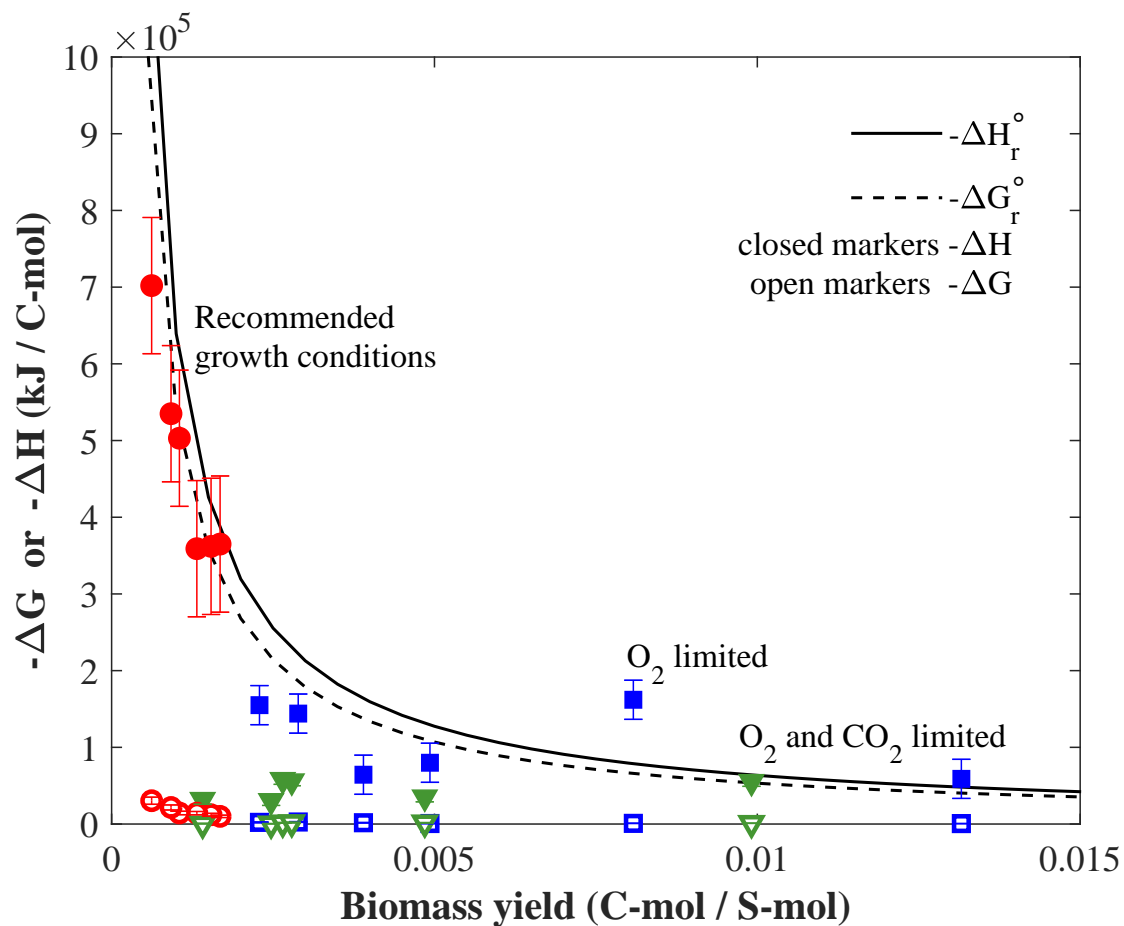


Figure 2.4: Black curves represent standard enthalpy ( $-\Delta H_r^\circ$ , solid line) and Gibbs energy ( $-\Delta G_r^\circ$ , dashed line) for the overall growth reaction for *A. ambivalens* as it relates to biomass yield. Standard state values for the overall growth reaction were calculated for 1 molal of pure reactants and products at 76°. The standard state curves act as theoretical results for how microbial growth will behave at different biomass yields. Plotted on top of the standard state curves are actual growth data; each symbol represents one replicate in the designated growth condition. The filled symbols represent measured enthalpies of growth ( $-\Delta H$ ) determined via calorimetry and open symbols represent Gibbs energy consumed ( $-\Delta G$ ) calculated from chemical data for all three growth conditions (recommended growth: red circles; O<sub>2</sub>-limited: blue squares; O<sub>2</sub>- and CO<sub>2</sub>-limited: green triangles). The measured enthalpies of growth fall along or close to the theoretical enthalpy of growth (solid line). All  $-\Delta G$  values were greater than zero, but much smaller than the theoretical Gibbs energy of growth (dashed line). Error bars are included for all measurements.

When standard state values of  $-\Delta G_r^\circ$  and  $-\Delta H_r^\circ$  of the modeled overall growth reaction for *A. ambivalens* were compared,  $-\Delta H_r^\circ$  was always greater than  $-\Delta G_r^\circ$  across the biomass yield values, with the difference between the lines representing entropic thermal energy ( $T\Delta S_r^\circ$ , [150, 164]) as shown in Figure 2.4. Therefore, enthalpy released during growth must be large to compensate for an unfavorable change in  $T\Delta S_r^\circ$  that would otherwise hinder microbial growth. The behavior of the standard state values predicts the primary mode of Gibbs energy dissipation will be through the release of heat and growth will be highly exothermic. This prediction held true for all experiments ( $-\Delta H > -\Delta G$ ) and measured  $-\Delta H$  fell along or near  $-\Delta H_r^\circ$  modeled with the exception of some OCL replicates. Calculated  $-\Delta G$ , however, was considerably less than  $-\Delta G_r^\circ$  modeled for all three growth scenarios. Though Gibbs energy was primarily dissipated as enthalpy ( $-\Delta H > -\Delta G$ ), the results suggest that a substantial portion of Gibbs energy is dissipated as  $T\Delta S$ . In all experiments,  $-\Delta G$  was smaller than the amount of enthalpy produced ( $-\Delta H > -\Delta G$ ) following standard state predictions; however, the standard state values did not accurately predict  $T\Delta S$  or  $-\Delta G$ .

#### 2.3.4 Response to carbon and oxygen availability

To evaluate the energetics of growth in response to oxygen and inorganic carbon availability, both initial dissolved oxygen activity and initial  $\text{CO}_2$  activity were plotted against  $-\Delta G$  (Figure 2.5 and 2.6, respectively). Two sample t-tests showed oxygen values for each growth condition were statistically different from each other ( $P < 0.05$  for all three tests). ANOVA and post analysis Tukey tests revealed RG  $-\Delta G$  values were statistically different from OL and OCL data (0.05 confidence level), but OL and OCL were statistically indistinguishable. ANOVA and Tukey tests were conducted for initial  $\text{CO}_2$  and showed OL contained significantly more inorganic carbon, while RG and OCL were the same. There were significant differences in initial activity of  $\text{CO}_2$  between OL and OCL experiments, but insignificant differences in  $-\Delta G$  during growth. This suggests the differences in Gibbs energy consumption and enthalpy across the three tested conditions were directly related to the initial dissolved oxygen activity in the medium while initial  $\text{CO}_2$  activity had no measurable effect.

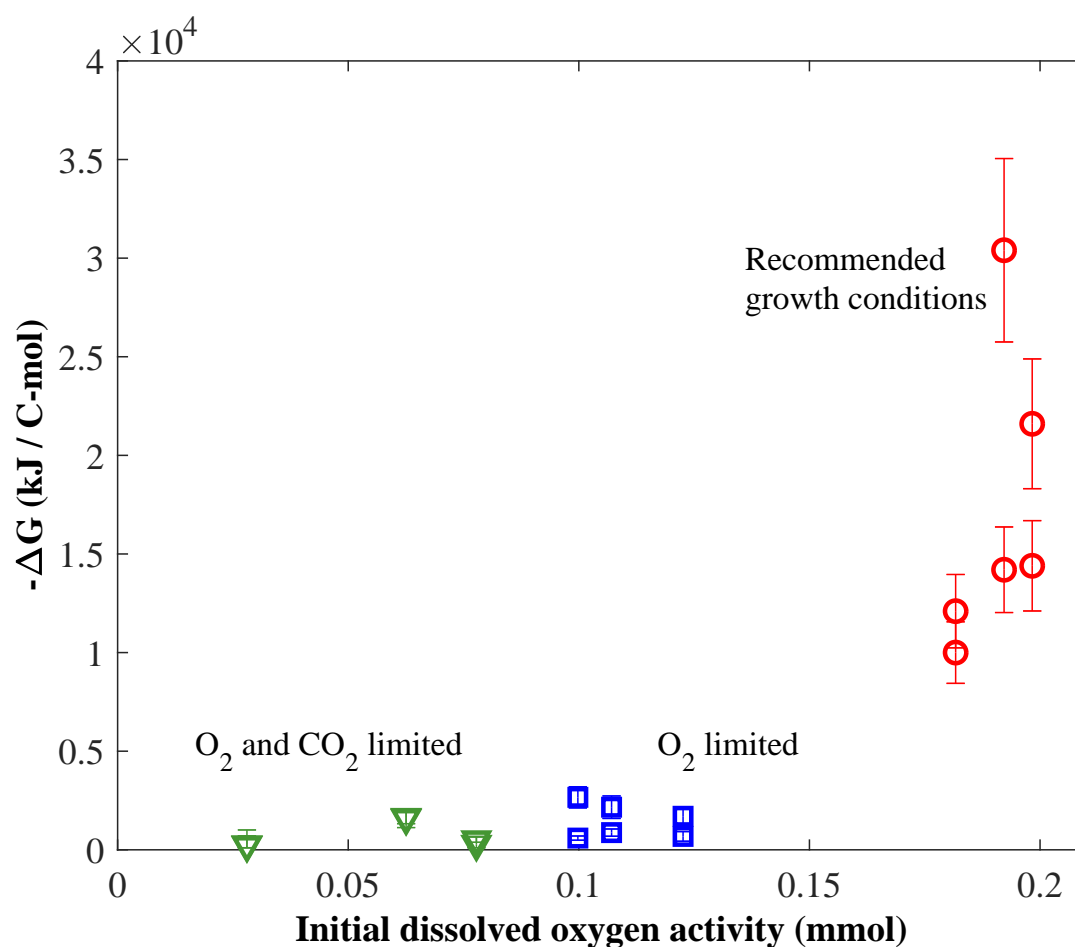


Figure 2.5: Gibbs energy consumed per C-mol biomass produced for the tested oxygen treatments. All three oxygen treatments had significantly different beginning dissolved oxygen concentrations ( $P \ll 0.001$ ). Gibbs energy consumed during growth significantly decreased between the fully aerobic recommended growth (RG, red circles) conditions and the two microaerophilic conditions, oxygen-limited (green triangles) and  $O_2$ - and  $CO_2$ -limited conditions (blue squares).

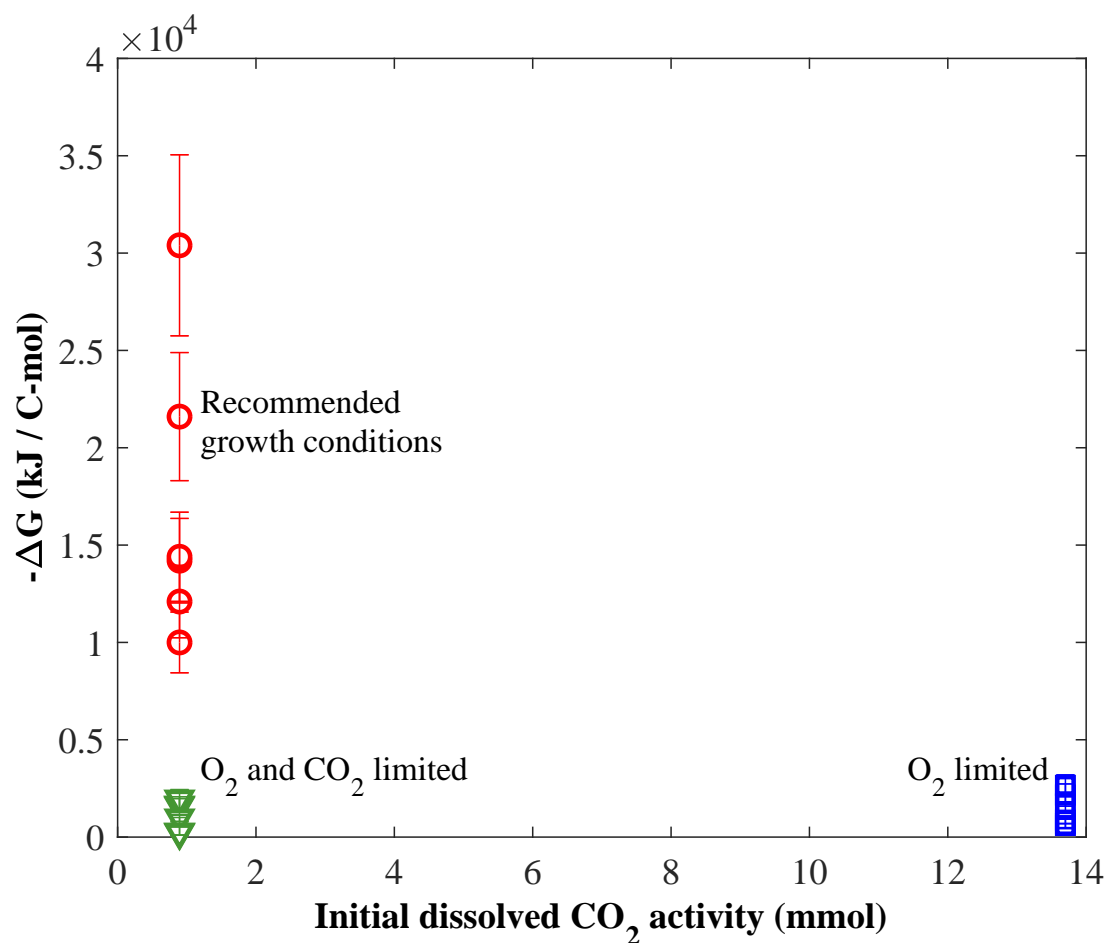


Figure 2.6: Gibbs energy consumed (kJ/C-mol biomass) and initial dissolved CO<sub>2</sub> activity (mM). Recommended growth (red circles) and O<sub>2</sub>- and CO<sub>2</sub>-limited conditions (OCL; green triangles) had the same initial dissolved CO<sub>2</sub> activities ( $P = 0.9$ ). Gibbs energy consumed during growth was significantly different between the fully aerobic recommended growth conditions and OCL conditions. The two microaerophilic conditions (OCL and oxygen-limited conditions, blue squares) had significantly different inorganic carbon available, but Gibbs energy consumed during growth was statistically the same.

## 2.4 Discussion

### 2.4.1 Energetic costs for life

*A. ambivalens* shows an increase in growth efficiency as oxygen availability decreases in the form of higher yields, lower heat production, and lower chemical energy consumption, but the mechanism(s) responsible for the change are not clear. The energy gained via catabolism drives many cellular processes besides anabolism. Energy is also partitioned for maintenance reactions, or the energy required for non-growth processes such as motility, turnover of macromolecules (e.g. proteins), and re-establishing chemical gradients across the cellular membrane [132].

The near-saturated oxygen concentrations in RG conditions may be more detrimental than advantageous, causing oxidative stress, leading to a greater maintenance energy demand and thus increasing overall energetic demands. Reactive oxygen species (ROS) are generated in several ways, including incomplete oxygen reduction during metabolism or increased partial pressure of oxygen. ROS are chemically damaging to all life by reacting with DNA, RNA, protein, lipids, and cofactors [11, 49]. ROS may be responsible for the increased maintenance energy demand in *A. ambivalens* by attacking the carbon fixation cycle. A key enzyme used in carbon fixation, 4-hydroxybutyryl-CoA dehydratase, is slowly inactivated by oxygen, though the enzyme can maintain sufficient activity within the protective, lower-oxygen environment of the cell [22]. Responses to oxidative and other environmental stresses have been researched in the archaea *Sulfolobus solfataricus* (*S. solfataricus*), a related sulfur-oxidizing thermoacidophile. Oxidative stress has been shown to result in a number of gene regulations [101], including a substantial upregulation in a Dps-like protein (DNA-binding protein from starved cells) known to act as an antioxidant [173] and increases in superoxide dismutase and peroxiredoxin.

As cell maintenance reactions are driven by energy gained through catabolism, an increase in maintenance energy demands may be accompanied by an increase in the catabolic reaction products. Continued use of the catabolic reaction by *A. ambivalens* and production

of sulfuric acid could further exacerbate the issue of increased maintenance energy. RG experiments consumed a greater amount of sulfur than the microaerophilic experiments, which lead to a greater production of sulfuric acid and a larger change in pH ( $\sim 0.25$  decrease) in the growth medium. McCarthy *et al.* [107] showed an increase in oxidative stress in *S. solfataricus* as pH decreased. These authors found genes consisting of membrane lipid biogenesis proteins were upregulated as a response to stress that likely aid in membrane repair due to oxidative damage. This indicates there may be further energy demands in order to regulate intracellular pH and re-establish proton gradients across the membrane in recommended growth experiments with *A. ambivalens* as pH decreases. Both microaerophilic experiments, conversely, produced significantly less sulfuric acid and resulted in a smaller change in pH in the growth medium ( $\sim 0.1$  to negligible change).

Although oxygen can be destructive in the cell in the form of ROS, oxygen is a necessary terminal electron acceptor for *A. ambivalens* under aerobic growth conditions. In looking at the summary of overall energetics in Figure 2.3, it seems as though some OCL replicates may have been under greater stress due to too little oxygen than other the replicates based on their deviation from the trend. Most data follow the simple trend of decreasing  $-\Delta H$  and  $-\Delta G$  as biomass yield increases in the shape of the standard state curves for the overall growth reaction (Figure 2.4). Two  $-\Delta H$  and  $-\Delta G$  points from OCL growth conditions fall below the rest. These replications had lower initial oxygen concentrations (28  $\mu\text{M}$ ; refer to Table 1). *A. ambivalens* requires  $\text{O}_2$  for anabolism as the final electron acceptor in the respiratory chain [174].

It is unlikely that energetic differences across the tested oxygen regimes were due to substantial differences in the anabolic energy costs, such as producing an alternate cellular composition (C:N:P ratios). In natural environments, in situ microorganisms living in extreme conditions in YNP can acclimate to nitrogen or phosphate limitations by altering cell composition in terms of nitrogen, phosphorous, or carbon [114]. Concentrations of key nutrients such as nitrogen and phosphorus were abundant and consistent across all tested growth conditions. Studying anabolic nutrient limitation was not the goal of the current

work and we assumed cell composition remained the same in all experiments.

#### 2.4.2 Energetic demands in aerobic and microaerobic conditions

In addition to indirectly measuring a change in maintenance energy demands, quantifying microbial energetics has also been used as a predictor for preferential growth conditions. Despite the common belief that microbes will preferentially grow on the most energetically favorable substrate, some energetic studies have shown this is not always the case [66, 4]. Laboratory studies with pure cultures under substrate-limited or substrate-competitive conditions can be conducted to test this.

A recent study isolated a native strain of *A. ambivalens* from YNP and characterized Gibbs energy demand for growth by measuring the change in catabolic chemical species [4]. Catabolic  $\Delta G$  consumed was calculated for various anaerobic metabolisms:  $H_2$  oxidation with sulfur,  $H_2$  oxidation with  $Fe^{3+}$ , and sulfur oxidation with  $Fe^{3+}$ . The authors found growth to be most efficient on  $H_2/S^0$  ( $\Delta G_r^\circ = -47.74$  kJ/mol at  $85^\circ C$ ; [9]), resulting in energetic yields (C-mol biomass produced per joule Gibbs energy consumed) averaging around 267 fmol-C/ $\mu J$ . Both  $Fe^{3+}$  metabolisms were less efficient, averaging around 32 fmol-C/ $\mu J$ , despite the greater energetic potential of the  $S^0/Fe^{3+}$  redox reaction ( $\Delta G_r^\circ = -302.94$  kJ/mol at  $85^\circ C$ ; [9]). Competition experiments containing  $H_2/S^0/Fe^{3+}$  indicated preferential growth on  $H_2/S^0$  over the other redox couples, suggesting substrate preference is dictated by energetic demand of the organism (highest energetic yield) as opposed to energetic potential (most negative  $\Delta G_r^\circ$ ).

While our findings with *A. ambivalens* are not directly comparable to Amenabar *et al.* [4] due to considerable differences (experimental methods and culture vials, growth temperatures, native *A. ambivalens* strain as opposed to ATCC strain), we can use this approach to understand preferential growth conditions. Fully aerobic recommended growth conditions yielded mean energetic yields of 67 /*pm* 24 fmol-C/ $\mu J$ , calculated using only the catabolic chemical species. In the microaerophilic growth conditions, the overall energetic yields of both OL and OCL conditions were much higher but highly variable, with a mean of 855 /*pm*

464 fmol-C/ $\mu$ J. The increase in energetic yield in OL and OCL conditions may indicate a preference for microaerophilic conditions over fully aerobic conditions. These results mirror those found by Simon *et al.* [143] with *S. solfataricus*. Microaerophilic conditions resulted in higher biomass yields and more efficient use of oxygen. At oxygen concentrations higher than atmospheric levels (35%), no growth was observed, indicating toxic levels. The preference for microaerophilic growth conditions demonstrated by *A. ambivalens*, *S. solfataricus*, and other thermophiles [76, 137, 149] could be the result of evolving in hot spring environments where concentrations of oxygen are naturally lower due to lower solubility as temperature increases.

#### 2.4.3 Thermodynamics of microbial growth

This is not the first study to report an increased growth efficiency in response to substrate limitation, but it is one of the few studies to characterize chemolithoautotrophic growth in thermodynamic terms. Several studies have investigated substrate limitations in heterotrophs, especially in moderate growth temperatures and circum-neutral pH (e.g. [133, 39, 52]), fewer have focused on extreme chemolithotrophs (e.g. [96, 89, 143, 36]), and even less have quantified growth efficiency in terms of  $\Delta G$  consumed [147, 4]. Using calorimetry to measure microbial growth has also proved useful for determining enthalpies of growth [64, 131], though very few studies have incorporated both  $\Delta G$  and  $\Delta H$  in microbial energetics studies [163, 135, 164].

As shown with *A. ambivalens*, incorporating calorimetric results with  $\Delta G$  consumption results in many orders of magnitude difference between the Gibbs energy consumed and enthalpy of growth during sulfur oxidation. The results were not accurately represented by  $\Delta G_r^\circ$  and, primarily in microaerophilic conditions,  $\Delta H_r^\circ$  (refer to Figure 2.4). It is clear by looking at the difference between  $\Delta H$  and  $\Delta G$  in all growth conditions oxidizing sulfur is highly exothermic. Irreversible reactions, such as cell growth and maintenance reactions, are accompanied with the production of entropy [162, 150]. To overcome internal entropy production, microorganisms must consume Gibbs energy and dissipate it as heat and/or



producing highly entropic products relative to the entropy of the nutrients ( $\Delta S > 0$ ). The primary mode of Gibbs energy dissipation is another approach to characterize how microbial life grows from a thermodynamic perspective. Microbial growth of *A. ambivalens* by sulfur oxidation is an excellent example of enthalpy-driven growth ( $\Delta H \ll 0$ ). Additional studies characterizing both  $\Delta G$  and  $\Delta H$  to determine mode of Gibbs energy dissipation will provide a more complete energetic description of microbial growth that can be compared between many species.

## 2.5 Conclusion

In this study, we have provided an energetic characterization of microbial growth for the thermoacidophilic sulfur-oxidizer *A. ambivalens* in response to oxygen availability. *A. ambivalens* produced the highest amount of biomass when oxygen concentrations were higher, but growth progressed very inefficiently with large chemical energy consumption ( $-\Delta G$ ), large enthalpy produced ( $-\Delta H$ ), and low biomass yield in moles of carbon produced per mole of sulfur used. When oxygen was limited, growth experiments resulted in less overall biomass, but the energy required for growth was significantly reduced and growth was more efficient in terms of  $\Delta G$ ,  $\Delta H$  produced, and biomass yield. We propose that the increase in overall efficiency from high oxygen to limited oxygen is due to the removal of oxidative stress on the organism. By limiting oxygen and oxidative stresses, the maintenance energy demand decreases and allows more catabolic energy to be partitioned into biomass production. This indicates a preference for growth under microaerophilic conditions in natural environments.

There are interesting implications for by continued research in the field of bioenergetics and understanding overall energy demand (and, indirectly, maintenance energy requirements) under different environmental conditions. The composition of chemotrophic communities in high-temperature environments is affected primarily by temperature and pH, but secondary controls involve the availability of dissolved nutrients. To further understand the heterogeneity we find in the biosphere of natural environments, we need a firmer grasp on energetics of individual species and metabolisms, in what way geochemical factors such as changes to en-

ergy source availability alter energetics, and what factors can measurably affect maintenance energy demands.

## Chapter 3

**ENERGETICS OF *A. AMBIVALENS* DURING ANAEROBIC SULFUR REDUCTION AND EFFECTS OF OXIDATION STATE ON GROWTH**

*This manuscript will be submitted to the journal Geomicrobiology.*

Co-authored by Chloe E. Hart, Drew Gorman-Lewis

**3.1 Introduction**

The energetic demands of microbial growth can be affected by a number of chemical and physical changes. Fluctuations in energy sources [39, 143, 52, 36], key nutrients [95, 19], temperature [92], and environmental stresses [127] can change the overall energy requirements and efficiency of microbial growth and, thus, affect microbial activity in the environment. In high-temperature environments, above the photosynthesis temperature limit of approximately 72°C [87, 169, 2], chemolithoautotrophic organisms play a vital role in geochemical cycles by metabolizing inorganic substrates and assimilating CO<sub>2</sub> to produce new cell material [130, 146, 24, 93]. Biosynthetic reactions, or the anabolic portion of metabolism, is most impacted by the oxidation state of the environment [108]. To understand how changes in oxidation state affect anabolism and overall microbial energetics, microbial growth energetics were determined for *Acidianus ambivalens* under anaerobic conditions and compared to fully aerobic and microaerobic growth conditions.

In volcanically-driven hot spring regions, such as Yellowstone National Park, geochemical fluctuations can occur within a geothermal region and within a single hot spring (e.g. [8, 35, 116, 23, 33]). The changes in geochemistry can be a result of abiotic processes relating to the reduced, thermal waters reaching the surface or due to microbial activity altering

the chemistry during growth (e.g. [176, 48, 23, 33]). Despite the extreme conditions of hot springs and fluctuations in chemistry, these regions support a wealth of microbial activity and metabolisms, with hydrogen- and oxygen-consuming metabolisms having high metabolic energy potentials (e.g. [8, 148, 109, 140, 33]). *In situ* data collected from hot springs have shown there can be micro-environments with gradients in O<sub>2</sub> and H<sub>2</sub>S due to microbial activity on  $\mu\text{m}$ -mm scales [129, 106, 23]. Microorganisms that are able to grow under these different redox conditions may experience changes in energetic demands as the cost of biosynthesis varies [108].

*Acidianus ambivalens* (*A. ambivalens*) is the ideal microorganism to study to understand the energetic responses to environmental oxidation state. *A. ambivalens* is a thermoacidophilic Archaea that grows optimally in temperatures around 75-85°C and pH around 2-3 [180, 181, 51]. *A. ambivalens* is a facultative anaerobe and metabolically flexible; *A. ambivalens* is able to grow in aerobic conditions by oxidizing sulfur with O<sub>2</sub> or in anaerobic conditions through sulfur oxidation with Fe<sup>3+</sup>, H<sub>2</sub> oxidation with sulfur, or H<sub>2</sub> oxidation with Fe<sup>3+</sup> [180, 181, 4]. *A. ambivalens* is also distributed globally in different geothermal settings [181, 8, 4].

Energetics of growth have been previously determined for *A. ambivalens* during sulfur oxidation under fully aerobic (100% O<sub>2</sub> saturation) and microaerobic (50% O<sub>2</sub> saturation) growth conditions (Chapter 2; [67]). The results showed an increase in biomass yield and a decrease in overall energetic demand as the availability of oxygen decreased. As a facultative anaerobe, growth should preferentially occur in aerobic conditions, indicated as the highest energetic yield (biomass produced per joule energy consumed; e.g. [4]). However, it is not known how lower energetic costs of anabolism in anaerobic conditions affects overall growth energetics. To address this gap in our knowledge, we characterized microbial growth in thermodynamic terms for *A. ambivalens* during anaerobic growth on H<sub>2</sub> and elemental sulfur (S<sup>0</sup>). The overall Gibbs energy consumed, enthalpies of growth, and biomass yields were compared to previously determined results under aerobic and microaerobic growth conditions.

## 3.2 Methods

### 3.2.1 Culture maintenance

*A. ambivalens* (ATCC 49204) was maintained according to anaerobic growth conditions described by Zillig et al. [181], using Brocks basal salt medium containing the following (per liter): 1.3 g  $(\text{NH}_4)_2\text{SO}_4$ , 0.28 g  $\text{KH}_2\text{PO}_4$ , 0.25 g  $\text{MgSO}_4 \cdot 7\text{H}_2\text{O}$ , 0.07 g  $\text{CaCl}_2 \cdot 2\text{H}_2\text{O}$ , 0.02 g  $\text{FeCl}_3 \cdot 6\text{H}_2\text{O}$ , 1.8 mg  $\text{MnCl}_2 \cdot 4\text{H}_2\text{O}$ , 4.5 mg  $\text{Na}_2\text{B}_4\text{O}_7 \cdot 10\text{H}_2\text{O}$ , 0.22 mg  $\text{ZnSO}_4 \cdot 7\text{H}_2\text{O}$ , 0.05 mg  $\text{CuCl}_2 \cdot 2\text{H}_2\text{O}$ , 0.03 mg  $\text{NaMoO}_4 \cdot 2\text{H}_2\text{O}$ , 0.03 mg  $\text{VO}_2\text{SO}_4 \cdot 2\text{H}_2\text{O}$ , 0.01 mg  $\text{CoSO}_4$  [26] supplemented with additional  $\text{KH}_2\text{PO}_4$  (0.02 M) and adjusted to pH 2.8 with  $\text{H}_2\text{SO}_4$ . After autoclaving, the medium was brought into an anaerobic hood under an  $\text{N}_2/\text{H}_2$  atmosphere to equilibrate for at least 48 hours.

Maintenance cultures were aseptically prepared in 100 mL septa vials with 50 mL growth medium, 2 g/L sterile sulfur powder, and 1 mL inoculum. Once sealed, vials were pressurized to 150 kPa with  $\text{H}_2/\text{CO}_2$  gas (80:20) and incubated at 76°C for 6-7 days.

### 3.2.2 Cell growth

Growth experiments were prepared identically to maintenance cultures according to the procedures described above. Cultures were aseptically prepared in an anaerobic chamber under an atmosphere of  $\text{N}_2/\text{H}_2$ . Experiments contained 2 mL of medium in 3.2 mL glass calorimetric vials containing 2 g/L sterile sulfur and 2% inoculum. The calorimetric vials were sealed with butyl rubber stoppers, crimped with aluminum caps, and pressurized to 1.5 kPa with  $\text{H}_2/\text{CO}_2$  gas (80:20).

### 3.2.3 Calorimetric procedures

Enthalpies of growth were measured with a TA Instruments TAM III Nanocalorimeter that measures heat flow between a reaction vial and a cell-free reference vial [80, 165]. The calorimeter heat flow response was calibrated by an electrical heating procedure verified by measuring the heat of protonation of trishydroxymethylaminomethane [61].

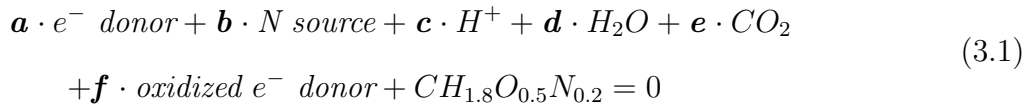
All calorimetric cells contained 2 mL total culture and 2 g/L sterile sulfur. Both reaction and reference glass cells were filled with identical media and headspace constituents. The reaction cell contained an aliquot of *A. ambivalens* with an initial cell density of  $10^5$  cells/mL and the reference cell was kept sterile. The heat flow of the samples was monitored over time. After the signal returned to baseline, integration of the signal after baseline correction resulted in the total heat produced during growth. The total heat produced was normalized to the total amount of cell material produced to calculate enthalpy.

#### 3.2.4 Chemical measurements

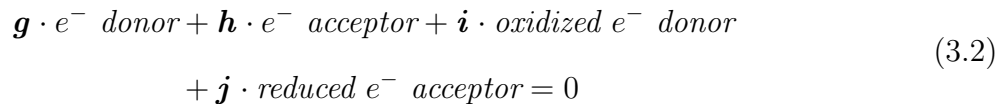
At the beginning and end of growth, chemical data were collected to measure the change in components of the growth medium. Sulfide concentrations were measured using a sulfide spectroscopic analysis [32], pH was measured with a combination microelectrode (Microelectrodes, Inc.) calibrated daily with four NIST standards, and dissolved hydrogen was measured with a Unisense Clark-type  $H_2$  microsensor. Slides for cell counts were prepared using a polycarbonate 0.2  $\mu$ m filter membrane with SYBR Green I dye following the procedure of Lunau et al. [100] and examined with appropriate filters on a Zeiss Axiostar Plus microscope. Cell counts were converted to C-mol based on the average value of 2.5 fmol-C per cell reported by Amenabar *et al.* [4].

#### 3.2.5 Overall growth modeling

To model overall metabolism in simplified macrochemical equations, equations reported by Heijnen and Kleerebezem [68] were applied to *A. ambivalens* growth. The equations are based on biosynthesis of one carbon-mole (C-mol) of generic biomass represented by the formula  $CH_{1.8}O_{0.5}N_{0.2}$  [63, 94, 162, 68]. The biomass formula is comprised of only the four major elements of cellular material and has a molar mass of 24.6 g/C-mol. *A. ambivalens* produces biomass during the anabolic reaction represented by Equation 3.1.



The Gibbs energy necessary to drive anabolism is generated through redox reactions during catabolism. A generic catabolic reaction is shown in Equation 3.2.



Metabolic coefficients  $\mathbf{a}$  through  $\mathbf{j}$  were determined by solving a series of linear equations to satisfy mass, charge, and degree of reduction balances, with positive coefficients for products and negative coefficients for reactants.

The energy gained through the catabolic reaction drives other cell reactions as well; therefore, catabolism and anabolism are not performed in equal quantities. The catabolic multiplicative factor ( $f_{cat}$ ) represents the number of times the catabolic reaction is performed to produce 1 C-mol biomass and is calculated using the amount of biomass yield ( $Y_{X/D}$ , defined as C-mol of biomass produced per mole electron donor consumed) and the anabolic coefficient of the electron donor ( $Y_{an}^D$ , Equation 3.3). Biomass produced in C-mol was calculated by converting grams of biomass to C-mol using the molar mass of the generic biomass formula (24.6 g/C-mol).

$$f_{cat} = \frac{-1}{Y_{X/D}} + Y_{an}^D \quad (3.3)$$

The overall growth coefficients are determined by combining  $f_{cat}$  (Equation 3.3), catabolic coefficients (Equation 3.2), and the anabolic coefficients (Equation 3.1), as shown in Equation 3.4.

$$\text{Overall growth reaction} = \text{Anabolism} + f_{cat} \cdot \text{Catabolism} \quad (3.4)$$

Individual catabolic factors (Equation 3.3) and overall growth reactions (Equation 3.4) were calculated for each experiment replicate based on the resulting biomass yield. Overall growth reactions for each experiment were used for further thermodynamic calculations.

### 3.2.6 Gibbs energy consumption

Gibbs energy consumed during growth ( $\Delta G$ ) was calculated for each experiment based on the change in available Gibbs energy, based on both the chemical species involved and stoichiometric coefficients of the overall growth reaction. The standard state Gibbs energies of formation ( $\Delta G_f^\circ$ ) for the chemical species in the growth reaction were calculated to at the experiment temperature with the revised Helgeson-Kirkham-Flowers (HKF) equations of state [72, 71] using SUPCRT92 [139, 83, 138, 141]. Standard states include unit activity of pure solid, unit activity of aqueous species in a hypothetical 1 molal solution to infinite dilution, and unit fugacity of a pure gas at 1 bar at any temperature and pressure. For biomass,  $\Delta G_f^\circ = -67$  kJ/mol was used for all growth experiments [69]. Standard state Gibbs energies of reactions ( $\Delta G_r^\circ$ ) of the overall growth reaction determined for each experiment were calculated using Equation 3.5, based on the Gibbs energy of formation of the products ( $\Delta G_{f,products}^\circ$ ) and of the reactants ( $\Delta G_{f,reactants}^\circ$ ) of the overall growth reaction.

$$\Delta G_r^\circ = \Delta G_{f,products}^\circ - \Delta G_{f,reactants}^\circ \quad (3.5)$$

Available Gibbs energy in the medium ( $\Delta G_r$ ) was calculated for the given growth reaction as demonstrated in Equation 3.6, using standard state Gibbs energies of reactions ( $\Delta G_r^\circ$ ) determined for each experiment from Equation 3.5, the universal gas constant ( $R$ ), absolute temperature ( $T$ ), and the reaction quotient ( $Q_r$ ).

$$\Delta G_r = \Delta G_r^\circ + RT \times \ln(Q_r) \quad (3.6)$$

The reaction quotient,  $Q_r$ , was using in Equation 3.7, where  $a_i^{Y^{ogr}}$  denotes thermodynamic activity of the  $i^{th}$  chemical species and  $Y^{ogr}$  represents the stoichiometric reaction coefficient



of the  $i^{th}$  species in the overall growth reaction (Equation 3.4).

$$Q_r = \prod a_i^{Y^{ogr}} \quad (3.7)$$

Activities of the aqueous species were calculated using PHREEQC [119] and solid sulfur was assumed to have an activity of 1. Biomass in solution, assuming an activity coefficient of 1, and was converted from molality (C-mol/kg solvent) to activity. Gibbs energy consumed for growth was calculated as the difference between initial ( $G_{r,initial}$ ) and final ( $G_{r,final}$ ) available Gibbs energy (Equation 3.8).

$$\Delta G = \Delta G_{r,initial} - \Delta G_{r,final} \quad (3.8)$$

### 3.3 Results

#### 3.3.1 Calorimetry results

Calorimetric experiments produced exothermic heat signals. In all replicates, microbial growth produced distinct heat flow curves that paralleled the growth phase of the culture. Lag, exponential, and stationary phase corresponded to the initial baseline, exponential increase and peak heat flow signal, and return to baseline, respectively, as shown in Figure 3.1. Exponential growth began after approximately 39 hours of growth. The peak heat signal was  $1.5 \mu\text{W}$  and occurred at about 58 hours. After 34 hours of exponential growth, the heat signal returned to baseline, resulting in 73 total hours of growth.

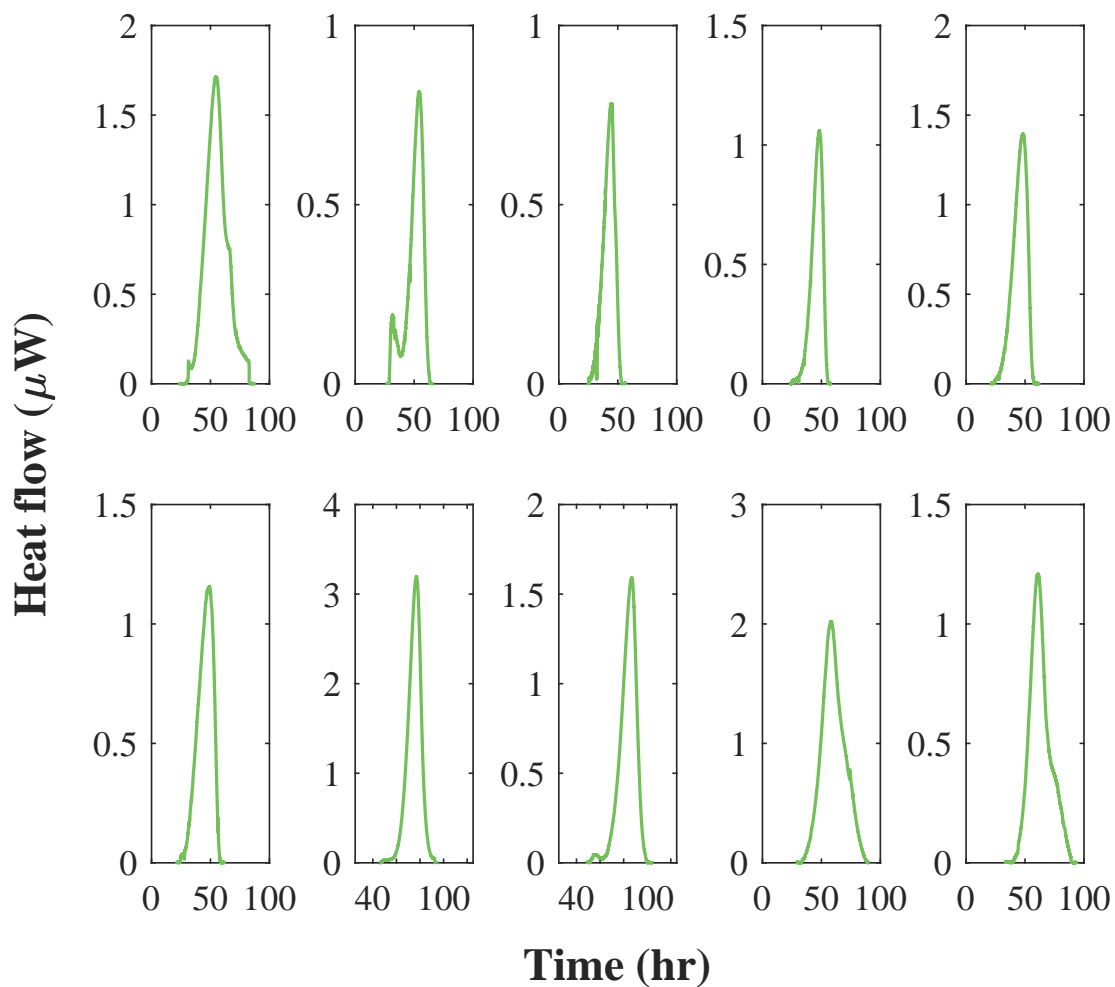


Figure 3.1: Calorimetric heat flow curves, in  $\mu\text{W}$  vs hours, for all *Acidianus ambivalens* replicates during microbial growth with  $\text{H}_2/\text{S}$ . Positive values indicates growth was exothermic ( $\Delta\text{H} < 0$ ).

### 3.3.2 Thermodynamic Description of Growth

Table 3.1 contains a summary of growth and energetics data collected from each replicate. The average biomass produced during growth was 35 nmol-C and consumed approximately 5.6  $\mu$ moles sulfur, leading to a biomass yield of 0.0064 C-mol/S.

Energetics of growth were normalized to the amount of biomass produced. Total heat produced during growth was determined for each replicate by integrating calorimetric heat flow curves. Enthalpy ( $-\Delta H$ ) of growth, shown in Table 3.1, had an average value of 3021 kJ/C-mol.  $-\Delta H$  generally approached zero as growth efficiency increased in terms of biomass yield (Figure 3.2). Total  $-\Delta G$  consumed during growth had an average value of 2116 kJ/C-mol and was generally less negative or similar to  $-\Delta H$  (Table 3.1). Figure 3.2 shows  $-\Delta G$  of growth followed a similar trend as  $-\Delta H$  and approached zero as biomass yield increased.

Standard state values of  $-\Delta G^\circ$  and  $-\Delta H^\circ$  of the modeled overall growth reaction for *A. ambivalens* were compared to measured  $-\Delta H$  and  $-\Delta G$  values, depicted in Figure 3.2. Standard states represent the theoretical energetics of growth for the overall growth reactions, based on pure substances at 1 molal, as a function of biomass yield. The standard state values for  $-\Delta G^\circ$  and  $-\Delta H^\circ$  predict Gibbs energy consumed and enthalpy produced during growth should be similar values, with  $-\Delta H$  resulting in slightly more negative values. Both  $-\Delta G^\circ$  and  $-\Delta H^\circ$  also approach zero as biomass yields increase. Though standard states and calculated  $-\Delta G$  and  $-\Delta H$  follow similar patterns,  $-\Delta H$  and  $-\Delta G$  fell substantially lower (less negative) than standard states predict.

Table 3.1: *Acidianus ambivalens* growth with H<sub>2</sub> / S°

Biomass (nmol-C)	S <sup>2-</sup> (μmoles)	Yield (C-mol/S)	-ΔH		-ΔG		Energy budget (kJ/C-mol)	
			(kJ/C-mol)	(kJ/e-mol)	(kJ/C-mol)	(kJ/e-mol)		
26	7.4	0.0036	4896	2448	3360	1680	3360	
29	5.9	0.0049	1360	680	2657	1328	2657	
55	7.5	0.0073	583	292	1769	885	1769	
54	5.2	0.0102	787	393	1066	533	1057	
20	4.6	0.0044	3548	1774	1985	993	1985	
24	3.3	0.0072	2731	1366	1156	578	1156	
38	6.4	0.0060	3832	1916	2627	1314	2627	
53	7.8	0.0067	1627	814	2159	1080	2148	
19	4.6	0.0041	8499	4249	3028	1514	3028	
35	3.5	0.0100	2351	1175	1355	678	1347	
<i>Avg</i>	35±14	5.6 ±1.6	0.0064±0.0023	3021±2372	1511±1190	2116±794	1058±397	2113±796

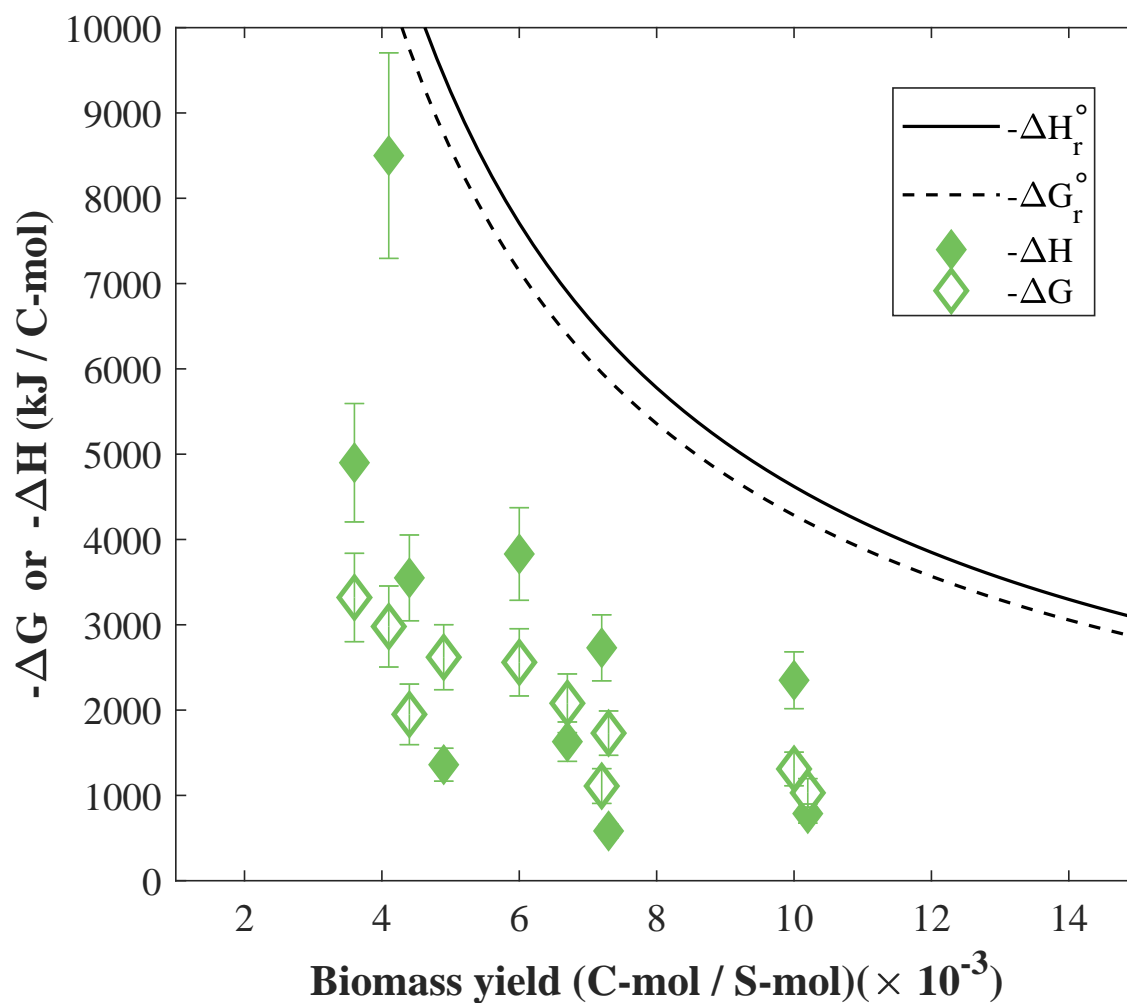


Figure 3.2: Gibbs energy ( $\Delta G$ ) consumed and enthalpies ( $\Delta H$ ) of growth for *A. ambivalens* growth on  $H_2/S$ . Filled diamonds indicate measured enthalpies by calorimetry and open diamonds are calculated Gibbs energy consumed for all replicates. Solid and dashed lines represent  $-\Delta H_r^\circ$  and  $-\Delta G_r^\circ$ , respectively, calculated at 76°C based on 1 mol of pure reactants and products.

### 3.4 Discussion

#### 3.4.1 Anaerobic and Aerobic Growth Energetics

In order to compare microbial energetics involving different catabolic reactions to gain energy, the number of electrons transferred per mole of substrate should be taken into consideration. During aerobic sulfur oxidation, *A. ambivalens* transfers six moles of electrons per mol-S to produce sulfuric acid, while anaerobic sulfur reduction involves two moles of electrons per mol-S to produce H<sub>2</sub>S. Therefore, energetics of growth ( $-\Delta G$  and  $-\Delta H$ ) were converted to kJ C-mol<sup>-1</sup> e-mol<sup>-1</sup> using the moles of substrate used and number of electrons per substrate (recorded in Table 3.1). The average growth and energetics data collected under aerobic and microaerobic conditions during sulfur oxidation are summarized in Table 3.2 and anaerobic data is compiled in Table 3.1.

Figure 3.3 shows previously determined energetics and biomass yield results for *A. ambivalens* during sulfur oxidation under fully aerobic and microaerobic growth conditions (Chapter 2, [67]) and the anaerobic sulfur reduction results from this study, normalized per mole electron transferred. Biomass yields for all three growth conditions were statistically distinct, with anaerobic growth producing higher yields than microaerobic growth (two-sample t-test,  $P < 0.05$ ) followed by aerobic growth (two-sample t-test,  $P < 0.05$ ). Enthalpies of growth (kJ C-mol<sup>-1</sup> e-mol<sup>-1</sup>) decreased as biomass yield increased and were also statistically distinct ( $P < 0.05$  for all two-sample t-tests).  $-\Delta H$  follows this trend due to the exothermic natures of the catabolic reactions. Sulfur oxidation is very exothermic;  $-\Delta H_r^\circ$  of the catabolic reaction alone is approximately 639 kJ/mol-S<sup>°</sup> at 76°C [83]. The amount of catabolism during growth is affected by the overall energetic demands of growth. In the aerobic growth experiments, energy demands were higher, likely due to an increase in maintenance energy demand due to oxidative stress (Chapter 2, [101, 107]). This led to an increase in catabolism and higher growth enthalpies as a result. In microaerobic growth conditions, the amount of catabolism decreased, likely due to the decrease in oxidative stress, resulting in lower growth enthalpies and higher biomass yields.

Table 3.2: Average growth data and energetic results for *Acidianus ambivalens* under aerobic and microaerobic conditions with  $S^\circ / O_2$  (Chapter 2, [67]).

Treatment	Biomass (nmol-C)	$S^\circ$ ( $\mu$ moles)	Yield (C-mol/S)	$-\Delta H$ (kJ/C-mol)	$-\Delta G$ (kJ/e-mol)	$-\Delta G$ (kJ/C-mol)	$-\Delta G$ (kJ/e-mol)	Energy budget (kJ/C-mol)
Aerobic	$12 \pm 4$	$10.1 \pm 0.9$	$0.0012 \pm 0.0004$	$4.71 \times 10^5 \pm 1.37 \times 10^5$	$78498 \pm 22841$	$17121 \pm 7585$	$2853 \pm 1264$	$17121 \pm 7585$
Microaerobic	$7 \pm 2$	$1.5 \pm 0.5$	$0.0059 \pm 0.0041$	$1.11 \times 10^5 \pm 4.80 \times 10^4$	$18462 \pm 8004$	$1444 \pm 859$	$241 \pm 143$	$1444 \pm 859$

The reaction to reduce sulfur, however, is far less exothermic than sulfur oxidation.  $-\Delta H_r^\circ$  of the catabolic reaction is  $\sim 34$  kJ/mol-S $^\circ$  at 76°C [83]. This is demonstrated in the significantly lower enthalpies of growth measured for anaerobic sulfur reduction.  $-\Delta G$  however, followed a different trend. Aerobic growth consumed the most energy, followed by anaerobic growth ( $P = 0.02$ , two-sample t-test), and, lastly, microaerobic growth ( $P \ll 0.05$ , two-sample t-test). The large Gibbs energy requirements during fully aerobic growth further supports the suggestion that high oxygen concentrations can cause stresses detrimental to growth (Chapter 2, [11, 101, 107]). The lower  $-\Delta G$  consumed in microaerobic growth, as previously discussed, probably reflects the decrease in oxidative stress. Despite the significantly higher biomass yields produced under anaerobic conditions ( $P = 0.0003$ , two-sample t-test), the amount of  $-\Delta G$  consumed during growth is larger than microaerobic conditions. Facultative anaerobes, such as *A. ambivalens*, tend to preferentially grow with oxygen due to the higher energetic potential oxygen-consuming reactions produce. In the case of *A. ambivalens*, the anaerobic catabolic reaction with H<sub>2</sub> and sulfur is endergonic with  $-\Delta G_r^\circ \sim 48$  kJ/mol-S $^\circ$  at 76°C, [83], but aerobic sulfur oxidation is far more energetic ( $-\Delta G_r^\circ \sim 520$  kJ/mol-S $^\circ$  at 76°C, [83]). The lower overall  $-\Delta G$ — consumed during growth in microaerobic conditions compared to anaerobic conditions suggests *A. ambivalens* conserves a higher amount energy during sulfur oxidation with O<sub>2</sub> than metabolizing H<sub>2</sub> and sulfur for ATP synthesis [156].



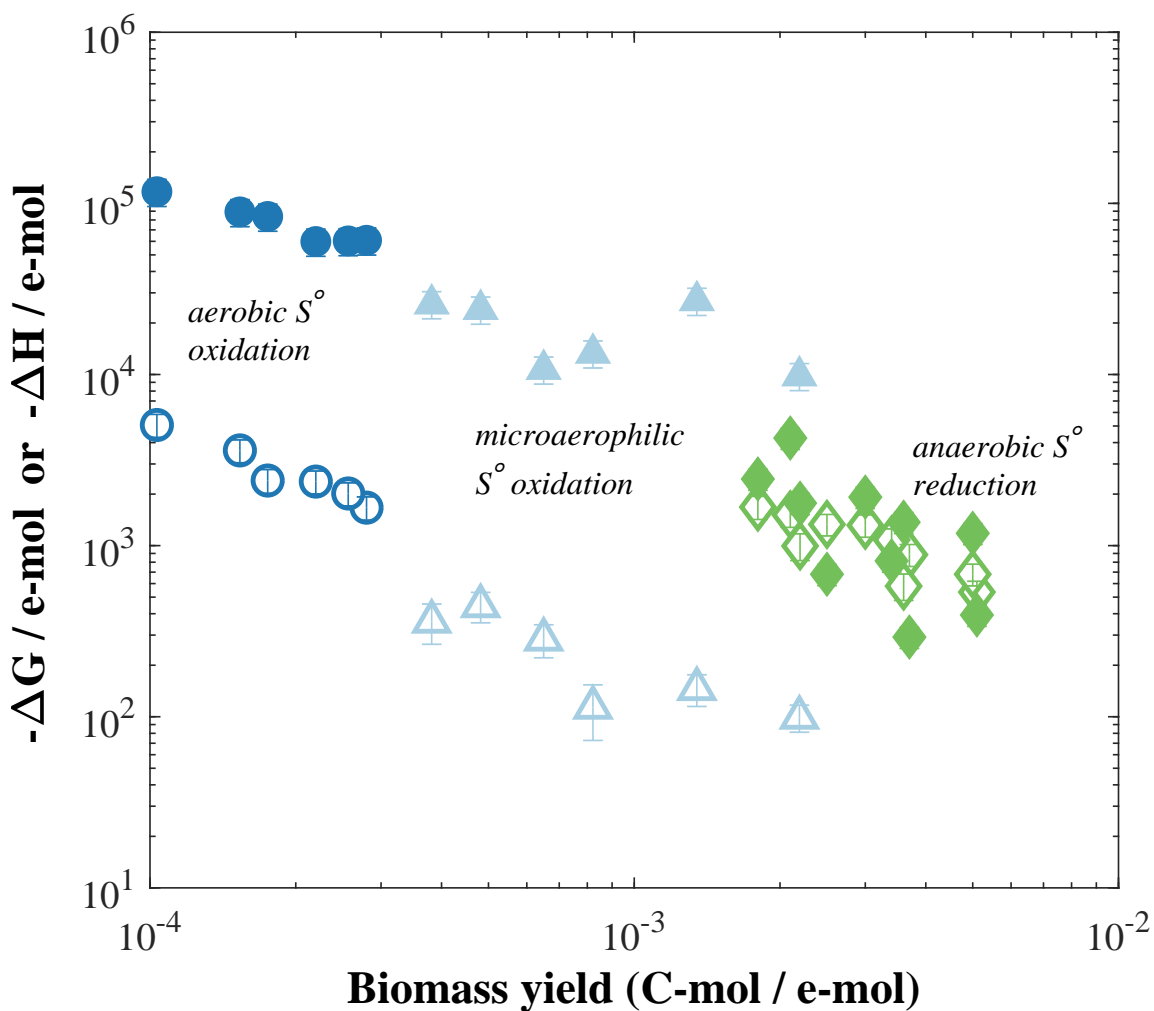


Figure 3.3: Energetics of aerobic, microaerobic, and anaerobic growth normalized to moles of electrons transferred ( $\text{kJ C-mol}^{-1} \text{ e-mol}^{-1}$ ). Aerobic growth with sulfur and  $\text{O}_2$  is represented by blue circles, microaerobic growth is represented by light blue triangles, and anaerobic growth with  $\text{H}_2$  and sulfur is denoted with green diamonds. All filled symbols indicate measured  $-\Delta H$  of growth and open symbols are  $-\Delta G$  consumed during growth. Aerobic and microaerobic data retrieved from [67] (Chapter 2).

### 3.4.2 Power Consumption and Energy Budgets

Microorganisms must consume energy over the duration of growth to drive processes such as cellular maintenance reactions, motility, and biosynthetic reactions [132, 86]. Using the amount of Gibbs energy consumed and the total growth time for each replicate, the power consumption was calculated in watts for all three redox conditions. Comparing the amount of biomass produced as a function of power consumption also considers rate of growth between redox treatments that may play a role in overall growth efficiency and energetics [57].

Figure 3.4 shows growth efficiency in terms of biomass produced versus power consumed [147]. Contour lines have been added to depict similar values of efficiency, calculated as  $\log \text{fmol-C/W}$ . Microaerobic growth was slightly more efficient than anaerobic growth and had an average value of  $2.01 \times 10^{14} \text{ fmol-C/W}$ . Although more overall biomass was produced under anaerobic conditions, the average efficiency was  $1.38 \times 10^{14} \text{ fmol-C/W}$  and was statistically similar to microaerobic results ( $P = 0.13$ , two-sample t-test). Aerobic growth was significantly less efficient and had an average efficiency of  $2.13 \times 10^{13} \text{ fmol-C/W}$  ( $P \ll 0.05$ , two-sample t-test), about 10-fold lower than microaerobic and anaerobic growth results. Though the aerobic growth conditions produced more overall biomass than microaerobic growth on average, the stress of high-oxygen concentrations required substantially more power during growth.

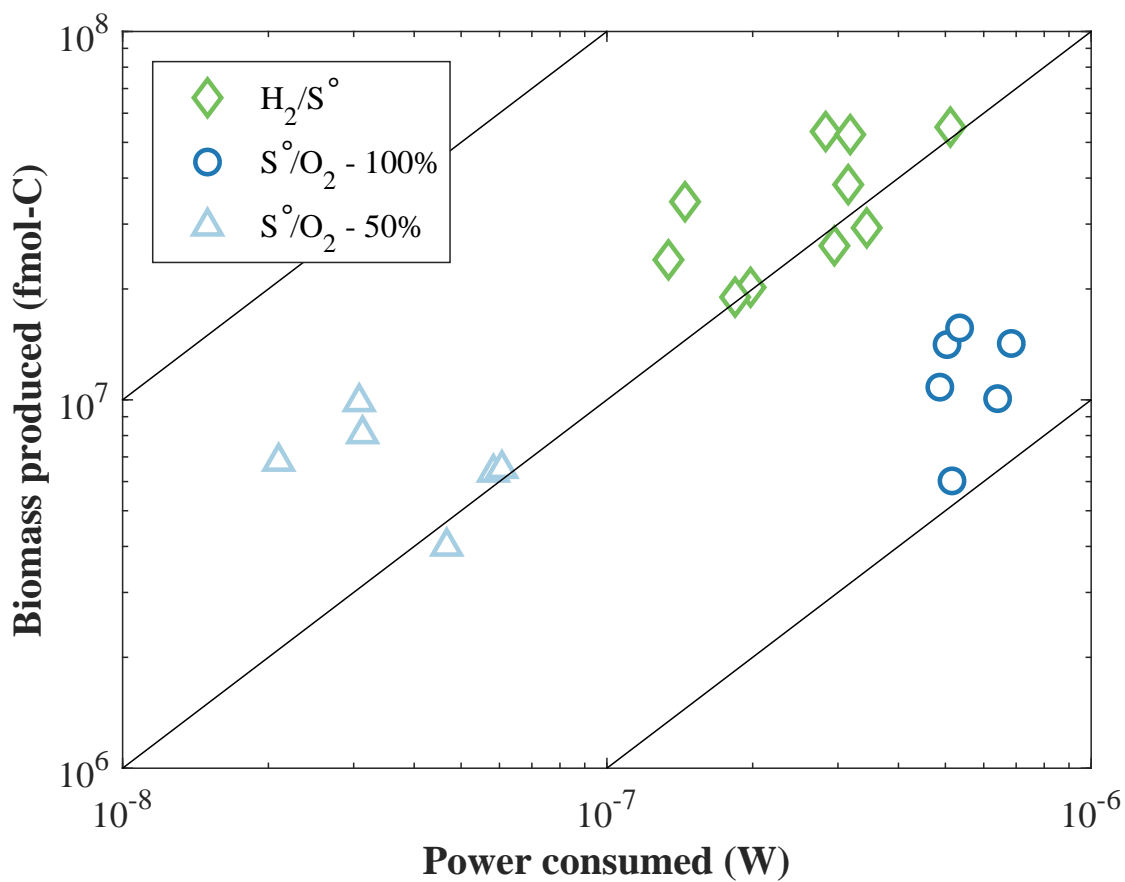


Figure 3.4: Amount of biomass produced (fmol-C) and power consumed (W) during microbial growth for *Acidianus ambivalens* grown under anaerobic, aerobic, and microaerophilic conditions. Contour lines indicate lines of similar growth efficiency, calculated as log fmol-C/watts. Green triangles represent growth on  $H_2/S$ , dark blue circles represent aerobic growth on  $S/O_2$  (100%  $O_2$  saturation), and light blue triangles represent microaerobic growth on  $S/O_2$  (100%  $O_2$  saturation). Aerobic and microaerobic data was retrieved from [67] (Chapter 2).

### 3.4.3 Energetic Costs for *A. ambivalens*

The geochemistry of an environment plays an important role in microbial activity and energetics. The effects of temperature and energy source availability have been previously explored, but laboratory studies isolating the energetic response to oxidation state are lacking. McCollom and Amend [108] conducted a thorough computational analysis of the theoretical cost of biomass production in oxic (microaerobic) and anoxic environments for chemolithoautotrophs. Their analysis was based on the cellular composition of *Escherichia coli* biomass and the respective  $\Delta G_f^\circ$  for the different biomolecules at standard temperature and pressure (25°C and 1 atm). They reported a substantial difference in energy requirements between the two environments, with aerobic chemolithotrophs requiring 18.4 kJ/g biomass and anaerobes requiring much less at 1.4 kJ/g biomass. The approximate 10-fold difference in anabolic costs is a substantial energetic difference, though anabolism may only make up a small portion of the overall energetic budget for growth ( $\sim 5\text{-}10\%$ , [108]).

The difference in anabolic energetics did not cause a significant difference in overall energetic demands in microaerobic and anaerobic growth of *A. ambivalens*; the average energy budget for anaerobic growth was  $\sim 2110$  kJ/C-mol (Table 3.1) and  $\sim 1440$  kJ/C-mol for microaerobic growth (Table 3.2,  $P = 0.15$ , two-sample t-test). However, the anabolic energy differences may explain the larger amount of biomass produced under anaerobic growth conditions (refer to Figure 3.4). There was about a 10-fold increase in energy budget for fully aerobic sulfur oxidation growth ( $\sim 17100$  kJ/C-mol) compared to microaerobic or anaerobic growth conditions. The large energetic demand in fully aerobic conditions has been attributed to higher maintenance energy demands [101, 107], though differences in anabolic costs could likely play a small role in the observed energetic differences as well [108].

Overall, changes in oxidation state between microaerobic and anaerobic conditions did not significantly impact *A. ambivalens* growth in terms of growth efficiency (biomass produced per W power) or in the energy budget for growth (kJ per C-mol biomass).  $-\Delta G$  consumed during growth (kJ C-mol<sup>-1</sup> e-mol<sup>-1</sup>) was lower in microaerobic conditions than anaerobic

conditions, suggesting a slight preference for growth using  $O_2$  as the terminal electron acceptor. The high energetic potential of the reaction with sulfur and oxygen may result in higher energy conservation as ATP [156]. In natural environments, hot springs supporting *A. ambivalens* growth typically have low oxygen concentrations due to the decrease in solubility at high temperatures, allowing redox gradients to develop in micro-environments ( $\mu\text{m}$ - $\text{mm}$ 's, [129, 106, 23]). In these situations, *A. ambivalens* will likely grow preferentially on sulfur and  $O_2$  under microaerobic conditions compared to fully aerobic or anaerobic conditions with  $H_2$  and sulfur due to the lower overall  $-\Delta G$  requirements for growth. However, the similarities in growth efficiency and energy budgets under microaerobic and anaerobic conditions may allow *A. ambivalens* to be competitive with either catabolic reaction.

### **3.5 Conclusion**

Gibbs energies and enthalpies of growth were determined for *A. ambivalens* under anaerobic conditions with  $H_2$  oxidation with elemental sulfur serving the energy yielding reaction. Energetics of growth were compared to sulfur-oxidizing growth under aerobic and microaerobic growth to determine the effects of oxidation state on overall energetic requirements. Despite the higher anabolic costs of creating biomass under aerobic conditions, growth under anaerobic and microaerobic conditions had very similar energy budgets and growth efficiencies, though fully aerobic growth was highly inefficient evidently due to oxidative stress. Overall Gibbs energy consumed during growth was lowest in microaerobic conditions, suggesting a slight preference for sulfur and  $O_2$  as energy sources in low- $O_2$  environments. However, the similarities in growth efficiency and energy budgets under microaerobic and anaerobic conditions may allow *A. ambivalens* to be competitive in natural environments with either catabolic reaction.

## Chapter 4

**ENERGETICS OF *ACIDITHIOBACILLUS* SPP. DURING  
SULFUR AND IRON(II) OXIDATION**

*This manuscript will be submitted to the journal Geochimica et Cosmochimica Acta.*

Co-authored by Chloe E. Hart, Drew Gorman-Lewis

**4.1 Introduction**

*Acidithiobacillus* spp. are chemolithoautotrophic gammaproteobacteria that dominate in both anthropogenic and naturally occurring acidic environments (pH < 3, [47, 134, 152]). They can metabolize iron and reduced inorganic sulfur compounds (RISCs), including iron sulfide minerals such as pyrite (FeS<sub>2</sub>), chalcopyrite (CuFeS<sub>2</sub>), and sphalerite ([Zn, Fe]S), making these species key players in iron and sulfur biogeochemical cycles in acidic waters. As these acidophiles grow and metabolize, they change the environment around them; the oxidation of RISCs and sulfide-rich rocks ultimately leads to the production of sulfuric acid and acid rock/mine drainage (AMD/ARD). Acid production and dissolution of sulfide-bearing rocks release metals (e.g. Zn, Cu, As) found in these ores and abandoned mining regions, producing metal-rich acid waters and contaminated drinking water (e.g. [53, 42]). Consequently, understanding the metabolism of *Acidithiobacillus* spp. from a thermodynamic perspective is essential for determining the impact on the surrounding environment by microbial activity.

*A. ferrooxidans* (formerly *Thiobacillus ferrooxidans*, [85]), one of the most abundant species found in AMD [82, 54, 134], is known for its ability to adapt to different environmental conditions, mainly different growth substrates and heavy metal concentrations. *A. ferrooxidans* can metabolize Fe<sup>2+</sup>, elemental sulfur, and Fe<sup>2+</sup> contained in iron sulfide minerals such as pyrite [153]. *A. ferrooxidans* has been shown to regulate different sets of proteins

based on the substrate on which it is growing [126]. *A. ferrooxidans* upregulates a different set of proteins during growth on sulfur and iron, while both sets are upregulated when grown on pyrite. At some AMD sites, both  $\text{Fe}^{2+}$  and elemental sulfur are available as substrates for *A. ferrooxidans* to metabolize. *A. thiooxidans* (formerly *Thiobacillus thiooxidans*, [85]) is also a prominent species in AMD regions. *A. thiooxidans* displays metabolic flexibility as well and is able to oxidize different RISCs, primarily thiosulfate and elemental sulfur, leading to sulfuric acid production. *A. thiooxidans* is unable to oxidize  $\text{Fe}^{2+}$ , but can couple sulfur oxidation to dissimilatory iron reduction [98]. Both *A. ferrooxidans* and *A. thiooxidans* have a high tolerance to heavy metals (e.g. [159, 40]) and the ability to recover valuable metals (e.g. copper, chromium) from solution, leading to the extensive use of these species in industrial bioleaching operations [168, 160, 167].

The environmental impacts due to metabolism, the significant influences on iron and sulfur cycling, and their extensive use in industrial bioleaching have prompted a wealth of research on *A. ferrooxidans* and *A. thiooxidans*, but we lack a complete quantification of their bioenergetics during growth. In this work, we describe microbial activity in thermodynamic terms for *A. ferrooxidans* and *A. thiooxidans*. We quantified biomass yields, Gibbs energy consumption, and enthalpies of growth for *A. ferrooxidans* during sulfur and iron oxidation and for *A. thiooxidans* during sulfur oxidation. Sulfur oxidation experiments were conducted under two different growth conditions to understand nutrient-limiting effects on biomass yields and how energetics change as a result. These results were used to infer preferential substrates for *A. ferrooxidans* growth. Ultimately, the sulfur energetics reported here will help predict energetics, such as heat production, for other sulfur-oxidizers based on growth yields, a useful tool for bioleaching operational designs [31].

## 4.2 Methods

### 4.2.1 Culture maintenance

All *Acidithiobacillus* cultures were purchased from ATCC and maintenance media followed ATCC recommendations as described below.

*A. ferrooxidans* (ATCC 23270) was maintained on different substrates prior to experimentation. Cultures performing sulfur oxidation were grown in ATCC Medium 2039 containing the following (g/L):  $(\text{NH}_4)_2\text{SO}_4$  (0.8),  $\text{MgSO}_4 \cdot 7 \text{H}_2\text{O}$  (2.0),  $\text{K}_2\text{HPO}_4$  (0.4), and 0.5% (v/v) Wolfe's mineral solution. This medium was adjusted to pH 2.3 with  $\text{H}_2\text{SO}_4$  and autoclaved. Sulfur was sterilized through three successive autoclave steam cycles at 100°C for 30 minutes (ATCC Medium 125 protocol). Sulfur powder was aseptically added to cultures to a concentration of 2 g/L. Cultures were transferred every week with a 5% inoculum.

Iron oxidation cultures of *A. ferrooxidans* were maintained in the same ATCC medium 2039 with the addition of a filter sterilized iron solution ( $\text{FeSO}_4 \cdot 7 \text{H}_2\text{O}$ , 20.0 g/L). Cultures were transferred every week with a 5% inoculum.

*A. thiooxidans* (ATCC 19377) was maintained in ATCC Medium 125 that contained the following (g/L):  $(\text{NH}_4)_2\text{SO}_4$  (0.2),  $\text{MgSO}_4 \cdot 7 \text{H}_2\text{O}$  (0.5),  $\text{CaCl}_2 \cdot 2 \text{H}_2\text{O}$  (0.33),  $\text{K}_2\text{HPO}_4$  (3.0),  $\text{FeSO}_4 \cdot 7 \text{H}_2\text{O}$  (9.0 mg/L), and 0.5% (v/v) Wolfe's mineral solution. The medium was adjusted to pH 2.1 with  $\text{H}_2\text{SO}_4$  and autoclaved. Sulfur powder was aseptically added to cultures for a final concentration of 2 g/L. Cultures were transferred every four weeks with a 5% inoculum.

All maintenance cultures were aseptically prepared in 500 ml Erlenmeyer flasks containing 100 ml medium and grown at 30°C without agitation.

### 4.2.2 Calorimetric experiments

All experimental cultures were inoculated from maintenance cultures grown on the same substrate. With the medium described above, iron-oxidizing cultures with *A. ferrooxidans* were prepared with 1 mL medium in 4 mL Hastelloy calorimeter vials. The calorimeter vials



were attached to open titration shafts covered with foil to allow a small degree of atmosphere exchange but prevent debris from entering.

Both *A. ferrooxidans* and *A. thiooxidans* sulfur-oxidizing cultures were grown in the same "open system" manner, with 1 mL of their respective medium and 2 g/L sulfur in 4 mL Hastelloy vials attached to open titration shafts. Additionally, *A. ferrooxidans* and *A. thiooxidans* were grown in "closed system" experiments to measure energetics over different growth yields. Closed system experiments were prepared with 2 mL medium, 2 g/L sulfur, and prepared in 3.2 mL glass vials sealed with butyl rubber stoppers and aluminum seals. Closed system experiments did not allow atmospheric exchange in order to limit growth.

Enthalpies of growth were measured with a TA Instruments TAM III Nanocalorimeter that measures heat flow between a reaction vial containing the growth experiment and a reference vial [80, 165]. The calorimeter heat flow response was calibrated by an electrical heating procedure verified by measuring the heat of protonation of trishydroxymethylaminomethane [61].

Experimental and reference vials were filled with identical media and atmospheric constituents. The experimental vial contained an aliquot from the appropriate maintenance culture to provide an initial cell density of  $10^6$  cells/ml and the reference vial was kept sterile and void of cells. The heat flow of the samples was monitored over time. After the signal returned to baseline, the signal was integrated after baseline correction to determine the total heat produced during growth. The total heat produced was normalized to the change in total cell material produced to calculate enthalpy (kJ/C-mol).

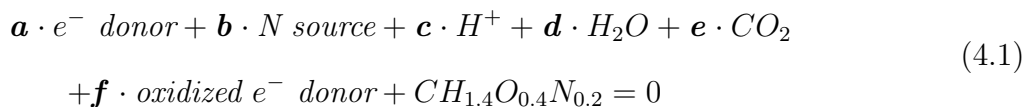
#### 4.2.3 Chemical measurements

At the beginning and end of growth, chemical data was collected to measure the change in components of the growth medium. Sulfate concentrations were determined through Hach TNTplus spectrophotometric sulfate test vials, pH was measured with a combination microelectrode (Microelectrodes, Inc.) calibrated daily with four NIST standards, dissolved oxygen was measured with a Unisense Clark-type D.O. microsensor, and Fe(II) and Fe(III)

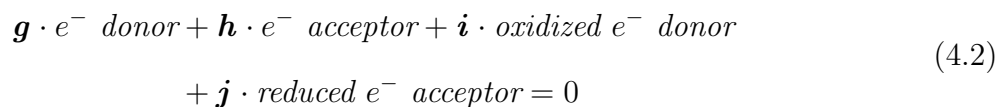
concentrations were measured using the ferrozine analysis [161]. Slides for cell counts were prepared using a polycarbonate 0.2  $\mu\text{m}$  filter membrane with SYBR Green I dye following the procedure of Lunau et al. [100] and examine with appropriate filters on a Zeiss Axiostar Plus microscope. The total grams of protein per cell was determined according to Lowry *et al.* [99] by colorimetric assay. Cell counts were converted to grams of biomass by doubling the determined grams of protein per cell, assuming total protein comprises 50% of cell mass, and multiplying it by the total cell count [144].

#### 4.2.4 Overall growth modeling

Overall metabolism was modeled as macrochemical equations following equations reported by Heijnen and Kleerebezem [68]. The basis of the equations is the biosynthesis of one carbon-mole (C-mol) of biomass, represented by the formula  $\text{CH}_{1.4}\text{O}_{0.4}\text{N}_{0.2}$  reported for *A. ferrooxidans* [88]. The formula for biomass includes only the four major elements of cellular material and has a molar mass of 22.6 g/C-mol. As autotrophic organisms, *A. ferrooxidans* and *A. thiooxidans* synthesize biomass through the anabolic reaction, represented by Equation 4.1.



Biosynthesis is an endergonic reaction ( $\Delta G > 0$ ) or slightly exergonic ( $\Delta G \leq 0$ ) [150]. Therefore, the reaction requires energy to proceed. Catabolism generates the Gibbs energy through redox reactions and drives anabolism. A generic catabolic reaction is shown in Equation 4.2.



Metabolic coefficients  $\mathbf{a}$  through  $\mathbf{j}$  were determined by solving a series of linear equations to satisfy mass, charge, and degree of reduction balances. Reactants consumed during growth

result in negative coefficients while products result in positive coefficients.

The energy gained through catabolism is also used for reactions such as protein turnover and cellular maintenance reactions [133], thus the anabolism and catabolism do not occur in a 1:1 ratio. The catabolic multiplicative factor ( $f_{cat}$ ) represents the number of times the catabolic reaction is performed to produce 1 C-mol biomass.  $f_{cat}$  is calculated with Equation 4.3 using the biomass yield ( $Y_{X/D}$ , defined as C-mol of biomass produced per mole electron donor consumed) and the anabolic coefficient of the electron donor ( $Y_D^{an}$ , or coefficient  $a$  in Equation 4.1). The total biomass produced in C-mol was calculated by converting grams of biomass to C-mol using the molar mass of the biomass formula (22.6 g/C-mol).

$$f_{cat} = \frac{-1}{Y_{X/D}} + Y_D^{an} \quad (4.3)$$

The overall growth coefficients are determined by combining  $f_{cat}$  (Equation 4.3), catabolic coefficients (Equation 4.2), and the anabolic coefficients (Equation 4.1), as shown in Equation 4.4.

$$\text{Overall growth reaction} = \text{Anabolism} + f_{cat} \cdot \text{Catabolism} \quad (4.4)$$

Individual  $f_{cat}$  values and overall growth reactions were calculated for each experimental replicate based on the resulting biomass yield. Overall growth reactions for each experimental were used for further thermodynamic calculations.

#### 4.2.5 Gibbs energy consumption

Gibbs energy consumed ( $\Delta G$ ) during growth was calculated for each experiment as the change of the amount of Gibbs energy available before and after growth, based on the the respective growth reaction derived. Calculating available Gibbs energy requires the use of activities of all the chemical species in the overall growth reaction. While the chemical species involved in all the growth reactions remain constant across all experiments, the stoichiometric coefficients vary as they are dependent on the biomass yield produced in each experiment

replicate. Thus, available Gibbs energy must be calculated for each experiment as it relies on both the species involved and the stoichiometric coefficients.

The standard state Gibbs energies of formation ( $\Delta G_f^\circ$ ) for the chemical species in the growth reaction were calculated at the experiment temperature with the revised Helgeson-Kirkham-Flowers (HKF) equations of state [72, 71] using SUPCRT92 [139, 83, 138, 141]. Standard states include unit activity of pure solid, unit activity of aqueous species in a hypothetical 1 molal solution to infinite dilution, and unit fugacity of a pure gas at 1 bar at any temperature and pressure. For biomass,  $\Delta G_f^\circ = -67$  kJ/mol was used for all growth experiments [69]. Standard state Gibbs energies of reactions ( $\Delta G_r^\circ$ ) of the overall growth reaction determined for each experiment were calculated using Equation 4.5, based on the Gibbs energy of formation of the products ( $\Delta G_{f,products}^\circ$ ) and of the reactants ( $\Delta G_{f,reactants}^\circ$ ) of the overall growth reaction.

$$\Delta G_r^\circ = \sum \Delta G_{f,products}^\circ - \sum \Delta G_{f,reactants}^\circ \quad (4.5)$$

Available Gibbs energy in the medium ( $\Delta G_r$ ) was calculated for the given growth reaction as demonstrated in Equation 4.6, using standard state Gibbs energies of reactions ( $\Delta G_r^\circ$ ) determined for each experiment from Equation 4.5, the universal gas constant ( $R$ ), absolute temperature ( $T$ ), and the reaction quotient ( $Q_r$ ).

$$\Delta G_r = \Delta G_r^\circ + RT \times \ln(Q_r) \quad (4.6)$$

The reaction quotient,  $Q_r$ , was calculated with the activities of the products and reactants involved in the overall growth equation and is shown in Equation 4.7, where  $a_i^{Y^{ogr}}$  denotes thermodynamic activity of the  $i^{th}$  chemical species and  $Y^{ogr}$  represents the stoichiometric reaction coefficient of the  $i^{th}$  species in the overall growth reaction (Equation 4.4).

$$Q_r = \prod a_i^{Y^{ogr}} \quad (4.7)$$

Activities of the aqueous species were calculated using PHREEQC [119] and solid sulfur

was assumed to have an activity of 1. Biomass in solution, assuming an activity coefficient of 1, was converted from molality (C-mol/kg solvent) to activity. Gibbs energy consumed for growth was calculated as the difference between initial ( $G_{r,initial}$ ) and final ( $G_{r,final}$ ) available Gibbs energy (Equation 4.8).

$$\Delta G = \Delta G_{r,initial} - \Delta G_{r,final} \quad (4.8)$$

### 4.3 Results

#### 4.3.1 *A. ferrooxidans* – Fe(II) oxidation

Calorimetry captured clear heat signals for all replicates during growth. The heat flow curve paralleled the growth phase of the culture with lag, exponential, and stationary phase corresponding to the initial baseline, exponential increase and peak heat flow signal, and return to baseline, respectively, as shown in Figure 4.1 with *A. ferrooxidans* growth on Fe<sup>2+</sup>. Exponential growth began after approximately 29 hours of growth. Peak heat signal was 22  $\mu$ W at about 62 hours. After 54 hours of exponential growth, the heat signal returned to baseline after a total of 83 hours for growth.

Protein colorimetric assays resulted in a calculated cell mass of  $2.19 \times 10^{-13}$  g/cell. This value, along with a biomass molar mass of 22.6 g/C-mol, was used to convert all cell counts to C-mol biomass. Growth data collected from each *A. ferrooxidans* replicate are summarized in Table 4.1. Cultures typically oxidized 70  $\mu$ moles of Fe<sup>2+</sup>, with visible iron precipitation in culture vials after growth. An average biomass of 0.34  $\mu$ mol-C was produced, resulting in a biomass yield of 0.0048 C-mol/Fe-mol.

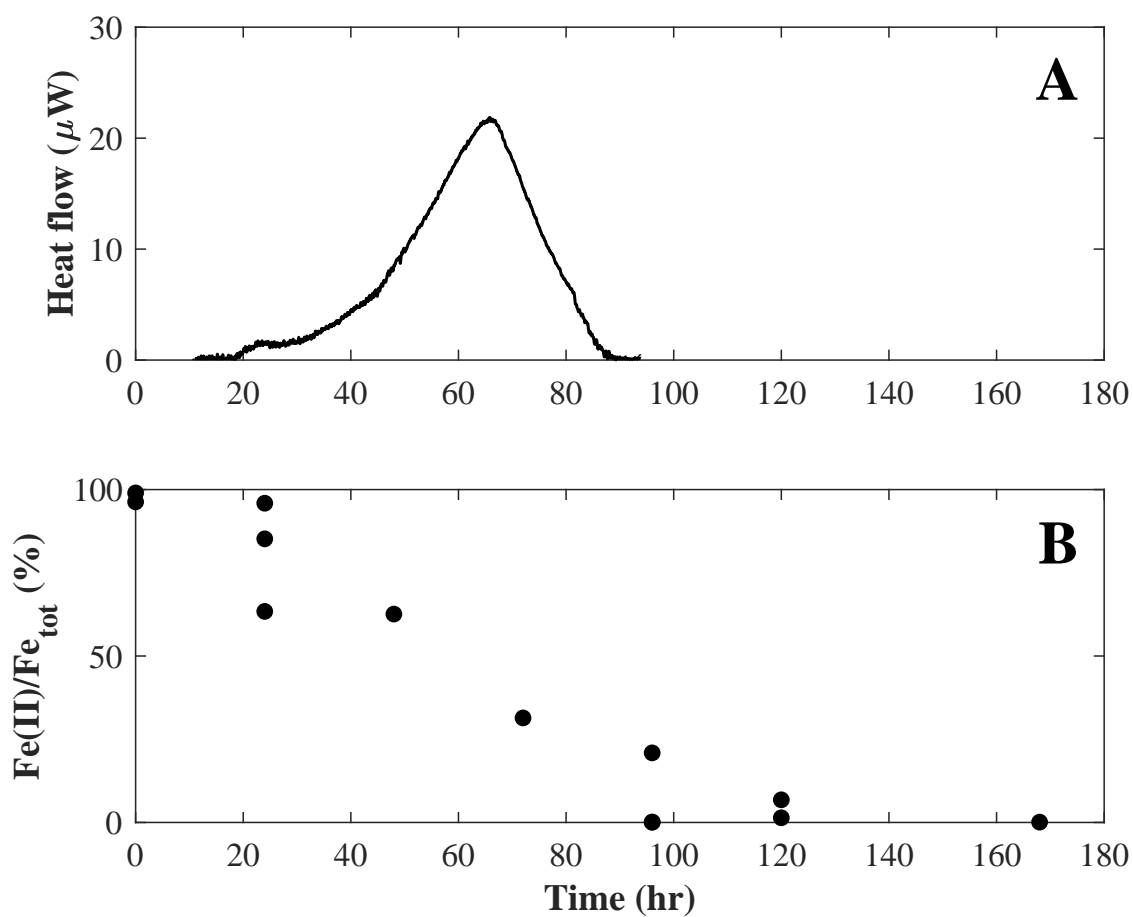


Figure 4.1: A) Example of a heat flow curve for *Acidithiobacillus ferrooxidans* during iron oxidation. B) Growth curve of *A. ferrooxidans* during iron oxidation, shown as percent  $\text{Fe}^{2+}$  of total iron ( $\text{Fe}^{2+}$  and  $\text{Fe}^{3+}$ ) over time. The heat flow and growth curves show cultures reach stationary phase around 100 hours.

Enthalpies of growth, or total heat produced per C-mol biomass produced, were determined for each replicate by integrating calorimetric heat flow curves. Due to iron precipitation, heat production due to microbial growth had to be corrected. PHREEQC chemical output showed goethite ( $\alpha$ -FeOOH) was supersaturated in solution, suggesting this was the iron mineral precipitating in the culture vials. Goethite precipitation is described by Equation 4.9.

Table 4.1: *Acidithiobacillus ferrooxidans* growth on Fe(II) / O<sub>2</sub>

	Biomass (C-mol)	Fe(II) ( $\mu$ mol)	Yield C-mol/Fe	$-\Delta H_{corr}$ (kJ/C-mol)	$-\Delta G$ (kJ/C-mol)
	$3.99 \times 10^{-7}$	52.9	0.0058	7341	$5494 \pm 1114$
	$4.06 \times 10^{-7}$	51.1	0.0059	9004	5408
	$3.32 \times 10^{-7}$	55.0	0.0043	13316	11040
	$3.72 \times 10^{-7}$	55.0	0.0048	10395	9864
	$2.95 \times 10^{-7}$	55.1	0.0047	13009	5353
	$3.37 \times 10^{-7}$	56.6	0.0054	6466	4767
<i>Avg</i>	$3.41 \times 10^{-7}$	70.7	0.0052	9921	6988



Goethite precipitation is an endothermic reaction ( $\Delta H_r^\circ = 58.8$  kJ/mol, [83]) and thus can dampen the heat signal produced by *A. ferrooxidans* growth. To correct for this, moles of total iron (Fe<sup>2+</sup> and Fe<sup>3+</sup>) after growth were compared to total iron at the beginning of the experiment. The number of moles missing from solution was assumed to be representative of the precipitated goethite in the vials. Moles of goethite were converted to enthalpies using the previously mentioned  $\Delta H_r^\circ$  and added to the total growth heat prior to calculating growth enthalpies. This is discussed in more detail below.

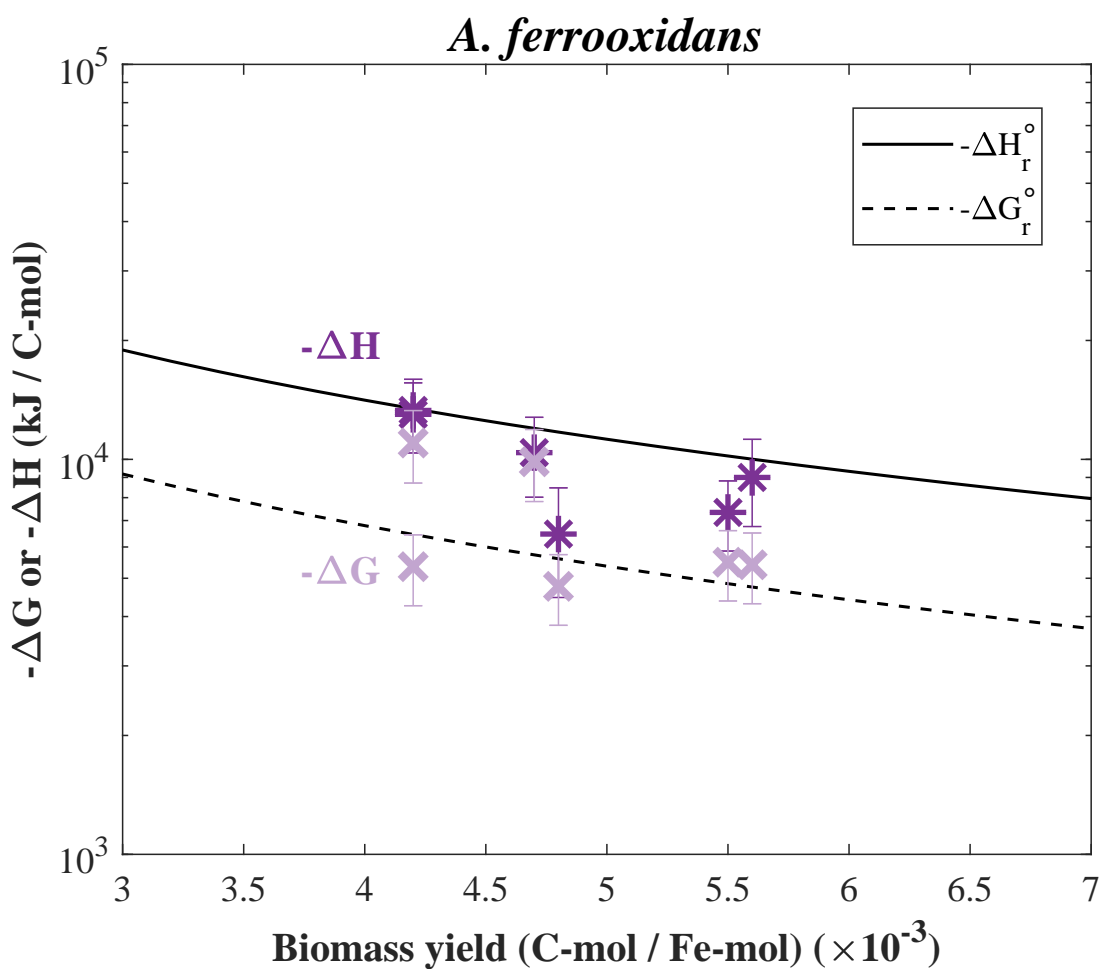


Figure 4.2: Energetics of *Acidithiobacillus ferrooxidans* during iron(II) oxidation compared to standard state  $\Delta G_r^\circ$  and  $\Delta H_r^\circ$  (all reported in kJ/C-mol) for given biomass yields (C-mol/Fe<sup>2+</sup>-mol). Standard states for the overall growth reaction were calculated for 1 molal of pure reactants and products at 30°C. The standard state curves act as theoretical results for how microbial growth will behave at different biomass yields. Asterisks (\*) represent measured  $\Delta H$  and crosses (×) represent calculated  $\Delta G$  for each replicate.



The  $\Delta G$  and  $\Delta H$  values determined for each *A. ferrooxidans* replicate were similar to the hypothetical standard state values, shown in Figure 4.2. The average corrected value for  $-\Delta H$  was 9920 kJ/C-mol and the  $-\Delta G$  consumed was slightly lower at 6990 kJ/C-mol (Table 4.1). As standard state calculations predict, Gibbs energy of the overall growth reaction was primarily dissipated as enthalpy for growth on  $\text{Fe}^{2+}$  depicted as more negative  $\Delta H$  values than  $\Delta G$ .

#### 4.3.2 *A. ferrooxidans* – $S^{\circ}$ oxidation

*A. ferrooxidans* produced distinct heat curve signals during growth on sulfur in all replicates (Appendix Figure A.5) and were different from growth on  $\text{Fe}^{2+}$ . In the open system setup, exponential growth began after approximately 32 hours of growth. Peak heat signal was 23  $\mu\text{W}$  and occurred about 68 hours into the experiments. After 86 hours of exponential growth, the heat signal returned to baseline, with total growth lasting for about 118 hours. In the closed system experiments, growth did not last as long and produced a smaller signal. Exponential growth began after approximately 7 hours of growth. The peak heat signal reached 9  $\mu\text{W}$  after about 15 hours. After 41 hours of exponential growth, the heat signal returned to baseline after a total growth time of 48 hours.

Growth data collected from all open and closed system replicates are summarized in Table 4.2. Open system experiments yielded more biomass than closed experiments, with an average of 2.2  $\mu\text{mol-C}$ . The average number of sulfur moles oxidized was 18.5  $\mu\text{moles}$ , resulting in a biomass yield of 0.1227 C-mol/S-mol. In the closed system experiments, the average amount of biomass was 0.17  $\mu\text{mol-C}$ . The amount of sulfur oxidized was 7.3  $\mu\text{moles}$ , resulting in a lower biomass yield than open experiments, with an average of 0.0270 C-mol/S-mol.

Enthalpies of growth and  $\Delta G$  consumed per C-mol biomass produced were determined for each replicate (Table 4.2). The average  $-\Delta G$  consumed for the open experiments was 125 kJ/C-mol and 760 kJ/C-mol for closed experiments. The average  $-\Delta H$  values were substantially higher at 1450 kJ/C-mol and 5080 kJ/C-mol for open and closed system experiments,

respectively. When  $-\Delta G$  and  $-\Delta H$  were plotted with standard state values as a function of biomass yield, both  $-\Delta G$  and  $-\Delta H$  were much lower than  $-\Delta G_r^\circ$  and  $-\Delta H_r^\circ$ . Standard state conditions did

Table 4.2: *Acidithiobacillus ferrooxidans* growth on S / O<sub>2</sub>

	Biomass (C-mol)	S <sup>o</sup> used ( $\mu$ mol)	C-mol/S	- $\Delta H$		- $\Delta G$	
				(kJ/C-mol)	(kJ/e-mol)	(kJ/C-mol)	(kJ/e-mol)
<i>Open system</i>							
	$1.88 \times 10^{-6}$	14.9	0.1260	1842	307	95	16
	$3.28 \times 10^{-6}$	17.7	0.1855	1070	178	81	13
	$1.64 \times 10^{-6}$	15.9	0.1027	1830	305	113	19
	$1.69 \times 10^{-6}$	13.1	0.1290	1595	266	77	13
	$2.56 \times 10^{-6}$	20.0	0.1280	1145	191	135	23
	$1.91 \times 10^{-6}$	29.3	0.0651	1219	20.	251	42
<i>Avg</i>	$2.16 \times 10^{-6}$	18.5	0.1227	1450	242	125	21
<i>Closed system</i>							
	$3.26 \times 10^{-7}$	6.4	0.0509	2054	342	204	34
	$1.76 \times 10^{-7}$	4.6	0.0353	3150	525	224	37
	$8.92 \times 10^{-8}$	8.6	0.0104	6347	1058	1345	224
	$7.95 \times 10^{-8}$	9.6	0.0083	8775	1463	1269	211
<i>Avg</i>	$1.68 \times 10^{-7}$	7.3	0.0270	5082	847	760	127

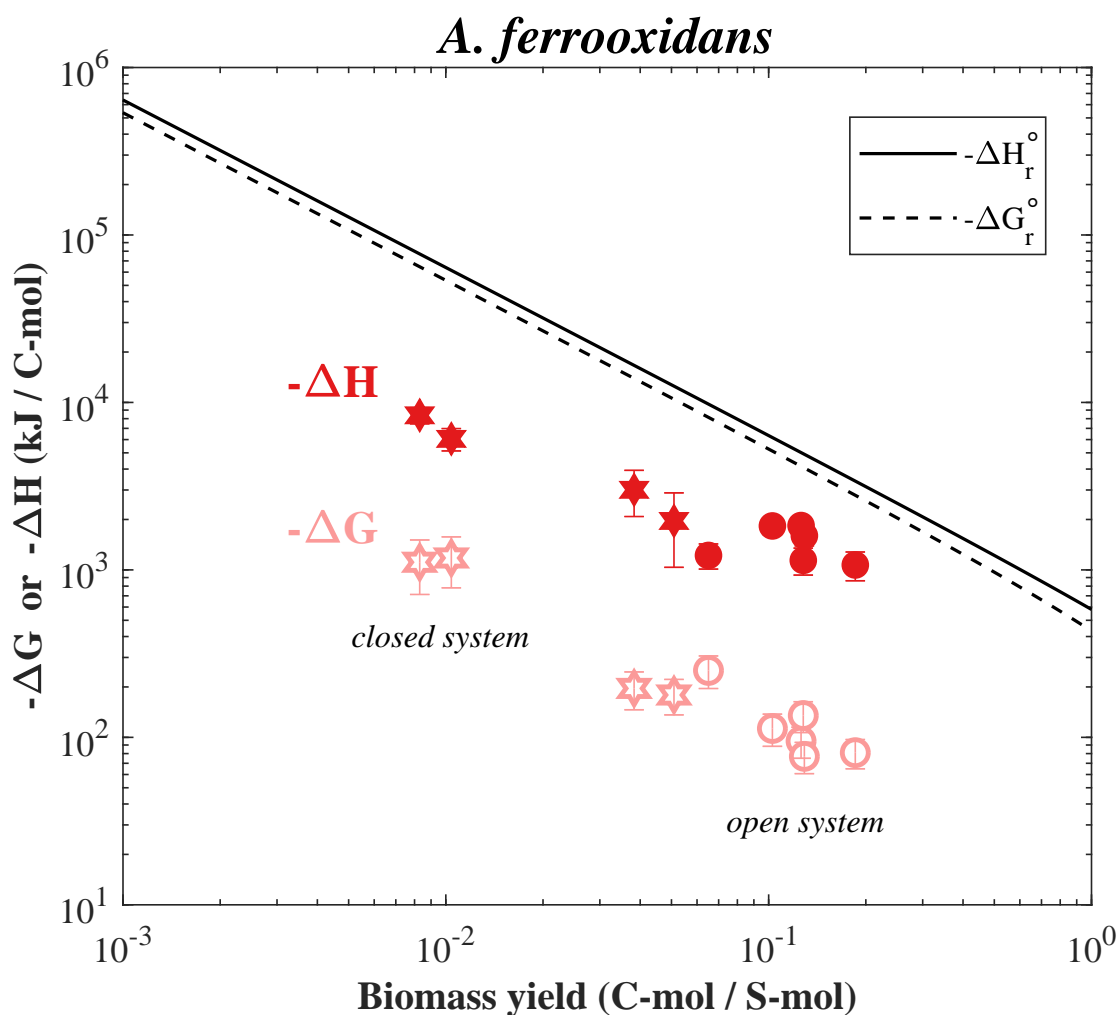


Figure 4.3: Energetics of *Acidithiobacillus ferrooxidans* oxidizing sulfur and standard state  $\Delta G_r^\circ$  and  $\Delta H_r^\circ$  (kJ/C-mol) for given biomass yields (C-mol/S $^\circ$ -mol). Standard states for the overall growth reaction were calculated for 1 molal of pure reactants and products at 30°C. Standard state curves act as theoretical results for microbial growth energetics as they relate to biomass yield. Filled symbols represent  $\Delta H$  measured by calorimetry and open symbols represent calculated  $\Delta G$  for each replicate. Closed and open system experiments are designated by stars (★) and circles (●), respectively.

not accurately represent *A. ferrooxidans* growth during sulfur oxidation for a given biomass yield, but did accurately predict the highly exothermic nature of growth ( $\Delta H$  more negative than  $\Delta G$ ). Both  $-\Delta G$  and  $-\Delta H$  increased as biomass yield decreases, which followed the same trend as the standard state values.

#### 4.3.3 *A. thiooxidans* – $S^{\circ}$ oxidation

*A. thiooxidans* produced very distinct heat curve signals during growth on sulfur in all replicates and produced the largest heat signals across all the tested growth conditions (Figure A.6). In the open system experiments, exponential growth began after approximately 9 hours. The peak heat signal reached  $91 \mu\text{W}$  around 64 hours of growth. After 225 hours of exponential growth, the heat signal returned to baseline, totaling 234 hours of growth. In the closed system experiments, exponential growth began after approximately 2 hours of growth. The peak heat signal was lower, approximately  $8 \mu\text{W}$ , at 12 hours into the experiment. Exponential growth lasted for 43 hours before the heat signal returned to baseline, totaling 45 hours of growth.

Table 4.3 contains a summary of growth data collected from each *A. thiooxidans* replicate. In the open system experiments, the average amount of biomass produced was  $1.5 \mu\text{mol-C}$ , with an average moles of sulfur oxidized of  $179 \mu\text{moles}$ . This resulted in an average biomass yield of  $0.0092 \text{ C-mol/S-mol}$ . Closed experiments did not grow as well, with an average amount of biomass production of  $0.04 \mu\text{mol-C}$ . The average amount of sulfur oxidized was also much lower, at  $15 \mu\text{moles}$ . This led to an average biomass yield of  $0.0028 \text{ C-mol/S-mol}$ .

Table 4.3: *Acidithiobacillus thiooxidans* growth on S / O<sub>2</sub>

	Biomass (C-mol)	S <sup>o</sup> used ( $\mu$ mol)	C-mol/S	- $\Delta$ H		- $\Delta$ G	
				(kJ/C-mol)	(kJ/e-mol)	(kJ/C-mol)	(kJ/e-mol)
<i>Open system</i>							
	$1.40 \times 10^{-6}$	106	0.0132	20516	3419	1121	187
	$1.04 \times 10^{-6}$	257	0.0041	50572	8429	5025	837
	$1.84 \times 10^{-6}$	200	0.0084	23673	3946	2243	374
	$7.13 \times 10^{-7}$	155	0.0046	48010	8002	3891	648
	$2.45 \times 10^{-6}$	157	0.0156	15659	2610	1104	184
<i>Avg</i>	$1.49 \times 10^{-6}$	179	0.0092	31686	6150	2677	630
<i>Closed system</i>							
	$4.28 \times 10^{-8}$	10	0.0043	13285	2214	1860	310
	$2.56 \times 10^{-8}$	10	0.0025	22832	3805	3582	597
	$4.96 \times 10^{-8}$	21	0.0024	9401	1567	6322	1054
	$3.95 \times 10^{-8}$	20	0.0020	12391	2065	7296	1216
<i>Avg</i>	$3.94 \times 10^{-8}$	15	0.0028	14477	2413	4765	794

Enthalpies of growth and Gibbs energy consumed were determined for each replicate given their respective overall growth reactions and then normalized to biomass produced. As shown in Table 4.3, average  $-\Delta G$  consumed for open experiments was 2680 kJ/C-mol and 4770 kJ/C-mol for closed experiments. Average  $-\Delta H$  were substantially higher at  $3.17 \times 10^4$  kJ/C-mol and  $1.45 \times 10^4$  kJ/C-mol for open and closed system experiments, respectively. Compared to standard state  $-\Delta G_r^\circ$  and  $-\Delta H_r^\circ$  as a function of biomass yield,  $-\Delta G$  and  $-\Delta H$  were much lower. Like *A. ferrooxidans* on sulfur, the standard state values of the overall growth reaction did not accurately represent experimental growth, but did predict enthalpy as the primary mode of Gibbs energy dissipation (more negative  $\Delta H$  than  $\Delta G$ ). Growth in both closed and open experiments was very exothermic. Both  $-\Delta G$  and  $-\Delta H$  for the open system replicates increased as biomass yield decreased, following the same trend as standard state values, but the closed system replicates did not. At the lower biomass yields recorded for the closed system experiments,  $-\Delta H$  began to decrease while  $-\Delta G$  consumption increased slightly, roughly following the trend of the open system replicates.

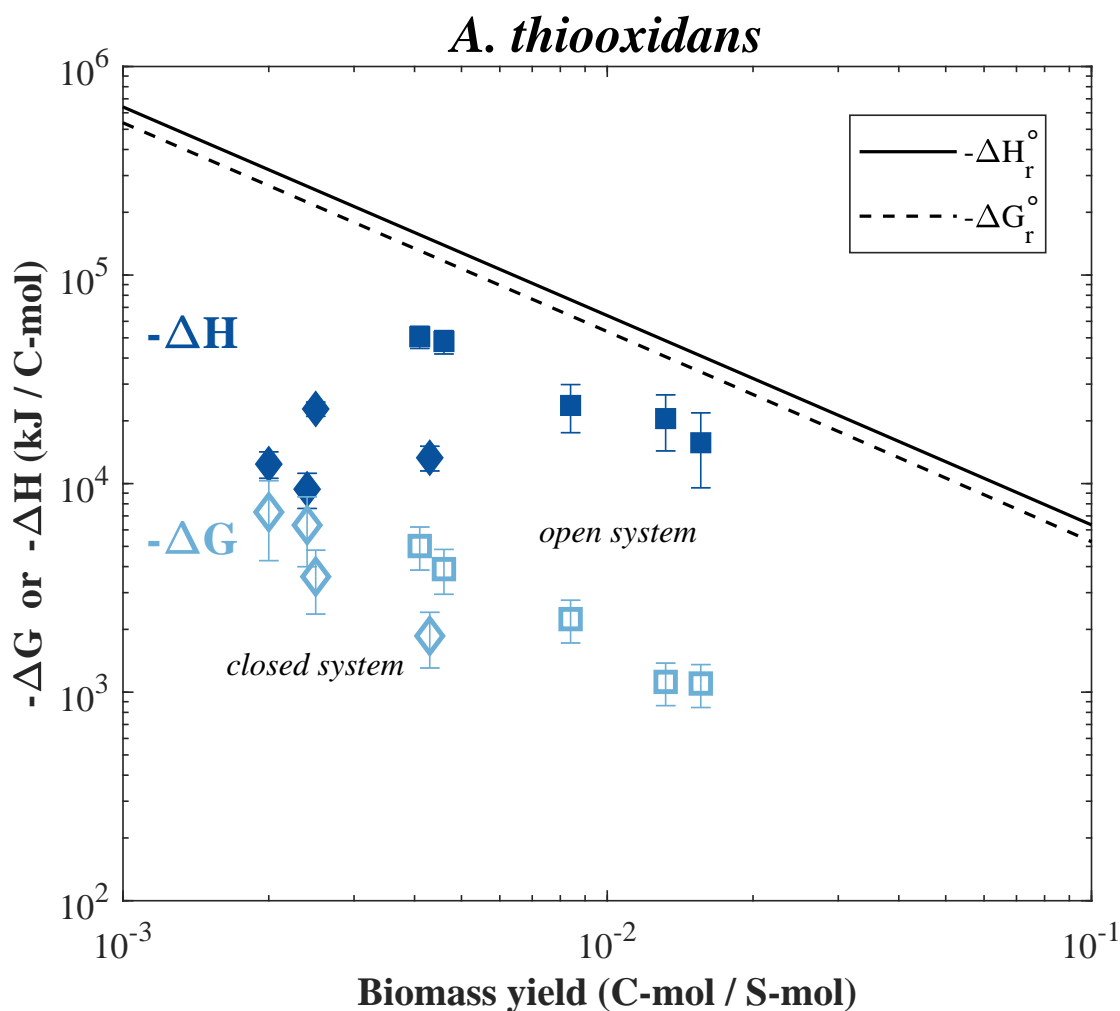


Figure 4.4: Energetics of growth (kJ/C-mol) for *Acidithiobacillus thiooxidans* during sulfur oxidation compared to theoretical standard state values for a range of biomass yields (C-mol/S-mol).  $-\Delta G_r^\circ$  (dashed line) and  $-\Delta H_r^\circ$  (solid line) were calculated for 1 molal of pure reactants and products at 30°C. Squares (■) represent replicates from open system experiments, diamonds (◆) represent closed system experiments, filled symbols are measured  $-\Delta H$  from calorimetry, and open symbols are calculated  $-\Delta G$  for all replicates.

## 4.4 Discussion

### 4.4.1 Iron oxidation by *A. ferrooxidans*

Precipitation of iron minerals from the growth medium affected  $\Delta G$ ,  $\Delta H$ , and biomass yield calculations for *A. ferrooxidans* despite analyzing abiotic controls. In correcting enthalpies of growth, the only data necessary were the type of iron mineral that precipitated and amount of total iron missing from solution. Using the  $\Delta H_r^\circ$  of the precipitation reaction, the heat production more accurately represents enthalpy due to growth. It is not necessary to know whether the  $\text{Fe}^{3+}$  in the mineral precipitate was oxidized due to biotic or abiotic processes. However, this is not the case in calculating biomass yields and  $\Delta G$  consumed during growth. Abiotic oxidation of  $\text{Fe}^{2+}$  leads to a larger change in available Gibbs energy in the medium after growth, making  $\Delta G$  consumption appear larger and biomass yield appear lower than their true values. Although control vials (without biomass) were prepared to measure abiotic oxidation of  $\text{Fe}^{2+}$ , the abiotic controls do not truly mimic experimental conditions in characteristics such as chemistry changes in the medium as biomass increases, changes in dissolved oxygen due to metabolism, and interactions with cell surfaces. Due to these complications, calorimetry data is more reliable for describing energetics of iron-oxidizing organisms like *A. ferrooxidans*.

### 4.4.2 Substrate utilization—*A. ferrooxidans*

In AMD environments, both sulfur and  $\text{Fe}^{2+}$  can be available as energy sources for *A. ferrooxidans* to metabolize. Regions containing pyrite tend to be popular research locations to study AMD ecology and microbial diversity due to the prevalence of pyrite on Earth. However, pyrite dissolution at ambient temperatures does not lead to a large supply of elemental sulfur (Nordstrom and Southam, 1997). At elevated temperatures, elemental sulfur and other RISCs can form, but the higher temperatures do not support *A. ferrooxidans* growth. A study by Schrenk *et al.* (1998) demonstrated that *A. ferrooxidans* was not responsible for acid production at the AMD site at Iron Mountain, CA, and instead was metabolizing  $\text{Fe}^{2+}$ .



over sulfur. The microorganism *Leptospirillum ferrooxidans* (*L. ferrooxidans*), a moderate thermophile, was found closer to the pyritic ore metabolizing RISCs where temperatures reached 50°C. Regions containing other iron sulfides, such as chalcopyrite ( $\text{CuFeS}_2$ ), do lead to a measurable production of elemental sulfur at temperatures favorable for *A. ferrooxidans* growth (near 30°C), providing *A. ferrooxidans* with two different electron donors to metabolize [118, 136].

It is widely thought that growth will likely occur preferentially on the substrate that releases the most energy (most negative  $\Delta G_r^\circ$ ). However, Amenabar *et al.* [4] presented a case where growth preferentially occurred on the substrate that generated the greatest energetic yield (C-mol/ $\mu\text{J}$ ) over the substrate that had the most energetic potential. Under the conditions tested in this investigation, *A. ferrooxidans* growth on elemental sulfur both maximized energetic yield (C-mol/ $\mu\text{J}$ ) and produced the largest growth yield (C-mol/mol substrate). As shown in Figure 4.5, normalized to the moles of electrons transferred, growth on iron ( $1 e^-$ -mol/Fe-mol), consumed significantly more substrate, and  $\Delta G$  as a result, while producing less biomass per mole of electrons transferred than growth on sulfur ( $6 e^-$ -mol/S-mol). When comparing growth on different substrates, it is also important to look at the power consumption, or rate of Gibbs energy consumed over time. Figure 4.6 shows the power consumed, calculated as joules of Gibbs energy consumed per second of growth, and the number of cells produced per ml for all open system growth experiments. These results are consistent with other research on iron-oxidizing microbes; iron oxidation is known to yield low levels of energy [142, 118]. Following this argument, *A. ferrooxidans* should grow preferentially on elemental sulfur over  $\text{Fe}^{2+}$  in environments favorable for growth where both substrates are present.

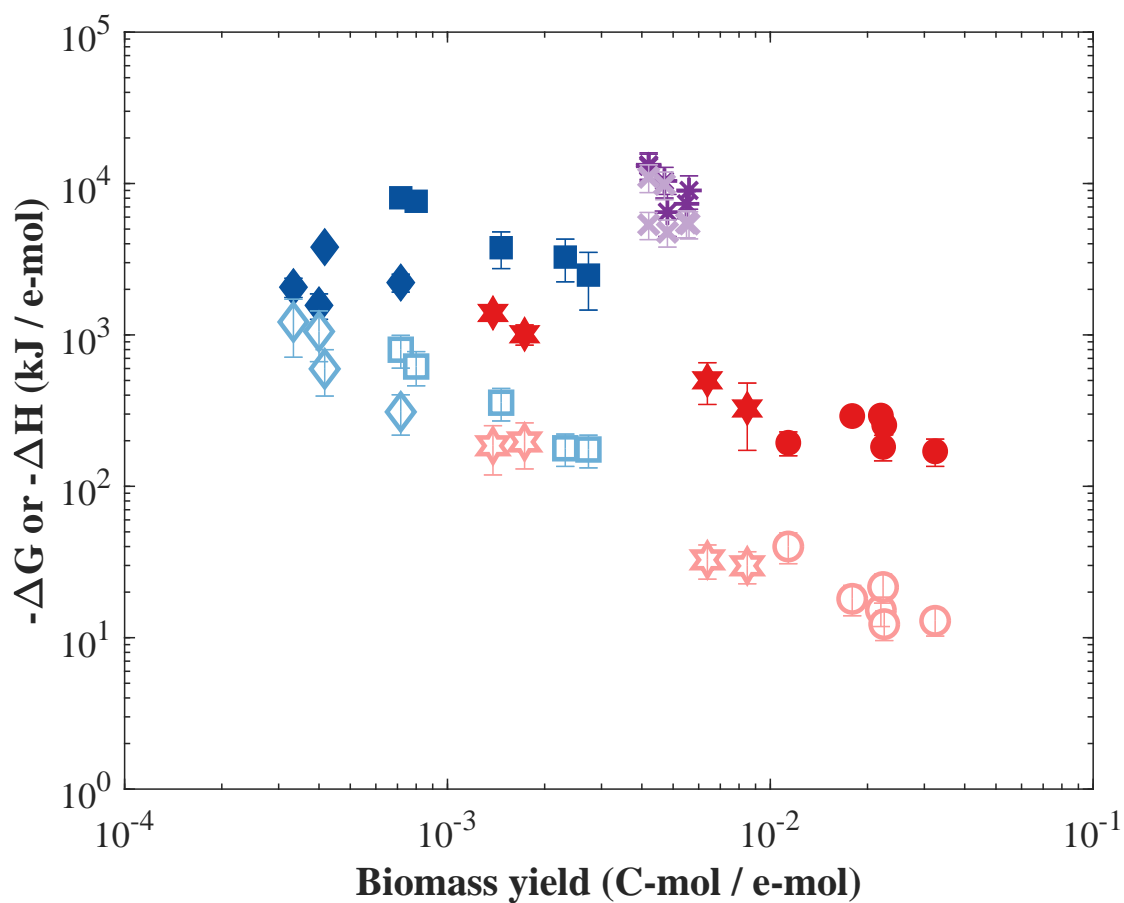


Figure 4.5: Combined energetics data and biomass yields from *Acidithiobacillus ferrooxidans* with sulfur (*A.f.*— $S^0$ , ●, ★), *Acidithiobacillus thiooxidans* with sulfur (*A.t.*— $S^0$ , ■, ◆) and *Acidithiobacillus ferrooxidans* during iron oxidation (*A.f.*— $Fe(II)$ , \*, ×), normalized to moles of electrons transferred. Filled symbols and asterisks represent  $-\Delta H$  and open and cross symbols represent  $-\Delta G$ .

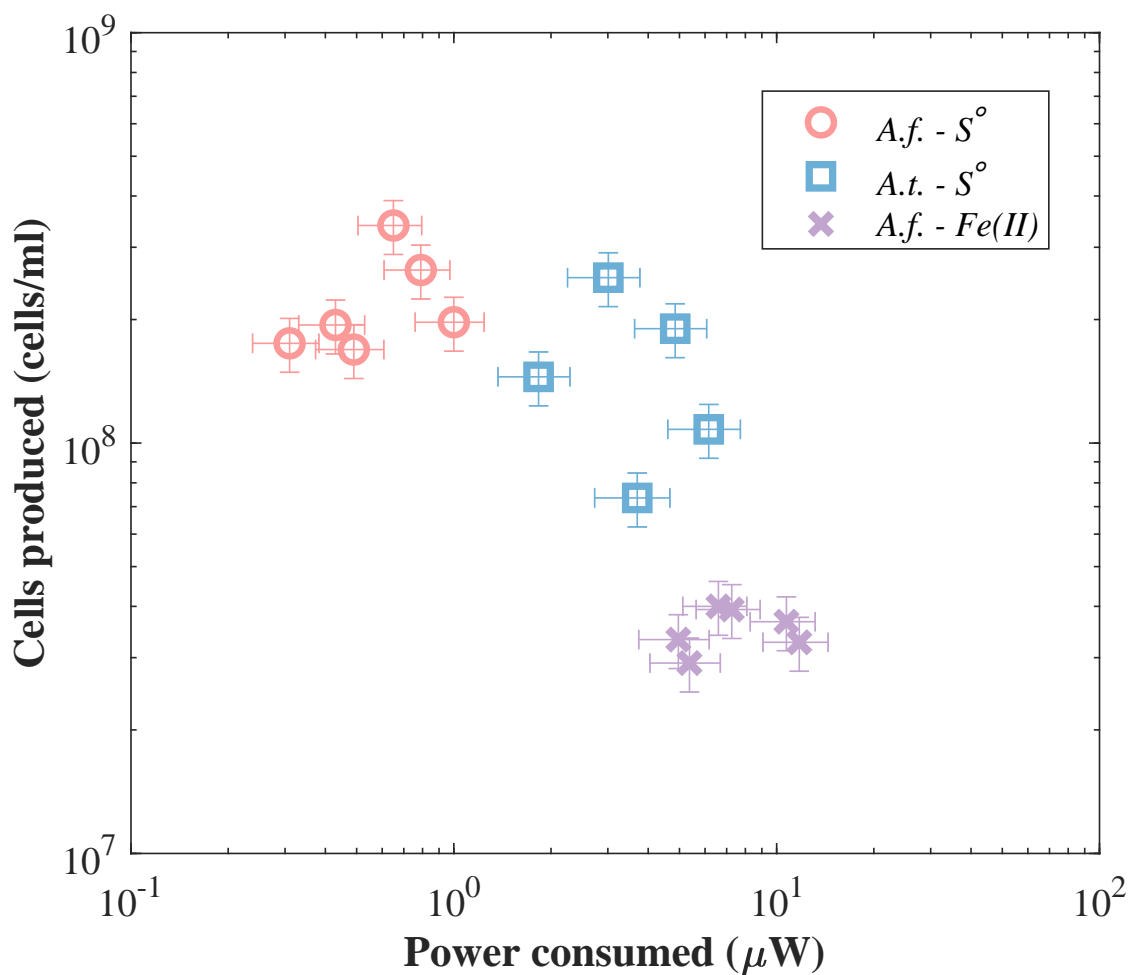


Figure 4.6: Total cells produced (cells/ml) and power consumed ( $\mu\text{W}$ ) for all open growth results. Results for *Acidithiobacillus ferrooxidans* with sulfur (*A.f.*— $S^\circ$ , ●), *Acidithiobacillus thiooxidans* with sulfur (*A.t.*— $S^\circ$ , ■) and *Acidithiobacillus ferrooxidans* during iron oxidation (*A.f.*— $Fe(II)$ , ×) are calculated as  $\Delta\text{G}$  consumed per seconds of growth, taking into account the different growth times. *A. ferrooxidans* growth on iron(II) consumed more power, but produced less cells compared to *A. ferrooxidans* and *A. thiooxidans* grown on sulfur.

#### 4.4.3 Open and closed system growth

Open and closed system experiments yielded very different results. Both in *A. thiooxidans* and *A. ferrooxidans* cultures, the closed system experiments produced significantly lower biomass yields than the open systems. In *A. ferrooxidans* sulfur-oxidizing experiments, lower yields were accompanied by higher  $-\Delta G$  consumption and higher dissipation of energy as  $-\Delta H$  (refer to Figure 4.3). These increases paralleled standard state curves for  $-\Delta G_r^\circ$  and  $-\Delta H_r^\circ$ . In *A. thiooxidans* cultures, the closed system led to lower than expected  $-\Delta H$  values, based on hypothetical values demonstrated by  $\Delta H_r^\circ$ , and similar  $-\Delta G$  values to the open system experiments (refer to Figure 4.4).

The response in growth efficiency was to be expected. Closed system experiments were completely sealed off from the atmosphere after inoculation. Unlike in the open system design, availability of both carbon source ( $\text{CO}_2$ ) and energy source ( $\text{O}_2$ ) were limited, leading to a depletion of nutrients as growth progressed without replenishment. A similar change in biomass yield was demonstrated in *L. ferrooxidans*, another prevalent acidophile in AMD environments, in response to energy source and  $\text{CO}_2$  limitations [19]. Under conditions limiting either  $\text{CO}_2$  or energy source (characterized as low  $\text{Fe}^{2+}$  in [19]), biomass yield (measured as g-protein/g- $\text{Fe}^{2+}$ ) increased 2- to nearly 4-fold compared to yields under double limitation. Under the open system design with no  $\text{CO}_2$  added to the headspace [73, 17], *A. ferrooxidans* and *A. thiooxidans* growth was only limited by  $\text{CO}_2$ , leading to an approximate 4-fold increase in yield for *A. ferrooxidans* and 3-fold increase for *A. thiooxidans*.

The change in energetics and biomass yield between open and closed system growth conditions may, in part, be due to genes responsible for carbon assimilation. It has been proposed that these species are capable of dealing with fluctuations in  $\text{O}_2$ ,  $\text{CO}_2$ , and other environmental conditions because their genomes contain copies of different forms of RuBisCO [14, 43], the main enzyme that catalyzes the  $\text{CO}_2$  fixation reaction in the Calvin-Bassham-Benson (CBB) pathway. Of the four known types of RuBisCO, both *A. ferrooxidans* and *A. thiooxidans* contain two copies of RuBisCO form I [70, 44] and one copy of RuBisCO form II

[43, 179]. *L. ferrooxidans* also contains copies of form I and form II RuBisCO. The change in energetics and biomass yield between the open and closed experimental designs could partly be due to a change in the type of RuBisCO being used for growth.

#### 4.4.4 Sulfur oxidation energetics

Despite the similarities between *A. thiooxidans* and *A. ferrooxidans*, there are genetic differences between the two species that may play a role in the energetic differences and biomass yields demonstrated here. A prominent difference is the enzymatic pathway responsible for sulfur oxidation. *A. thiooxidans* contains a cluster of genes belonging to the well-studied SOX system, or sulfur oxidases [160, 50]. *A. ferrooxidans*, however, evolved different mechanisms for sulfur oxidation and lacks all *sox* genes. Instead, *A. ferrooxidans* has genes encoding sulfide quinone oxidoreductases (SQR) [178].

Outside of the *Acidithiobacillus* genus, other prokaryotes have evolved different mechanisms to oxidize RISCs [50, 55]. In the Archaea domain, some organisms in the order Sulfolobales are also capable of metabolizing elemental sulfur and oxygen in acidic environments. *Acidianus ambivalens* (*A. ambivalens*) is a thermoacidophile found in geothermal regions such as Yellowstone National Park, growing at temperatures between 70 – 85°C [180, 181, 51]. *A. ambivalens* uses sulfur oxygenase-reductase (SOR) to oxidize sulfur in the presence of oxygen, producing sulfite, thiosulfate, and hydrogen sulfide ([90, 91]). Previous work by Hart and Gorman-Lewis (*in prep*) quantified the bioenergetics for *A. ambivalens* both for fully aerobic growth conditions (near 100% O<sub>2</sub> saturation) and microaerophilic conditions (50% O<sub>2</sub> saturation). The combined energetics data from *A. thiooxidans*, *A. ferrooxidans*, and *A. ambivalens* are shown in Figure 4.7.

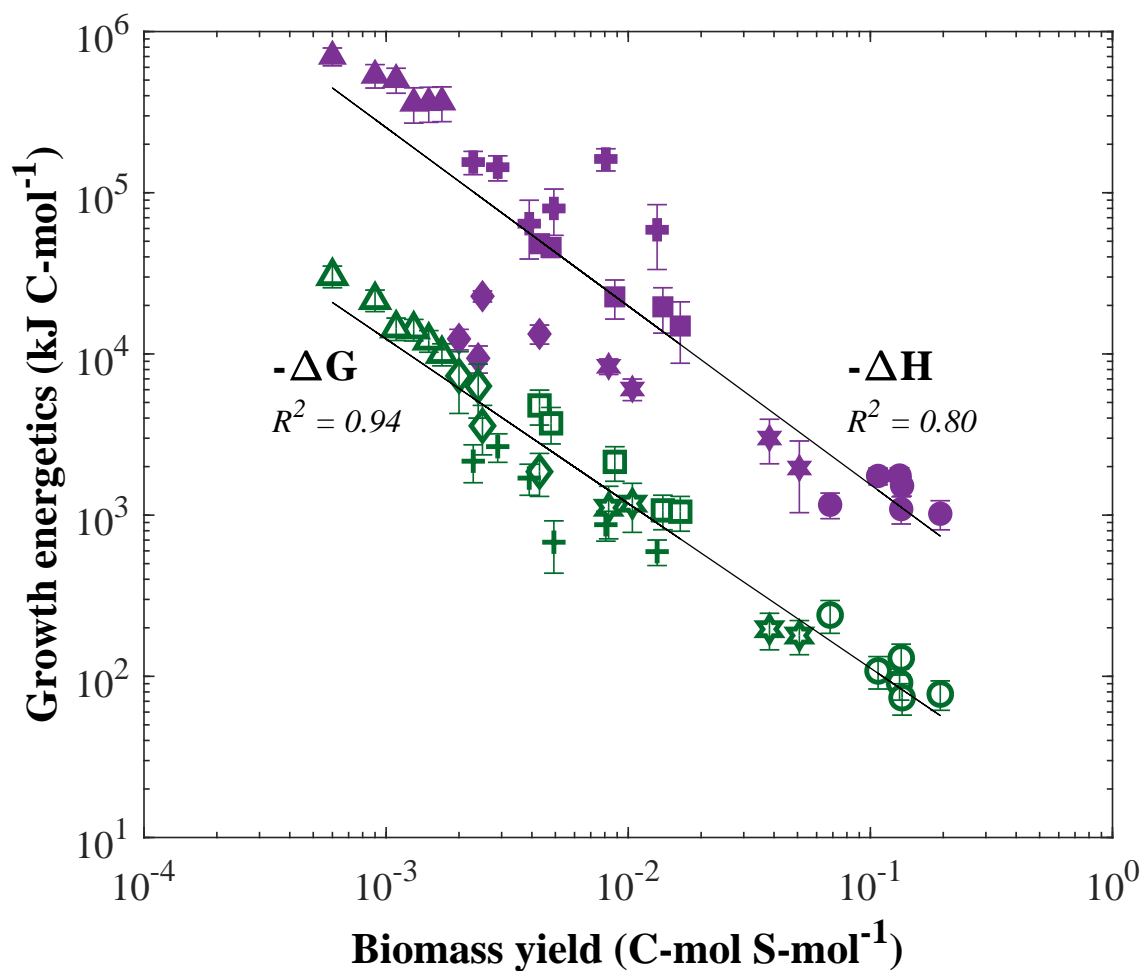


Figure 4.7: Combined energetics data from mesophilic Bacteria *Acidithiobacillus ferrooxidans* (open system — ●, closed system — ★) and *Acidithiobacillus thiooxidans* (open system — ■, closed system — ◆), and the thermoacidophilic Archaea *Acidianus ambivalens* (50% O<sub>2</sub> saturation — +, 100% O<sub>2</sub> saturation — ▲). Filled purple symbols represent  $\Delta H$  and open green symbols represent  $\Delta G$  of growth. Despite the vast differences in biochemistry and growth temperatures, the three species produced a significant correlation between  $\Delta G$ ,  $\Delta H$ , and biomass yields. Linear regressions are shown for both  $\Delta G$  ( $R^2 = 0.94$ ) and  $\Delta H$  ( $R^2 = 0.80$ ).

It is interesting to find correlating energetics between these three species given the extreme temperature and biochemical differences between the mesophilic Bacteria investigated in this study and *A. ambivalens*, a thermophilic Archaea. These three organisms also use different enzymes to oxidize sulfur. This suggests  $\Delta G$  and  $\Delta H$  of microbial growth is influenced more by the aqueous chemistry of the catabolic reaction than biochemical differences of the microorganisms in question. Bioenergetic trends of the sulfur oxidizers in this study may also hold true for other sulfur-oxidizing species and could help predict growth energetics for species not yet studied.

#### **4.5 Conclusion**

This is the first full thermodynamic characterization of microbial growth for *A. ferrooxidans* and *A. thiooxidans*. *A. ferrooxidans* grew more efficiently on sulfur, both in energetic yield and substrate yield, than on  $\text{Fe}^{2+}$ . Sulfur growth also produced significantly more cells per watt of power consumed. Closed system experiments ( $\text{CO}_2/\text{O}_2$  limited) with *A. ferrooxidans* and *A. thiooxidans* during sulfur oxidation led to inefficient growth represented as lower biomass yield and higher Gibbs energy consumed compared to open system experiments. All the sulfur oxidation results recorded for *A. ferrooxidans* and *A. thiooxidans* correlated with a high temperature Archaea, *Acidianus ambivalens*, in terms of growth energetics ( $\Delta G$  and  $\Delta H$ ) and biomass yields despite extreme differences in biochemistry and growth temperatures. This suggests that the changes in aqueous chemistry due to the catabolic reaction surpass biochemical differences between organisms when determining microbial energetics. The sulfur oxidation results presented here may help predict energetics with respect to biomass yield for other sulfur oxidizers.

## Chapter 5

**THERMODYNAMIC CHARACTERIZATION OF CADMIUM  
ADSORPTION ONTO CELLS OF THE  
THERMOACIDOPHILE *SULFOLOBUS ACIDOCALDARIUS***

*This manuscript will be submitted to Chemical Geology.*

Co-authored by Chloe E. Hart, Drew Gorman-Lewis

**5.1 Introduction**

Heavy metal contaminants enter the biosphere through natural processes and as a result of anthropogenic influences. Acidic environments in particular host high concentrations of toxic metals such as cadmium, copper, and zinc due to their increased solubility at low pH [30, 117, 42]. Adsorption to cell surfaces and organic ligands can control the bioavailability and mobility of metals in aqueous environments (e.g. [112, 166, 27, 177, 59, 58]). Therefore, quantifying the extent of metal accumulation on the surface of acidophiles is necessary to understand how their cell surfaces can impact metal partitioning in these systems.

Acidic systems are generated primarily through biological or geophysical/geochemical processes. Some biologically driven systems begin as the result of exposure of sulfidic ores to atmospheric oxygen, either through mining or natural weathering. Sulfide-bearing rocks oxidize abiotically when exposed to oxygen and biotically due to microbial activity, leading to the production of acidic waters best known as acid mine drainage [81]. In environments with geophysical and geochemical drivers, volcanic systems produce vapors (i.e.  $\text{H}_2\text{S}$ ,  $\text{CO}_2$ ) as hydrothermal waters boil in response to pressure/temperature changes. As the sulfide-bearing vapors condense, abiotic and biotic oxidation produces sulfuric acid, leading to the formation of acidic hot springs at the surface, such as the sulfuric acid-rich features in



Yellowstone National Park [176]. Hot springs within the same geothermal system can have a range of pH values, from  $< 2$  to near neutral [124, 151].

Microorganisms found in these extreme environments not only thrive in the low pH conditions, but grow despite the presence of toxic metals. Acidophiles display high tolerances for heavy metals compared to neutrophilic organisms [40, 128, 41, 172], leading to their use in industrial bioleaching and remediation research. Studies have been conducted to understand metal sorption to the cell surfaces of acidophiles, though bacterial species are typically the focus [170, 29, 56]. Of the acidophilic Archaea isolated in pure culture, *Sulfolobus acidocaldarius* (*S. acidocaldarius*) has one the highest tolerances for cadmium. *S. acidocaldarius*, first isolated from Yellowstone National Park, is a thermoacidophile that grows optimally at temperatures between 70-75°C and pH around 3, but can withstand a pH range of 0.9 to 5.8 [26, 47]. *S. acidocaldarius* can grow in the presence of Cd despite its toxicity [13], withstanding concentrations up to 10 mM ( $\sim 1,000$  ppm) before metabolic activity ceases [62, 110].

The high tolerance for Cd in metal-rich acidic environments makes *S. acidocaldarius* an excellent candidate for research on Cd complexation research by cell surfaces. Ideally, we want to understand Cd surface complexation at high temperatures to accurately represent environments that support *S. acidocaldarius*. However, conducting metal adsorption experiments at higher temperatures is difficult to accomplish [56]. To rectify the temperature discrepancy between experiments and thermophilic environments where *S. acidocaldarius* is found, temperature-dependent stability constants can be extrapolated to higher temperatures using the Van't Hoff equation.

In this investigation, we measured Cd adsorption onto *S. acidocaldarius* cells as a function of pH, ranging from 3-8, and two biomass concentrations. Adsorption results, combined with surface complexation modeling of *S. acidocaldarius* cells, were used to determine site-specific enthalpies of Cd adsorption through isothermal calorimetry.

## 5.2 Materials and Methods

### 5.2.1 Cell Growth

*S. acidocaldarius* was grown in liquid medium containing 1 g/L tryptone, 0.05 g/L yeast extract, 10 mM  $(\text{NH}_4)_2\text{SO}_4$ , 1 mM  $\text{MgSO}_4 \cdot 7\text{H}_2\text{O}$ , 5 mM  $\text{CaCl}_2 \cdot 2\text{H}_2\text{O}$ , 2 mM  $\text{KH}_2\text{PO}_4$ , 22  $\mu\text{M}$   $\text{Na}_2\text{B}_4\text{O}_7$ , 75  $\mu\text{M}$   $\text{FeCl}_3 \cdot 6\text{H}_2\text{O}$ , 124 nM  $\text{NaMoO}_4$ , 120 nM  $\text{MnCl}_2$ , 66 nM  $\text{CoSO}_4$ , 150 nM  $\text{VO}_2\text{SO}_4 \cdot 2\text{H}_2\text{O}$ , 77  $\mu\text{M}$   $\text{ZnSO}_4 \cdot 7\text{H}_2\text{O}$ , and 8 nM  $\text{CuCl}_2 \cdot 2\text{H}_2\text{O}$ . The medium was adjusted to pH 3 with  $\text{H}_2\text{SO}_4$  and cultures were grown at 70 °C. Cultures were transferred (10% inoculum size) to fresh medium after 6 to 7 days.

Biomass for experiments was harvested from culture via centrifugation when cells reached stationary phase. Cells were washed three times, which involved suspending the biomass in 0.1 M  $\text{NaClO}_4$  and vortexing for 15 seconds. Cells were reharvested via centrifugation and the supernatant decanted and replaced with fresh 0.1 M  $\text{NaClO}_4$ . The process was repeated two additional times.

### 5.2.2 Adsorption Experiments

All adsorption experiments conditions were performed with *S. acidocaldarius* suspended in 0.1 M  $\text{NaClO}_4$  in Nalgene Oak Ridge FEP centrifuge tubes. Two biomass concentrations were used, deemed low biomass (0.18 g/L dry weight) and high biomass (0.68 g/L dry weight). Cd added to the biomass suspension to create a solution with a final Cd concentration of  $4.4 \times 10^{-5}$  M. The Cd-containing suspension was separated into reaction vessels and the pH adjusted to between 3 and 8 using small volumes of concentrated NaOH and  $\text{HClO}_4$ . Reaction vessels were slowly agitated end over end for 45 min and the equilibrium pH was measured. The supernatant was filtered through a 0.22  $\mu\text{m}$  polycarbonate membrane filter. Cd in the supernatant was analyzed spectrophotometrically by its color reaction with 2-(5-bromo-2-pyridylazo)-5-diethylaminophenol (5-BrPADAP) following procedures by [74] adapted for Cd instead of Zn, without the preconcentration step and demasking steps as these were unnecessary. The analytical uncertainty of this procedure was 3%. By subtract-

ing the aqueous metal concentration in the supernatant from the initial concentration, the concentration of metal bound to cells was determined. Cell-free, Cd control experiments were performed in the same manner to ensure that Cd did not adsorb onto the polycarbonate filter membrane or other experimental apparatus.

### 5.2.3 Desorption Experiments

Desorption experiments were conducted to determine the reversibility of the Cd-cell adsorption reaction. Cd-bearing cell suspensions in 0.1 M NaClO<sub>4</sub> were adjusted to approximately pH 7.4 and 6.3, agitated for 45 min, and adsorbed Cd was determined on an aliquot of the sample using procedures describe above. The remaining suspensions were adjusted to pH 3.0 and agitated for an additional 45 min before remeasuring adsorbed Cd.

### 5.2.4 Calorimetric Experiments

Calorimetric experiments involved titrating a cadmium-bearing solution with a computer controlled Lund pump with a syringe and cannula into the reaction cell at a nearly constant pH. The reaction and reference cells were filled with 1 ml of microbial suspension in 0.1 M NaClO<sub>4</sub>. Cell-bearing suspensions were adjusted to pH 5.4 and 5.0. The pH of the suspension was adjusted to the appropriate pH by the addition of HClO<sub>4</sub> or NaOH prior to the titration. The titrant composition was 4.2 mM Cd(ClO<sub>4</sub>)<sub>2</sub> in 0.1 M NaClO<sub>4</sub> with the pH adjusted to match that of the bacterial suspension. Sequential 12 μL doses of titrant were added to the reaction cell followed by an 8 min period of monitoring heat flow.

Experimental heats associated with metal-adsorption reactions on the cell wall for the *i*th addition of titrant ( $Q_i^{corr}$ ) requires a background correction to subtract heats associated with the reactions intrinsic to the titration process. Background heats ( $Q_i^{bkg}$ ) were measured by titrating the same Cd-bearing solution into a cell-free solution of 0.1 M NaClO<sub>4</sub>. Corrected heats are produced by subtracting background heats from the experimentally measured heat ( $Q_i^{exp}$ ) as described by Equation 5.1.

$$Q_i^{corr} = Q_i^{exp} - Q_i^{bkg} \quad (5.1)$$

### 5.2.5 Derivation of model parameters

#### Surface complexation models

We modeled the adsorption data with a surface complexation model to quantify metal adsorption. The non-electrostatic model of [60] describes the proton-active sites on the surface of *S. acidocaldarius* (Table 5.1). Proton binding is ascribed to distinct reactions of the following stoichiometry:



where  $R$  is a bacterial cell to which a proton-active functional group,  $L_i$ , is attached.

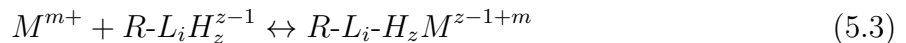
Table 5.1: *Sulfolobus acidocaldarius*

Parameter <sup>a</sup>	<i>S. acidocaldarius</i>			
$pK_a$	$3.6 \pm 0.1$	$4.6 \pm 0.1$	$6.6 \pm 0.1$	$9.9 \pm 0.2$
$[Sites](\mu mol/g)^b$	$363 \pm 10$	$389 \pm 10$	$1380 \pm 10$	$1995 \pm 10$
$\Delta G(kJ/mol)$	$-20.5 \pm 0.6$	$-26.1 \pm 0.7$	$-37.9 \pm 0.9$	$-56.5 \pm 1.0$
$\Delta H(kJ/mol)$	$-7.3 \pm 2.6$	$-6.2 \pm 2.3$	$-15.8 \pm 0.3$	$-24.6 \pm 0.4$
$\Delta S(J/molK)$	$44 \pm 9$	$67 \pm 8$	$74 \pm 3$	$107 \pm 4$

<sup>a</sup> According to the reaction  $R-L_i^- + H^+ \leftrightarrow R-L_iH^o$  for ionic strength of 0.1 M with 1  $\sigma$  errors reported.

<sup>b</sup> Normalized to dry weight.

Electric double layer interactions were not taken into account in the models of proton adsorption due to the lack of consensus on how to model electrostatic effects on bacterial surfaces [38, 46, 45, 65, 105, 115, 125]. A generic metal adsorption reaction can be represented with the balanced chemical equation:



where  $L_i$  represents one of the five surface functional groups present on the bacterial surface, and  $z$  can equal 0 or 1. A range of possible reaction stoichiometries were tested and derived each proposed stability constant as defined by Equation 5.4:

$$K = \frac{[R-L_i-H_zM^{z-1+m}]}{a_{M^{m+}}[R-L_iH_z^{z-1}]} \quad (5.4)$$

where  $a$  represents the aqueous activity of the subscripted species with activity coefficients calculated by FITEQL using the Davies equation [171], and the brackets represent surface site concentrations in moles per kilogram of solution.

Surface complexation reactions were modeled using FITEQL [171]. The general strategy started with modeling the data gathered as a function of pH with a one-site model involving monodentate complexation and adding additional reactions as necessary to achieve reasonable fits to the dataset.  $V_Y$  values are indicative of how well models fit the data. These values are calculated from the sum of squares difference between the experimental and calculated total concentrations of the metal investigated weighted according to the error estimated in the extent of adsorbed metal [171]. Reasonable model fits are typically those that produced  $V_Y$  values less than 20. In addition to reasonable  $V_Y$  values, the log  $K$  values for each biomass concentration needed to be within 1 log unit of each other to consider the model as reasonably representing the data. The average of the formation constants that described the datasets produced the overall log  $K$  values for the final model. Errors for the formation constants were calculated by propagating uncertainties produced by FITEQL from the inverse of the covariance matrix for each biomass concentration, based on analytical uncertainties of metal

analysis and pH measurements, through the averaging calculation and generating  $2\sigma$  errors for the formation constants of the final models.

*Derivation of enthalpies of Cd adsorption*

Equation 5.5 describes the relationship between the corrected heats of metal adsorption ( $Q_i^{corr}$ ) and the site-specific enthalpies of proton ( $\Delta H_{HL_y}$ ) and metal adsorption ( $\Delta H_{ML_y}$ ). The change in the number of moles of the protonated sites ( $\delta n_{HL_y}^i$ ) and surface-complexed metal ion ( $\delta n_{ML_y}^i$ ) caused by the  $i$ th addition of titrant, relate the enthalpies of protonation and metal adsorption to the corrected heats ( $Q_i^{corr}$ ).

$$-\sum Q_i^{corr} = \sum \Delta H_{ML_y} \times \sum \delta n_{ML_y}^i + \sum \Delta H_{HL_y} \times \sum \delta n_{HL_y}^i \quad (5.5)$$

The  $\delta n^i$  values—a function of pH,  $K_y$ , site concentrations, metal concentration, and volume—and site-specific enthalpies of protonation and metal adsorption determine the total heat produced with each addition of metal. The volume of metal solution added and pH were treated as independent variables to calculate  $\delta n^i$  values and subsequently derive site-specific enthalpies through optimization by minimizing the sum-of-squares difference between the measured experimental heats ( $Q_i^{corr}$ ) and the model derived heats ( $Q_i^{calc}$ ). Enthalpies of metal adsorption were only derived for the best-fit models that adequately represented the pH adsorption edges. Uncertainties in model parameters are given at the  $2\sigma$  confidence level and are calculated from the inverse covariance matrix of a given fit. Gibbs energy and the entropy of reaction were calculated using Equation 5.6 and Equation 5.7 with propagated errors representing  $2\sigma$ .

$$\Delta G = -2.3026RT \log K \quad (5.6)$$

$$\Delta G = \Delta H - T\Delta S \quad (5.7)$$

### 5.3 Results and Discussion

#### 5.3.1 Cd Adsorption

Cd adsorption onto *S. acidocaldarius* is depicted in Figure 5.1. In the low biomass system, Cd adsorption was near 0% up to pH 5 then adsorption increased substantially as pH increased with an average maximum adsorption of approximately 13% above pH 6. Increasing the biomass concentration approximately 4 times increased the extent of adsorption above pH 4 with a maximum extent of adsorption of approximately 70 – 75% around pH 7. Below pH 4 Cd adsorption was between 0 – 5%. Desorption experiments with initial samples at pH 6.3 and 7.4 adsorbed 10 – 28% Cd. Upon decreasing the pH to 3, Cd adsorption decreased to nearly 0%.

#### 5.3.2 Surface Complexation Modeling

Multiple surface complexation models of Cd adsorption onto *S. acidocaldarius* produced reasonable fits. All reasonable models included 2 reactions either involving sites 1 and 3 or 2 and 3. Monodentate models with Cd adsorbing onto sites 1 and 3 or 2 and 3 produced log K values between 2.9 – 3.4. Multiple models involving a combination of monodentate and bidentate binding also produced reasonable fits to the adsorption data. Similar to the monodentate models, these models all involved reactions onto either sites 1 and 3 or 2 and 3. Bidentate binding of Cd approximately doubled the monodentate log K values resulting in values between 6.5 – 7. Only one model involving two bidentate reactions with sites 2 and 3 fit the data. These models are described in Table 5.2, while all attempted models are described in the Supplemental Section. All reasonable models within each biomass concentration produced  $V_Y$  values that were statistically similar.

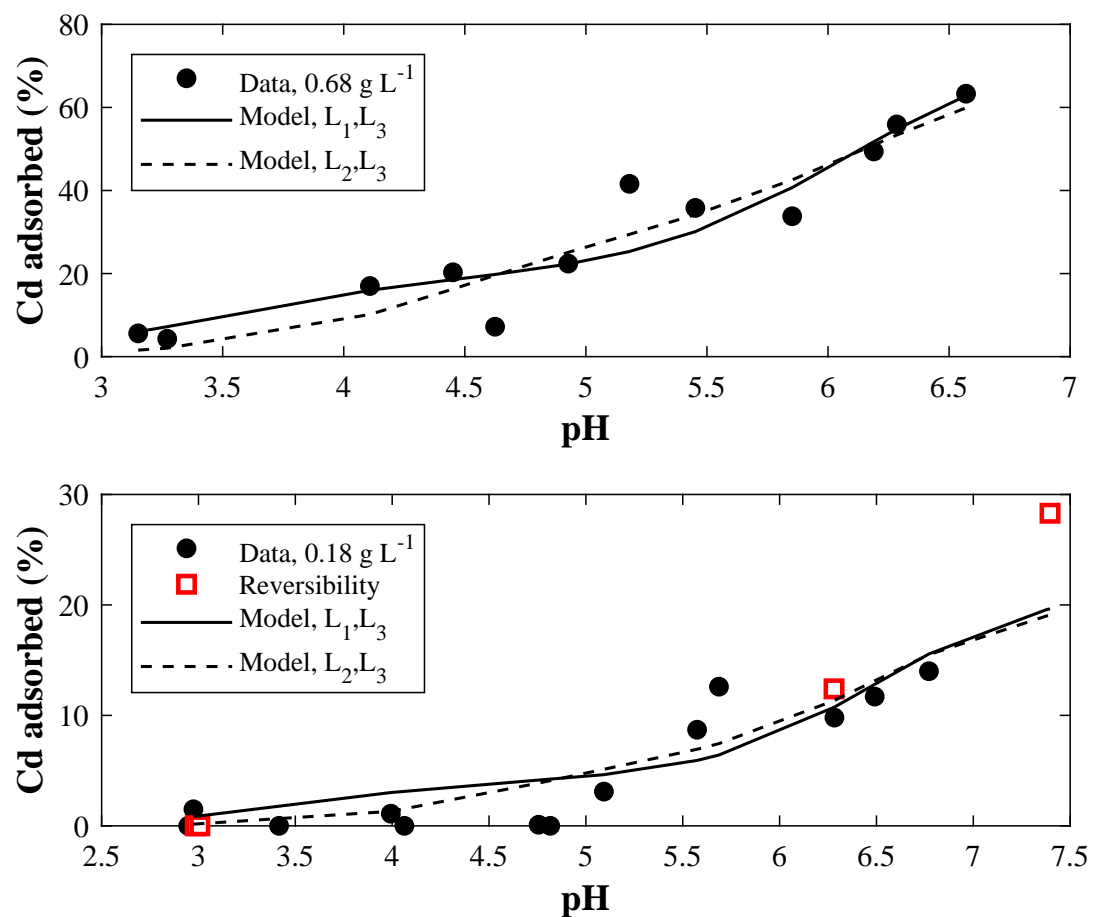


Figure 5.1: Cd adsorption by *S. acidocaldarius* (●) as a function of pH for 0.68 g/L biomass (top) and 0.18 g/L biomass (bottom). Reversibility experiments are indicated with open red squares. Solid and dashed lines represent the surface complexation models involving monodentate sites  $L_1$  and  $L_3$  and monodentate sites  $L_2$  and  $L_3$ , described in Table 5.2.



Table 5.2: Model Parameters

Reaction	Log K	$\Delta G$	$\Delta H$ (kJ/mol)	$\Delta S$ (J/molK)	Log K (75°C)
$R - L_2 + Cd^{2+} \leftrightarrow R - L_2 - Cd^+$	3.1	$-18 \pm 0.4$	$11 \pm 4.2$	$+97 \pm 14$	3.4
$R - L_3 + Cd^{2+} \leftrightarrow R - L_3 - Cd^+$	3.2	$-18 \pm 0.3$	$-31 \pm 2.2$	$-43 \pm 7$	2.4
$2R - L_2 + Cd^{2+} \leftrightarrow (R - L_2)_2 - Cd^\circ$	7.2	$-41 \pm 0.4$	$20 \pm 8.7$	$+205 \pm 29$	7.7
$R - L_3 + Cd^{2+} \leftrightarrow R - L_3 - Cd^+$	3.1	$-18 \pm 0.3$	$-27 \pm 1.7$	$-31 \pm 6$	2.4
$R - L_2 + Cd^{2+} \leftrightarrow R - L_2 - Cd^+$	3.3	$-19 \pm 0.2$	$-13 \pm 6.0$	$+19 \pm 20$	3.0
$2R - L_3 + Cd^{2+} \leftrightarrow (R - L_3)_2 - Cd^\circ$	6.8	$-39 \pm 0.3$	$-34 \pm 0.6$	$+16 \pm 2$	5.9
$2R - L_2 + Cd^{2+} \leftrightarrow (R - L_2)_2 - Cd^\circ$	7.3	$-42 \pm 0.2$	$-4 \pm 2.1$	$+127 \pm 7$	7.2
$2R - L_3 + Cd^{2+} \leftrightarrow (R - L_3)_2 - Cd^\circ$	6.7	$-38 \pm 0.4$	$-35 \pm 0.5$	$+10 \pm 2$	5.8
$R - L_1 + Cd^{2+} \leftrightarrow R - L_1 - Cd^+$	2.9	$-16 \pm 0.4$	$14 \pm 4.3$	$+102 \pm 14$	3.3
$R - L_3 + Cd^{2+} \leftrightarrow R - L_3 - Cd^+$	3.3	$-18 \pm 0.2$	$-31 \pm 2.2$	$-42 \pm 7$	2.5
$2R - L_1 + Cd^{2+} \leftrightarrow (R - L_1)_2 - Cd^\circ$	6.9	$-39 \pm 0.4$	$47 \pm 15.1$	$+289 \pm 51$	8.1
$R - L_3 + Cd^{2+} \leftrightarrow R - L_3 - Cd^+$	3.3	$-18 \pm 0.2$	$-32 \pm 3.0$	$-46 \pm 10$	2.5
$R - L_1 + Cd^{2+} \leftrightarrow R - L_1 - Cd^+$	3.1	$-17 \pm 0.2$	$-3 \pm 2.1$	$+48 \pm 7$	3.0
$2R - L_3 + Cd^{2+} \leftrightarrow (R - L_3)_2 - Cd^\circ$	6.8	$-39 \pm 0.2$	$-35 \pm 0.5$	$+13 \pm 2$	5.9

### 5.3.3 Enthalpies of Cd Adsorption

Figure 5.2 depicts cumulative corrected heats of Cd adsorption. These heats are exothermic and become more exothermic with increasing Cd. This is particularly pronounced at pH 5 where the cumulative corrected heats are 1 – 1.4 mJ after approximately 300  $\mu\text{mole}$  Cd was added. At pH 5.6, after the same amount of Cd was added, the cumulative corrected heats are only 0.3 – 0.5 mJ. Heats do not plateau at either pH value. These heats represent those from adsorption of Cd onto the *S. acidocaldarius* surface as well as heats resulting from a redistribution of protons on the surface. To deconvolve these contributions to the corrected heats, a surface complexation model must be applied to the data to speciate the system. Therefore, site-specific enthalpies of Cd adsorption are model dependent.

The surface complexation models for the reactions in Table 5.2 were used to calculate  $\delta n_{HL_y}^i$  and  $\delta n_{ML_y}^i$  values along with the previously determined enthalpies of protonation ( $\Delta H_{HL_y}$ ) necessary to apply Equation 5.5 to the data. Curves in Figure 5.2 represent the fit of Equation 5.5 to the calorimetric data and the enthalpies of Cd adsorption are reported in Table 5.2. Enthalpies of Cd adsorption are interpreted based on their equivalent aqueous reaction with organic ligands. This is a common framework for understanding the reactivity of bacterial surfaces due to their surface functional groups reacting similarly with equivalent aqueous organic ligands [125, 46, 115, 59, 28, 157].

The surface complexation models in Table 5.2 describing monodentate complexation onto sites 1 and 2 produced consistently mild exothermic to endothermic enthalpies of Cd adsorption. Calculated entropies of complexation (reported in Table 5.2) for these reactions were large and positive. Considering these enthalpy and calculated entropy values in conjunction with the electronic structure of donor and metal ions along with other ligand properties like denticity, steric constraints, etc. allows us to interpret the results in terms of aqueous complexation selectivity. Gorman-Lewis [60] suggested the identities of sites 1 and 2 were likely anionic oxygen ligands. In terms of the “hard” and “soft” classification scheme of atoms, anionic oxygen ligands are “hard”, and therefore, less polarizable. The driving force

for complexation with “hard” ligands comes from a large, positive entropic contribution resulting from the dehydration of the 1° and 2° hydration spheres of the metal ion and ligand [1, 21, 104, 120, 121]. Breaking the H<sub>2</sub>O-metal and H<sub>2</sub>O-ligands bonds results in the production of mildly exothermic to endothermic enthalpies of complexation. This is observed for a variety of anionic oxygen ligands complexing Cd [12, 103, 122]. Interpretation of monodentate enthalpies and entropies of Cd complexation onto sites 1 and 2 give results which are consistent with Cd complexation by an anionic oxygen ligand.

Bidentate complexation by anionic oxygen ligands should produce differences in the enthalpies of and entropies of complexation. With the increase in dehydration of the additional ligand, one would expect an increase in the endothermicity of complexation as well as a positive increase in the entropy of complexation. This is observed for two of the three models involving bidentate complexation with site 1 or 2. The model with bidentate complexation onto both sites 2 and 3 did not produce enthalpies and entropies with these trends; consequently, this model is not considered to produce reasonable thermodynamic parameters.

Gorman-Lewis [60] suggested site 3 was likely a “soft” ligand such as the N-containing compounds found in imidazole or histidine. Donors classified as “soft” are more polarizable than anionic oxygen ligands and create largely covalent bonds with donors “soft” metal ions such as Cd. These “soft-soft” complexes typically include some degree of back-bonding between *d* orbitals of the metal ion and vacant *d* or  $\pi^*$  orbitals of the ligand. The covalent nature of these complexes causes their complexation reactions to be exothermic. The drive to break the metal-H<sub>2</sub>O bonds comes from the formation of new covalent metal-ligand bonds. In all models, Cd complexation by site 3 produced exothermic enthalpies and small positive or negative entropies of complexation both consistent with Cd complexation by imidazole [10, 37, 145, 122]. The effect of bidentate complexation on the enthalpies of Cd complexation by N-ligands lacks definite trends as previous studies has shown that the enthalpies may become more or less exothermic. However, there is a definite trend in the entropies of complexation as monodentate binding produces negative values and bidentate binding produces slightly positive values. Negative values suggest the formation of outer sphere surface complexes,

and small positive values may reflect some dehydration as the Cd is bound more strongly in a bidentate manner.

#### 5.3.4 Temperature Dependence

The previously discussed results shows that the *S. acidocaldarius* surface has an affinity for Cd at 25°C; however, we are ultimately interested in its behavior at higher temperatures. Using the enthalpies of Cd adsorption and stability constants determined at 25°C, in conjunction with the Van't Hoff equation, allows us to predict the stability constants at higher temperature. These predictions assume the relative heat capacities of the products and of the reactants ( $\Delta C_P$ ) are zero for the reaction, which is a reasonable assumption over small (i.e.,  $\leq 75^\circ$ ) temperature changes.

The general endothermicity of reactions onto sites 1 and 2 suggest the most potential for stability constants to increase with an increase in temperature. As shown in Table 5.2, these reactions with endothermic enthalpies have increases in their stability constant of 0.3 – 1 near the optimal growth temperature of *S. acidocaldarius* of 75°C. Cd adsorption onto site 3 being exothermic had a decrease in its stability constant of approximately 0.8 when predicted at 75°C. To better understand how this temperature increase might affect the extent of Cd adsorption under similar conditions as the adsorption experiments, we used the predicted stability constants and those determined at 25°C to predict adsorption as depicted in Figure 5.3. With an increase in temperature a larger fraction of Cd is partitioned onto site 2, which also increases the total fraction of adsorbed Cd below pH 5.

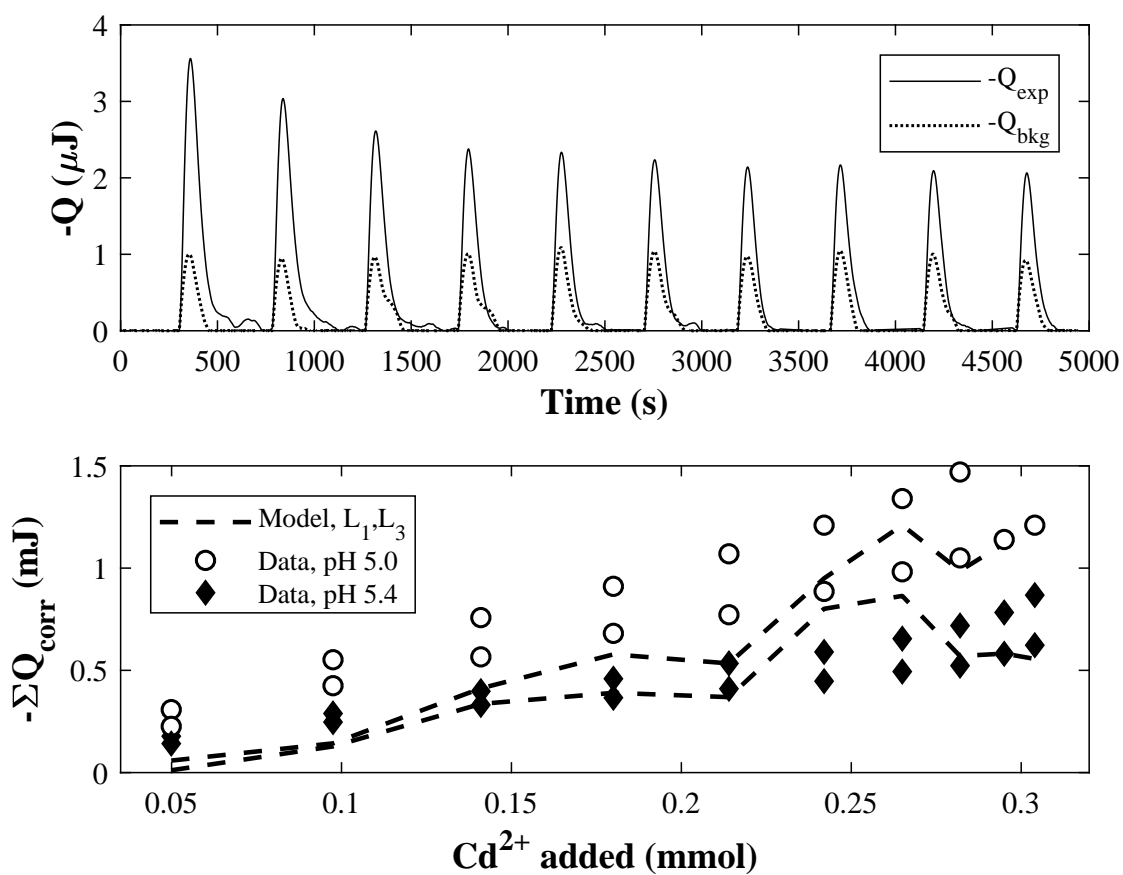


Figure 5.2: Top: Raw experimental data ( $-Q_{\text{exp}}$ ) with biomass and measured background heat ( $-Q_{\text{bkg}}$ ) during addition of Cd. Bottom: Corrected heat ( $-Q_{\text{corr}}$ ) from two high pH ( $\blacklozenge$ ) and two low pH ( $\circ$ ) adsorption titrations with the dashed curve representing a model fit using sites  $L_2$  and  $L_3$ .

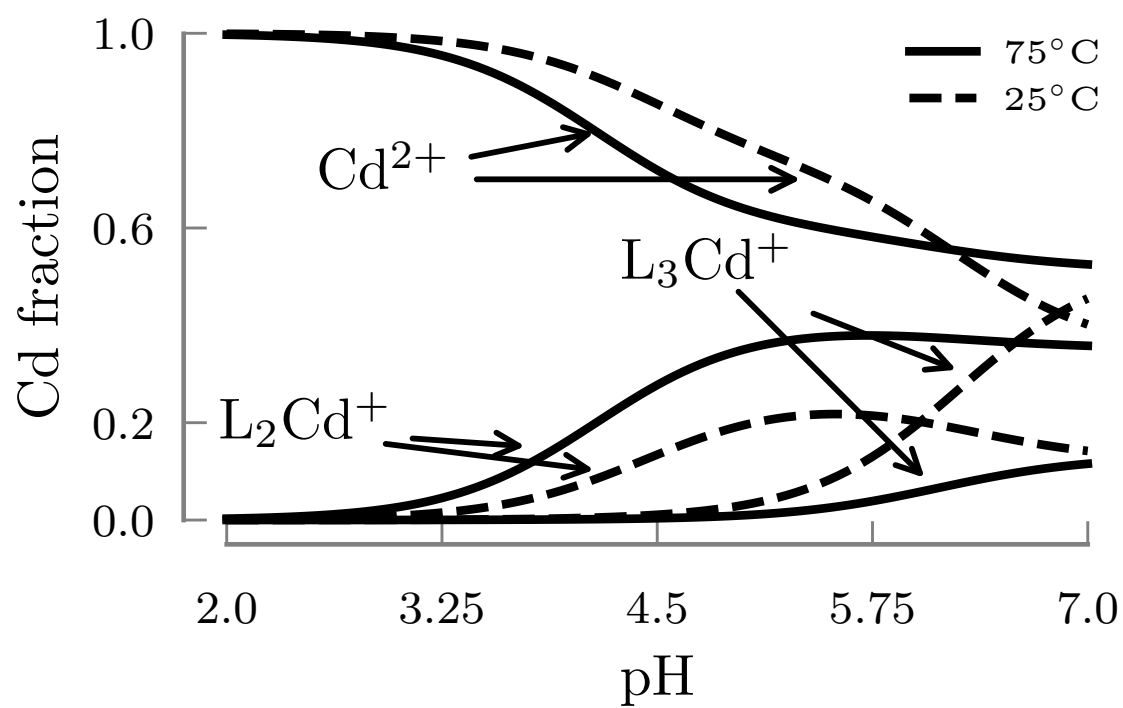


Figure 5.3: Cd partitioning onto *S. acidocaldarius* at 25°C and 75°C.

#### 5.4 Conclusions

The *S. acidocaldarius* surface readily adsorbs Cd, which can impact Cd partitioning. Surface complexation modeling of Cd adsorption revealed that multiple surface sites are involved in the complexation reactions. Combining the surface complexation models with isothermal calorimetric measurements allowed us to determine enthalpies and entropies of adsorption. The thermodynamic parameters describing Cd adsorption are consistent with surface sites 1 and 2 being anionic oxygen ligands and surface site 3 being a N-containing ligand consistent with imidazole. Predicting the temperature dependence of the adsorption reactions by using the Van't Hoff equation and enthalpies of adsorption revealed that as temperature increases the influence of sites 1 or 2 on the total Cd partitioning increases, which increases the potential for adsorption at lower pH. This type of thermodynamic predictive modeling is possible through our approach combining calorimetric measurements and surface complexation modeling to provide the first thermodynamic description of Cd adsorption onto *S. acidocaldarius*.

## Chapter 6

# CONCLUSIONS

Characterizing microbial growth of acidophiles in thermodynamic terms has the potential to improve our understanding of the distribution and abundances of microorganisms in extreme environments, determine the effects that environmental factors have on microbial activity, and help guide our search for life elsewhere by improving the quantification of energy budgets and growth efficiencies. The need to acquire energy to drive reactions such as maintenance, biosynthesis, and motility is a universal characteristic of all living organisms. Microbial growth can be modeled using macrochemical equations to describe overall metabolism and determine the amount of Gibbs energy consumed from the environment. With the addition of calorimetry, overall growth can be characterized in thermodynamic terms. This combined geochemical and thermodynamic framework was applied to the growth of three acidophiles in different growth conditions to understand how environmental factors can influence microbial efficiency and overall energetic requirements. The cell surface of a fourth acidophile was characterized in thermodynamic terms in order to understand interactions with heavy metals in extreme environments.

### 6.0.1 Summary of work

*Chapter 2* Energetics of growth were determined for the thermoacidophilic sulfur-oxidizer *Acidianus ambivalens* (*A. ambivalens*) under conditions designed to maximize biomass production and two different conditions of oxygen limitation to determine the effects of energy source availability on energy usage. In all experiments, Gibbs energy was primarily dissipated through the release of heat. In oxygen-limited conditions, growth was significantly more efficient and resulted in a tighter coupling of energy consumption to biomass pro-



duction (biomass yield, C-mol/S) and lower overall Gibbs energy consumption for growth. High-oxygen experiments resulted in decoupling between catabolic and anabolic reactions, indicated by low biomass yield values. The increase in Gibbs energy consumption observed in high-oxygen conditions likely reflects larger maintenance energy demand as a result of oxidative stress. Continued research investigating microbial bioenergetics will improve our understanding of maintenance energy requirements in extreme environments and aid in quantifying energy budgets for microbial growth and cell maintenance.

*Chapter 3* Microbial activity can be affected by a number of physical and chemical changes in the environment, but the effects of environmental oxidation state on overall energetics is not fully understood. Energetics of growth were determined for *A. ambivalens* during anaerobic sulfur reduction with hydrogen. Gibbs energy consumed, enthalpy of growth, and growth efficiency under anaerobic conditions were compared to growth via sulfur oxidation in aerobic and microaerobic conditions. Despite higher energetic costs to create biomass under oxic conditions, microaerobic growth with sulfur and O<sub>2</sub> required the least amount of Gibbs energy for growth. Growth efficiencies and energy budgets between microaerobic and anaerobic growth conditions were statistically similar, however, suggesting only a slight preference for growth with S<sup>0</sup>/O<sub>2</sub> in microaerobic environments.

*Chapter 4* *Acidithiobacillus ferrooxidans* and *Acidithiobacillus thiooxidans* are prevalent species in acid mine drainage areas. Their metabolisms drive acid production and heavy metal leaching through the oxidation of elemental sulfur and Fe<sup>2+</sup>. To further understand growth efficiency and energetic demands, energetics of growth were determined for *A. ferrooxidans* during iron and sulfur oxidation and for *A. thiooxidans* during sulfur oxidation. *A. ferrooxidans* growth was more efficient on elemental sulfur than Fe<sup>2+</sup>, producing higher biomass yields and consuming less power per cell produced, suggesting growth preferentially occurs on elemental sulfur with O<sub>2</sub> as opposed to Fe<sup>2+</sup>. *A. thiooxidans* and *A. ferrooxidans* energetics, in terms of Gibbs energy consumed and enthalpy of growth, produced correlating results with biomass yield. Energetics of *Acidianus ambivalens* during sulfur oxidation was combined with *Acidithiobacillus* species and resulted in significant linear regression trends

between  $-\Delta G$  and  $-\Delta H$  with biomass yield, suggesting Gibbs energy consumption and heat production can be predicted for other sulfur-oxidizing organisms based on their biomass yields.

*Chapter 5* Acidic environments can contain high toxic metal concentrations due to their increased solubility at low pH. Acidophiles display high tolerances to a number of these metals and thrive in such environments despite high levels of heavy metals. *Sulfolobus acidocaldarius*, a thermoacidophilic Archaea, is known to have a high tolerance to cadmium, a metal that is toxic to all life. Understanding metal adsorption by acidophile cell surfaces is important because microbial surfaces play an important role regulating bioavailability and mobility of metals in the environment. Therefore, I measured cadmium adsorption by *S. acidocaldarius* cell surfaces as a function of pH and concentration of biomass. With surface complexation models and isothermal calorimetry, I determined Gibbs energies, enthalpies, and entropies of Cd adsorption onto cell surfaces, providing the first thermodynamic characterization of *S. acidocaldarius* with Cd.

## BIBLIOGRAPHY

- [1] S. Ahrland, J. Chatt, and N. R. Davies. The relative affinities of ligand atoms for acceptor molecules and ions. *Quarterly Reviews of the Chemical Society*, 12:265–276, 1958.
- [2] J. P. Allewalt, N. P. Revsbech, K. Slack, and D. M. Ward. Effect of Temperature and Light on Growth of and Photosynthesis by *Synechococcus* isolates typical of those predominating in the Octopus Spring microbial mat community of Yellowstone National Park. *Applied and Environmental Microbiology*, 72(1):544–550, 2006.
- [3] E. B. Alsop, E. S. Boyd, and J. Raymond. Merging metagenomics and geochemistry reveals environmental controls on biological diversity and evolution. *BMC Ecology*, 14:1–12, 2014.
- [4] M. J. Amenabar, E. L. Shock, E. E. Roden, J. W. Peters, and E. S. Boyd. Microbial substrate preference dictated by energy demand rather than supply. *Nature Geoscience*, 10(8):577–581, 2017.
- [5] J. P. Amend and H. C. Helgeson. Calculation of the standard molal thermodynamic properties of aqueous biomolecules at elevated temperatures and pressures Part 1L- $\alpha$ -Amino acids. *Journal of the Chemical Society, Faraday Transactions*, 93(10):1927–1941, 1997.
- [6] J. P. Amend, D. E. LaRowe, T. M. McCollom, and E. L. Shock. The energetics of organic synthesis inside and outside the cell. *Philosophical Transactions of the Royal Society B: Biological Sciences*, 368(1622):1–15, 2013.
- [7] J. P. Amend and A. V. Plyasunov. Carbohydrates in thermophile metabolism: Calculation of the standard molal thermodynamic properties of aqueous pentoses and hexoses at elevated temperatures and pressures. *Geochimica et Cosmochimica Acta*, 65(21):3901–3916, 2001.
- [8] J. P. Amend, K. L. Rogers, E. L. Shock, S. Gurrieri, and S. Inguaggiato. Energetics of chemolithoautotrophy in the hydrothermal system of Vulcano Island, southern Italy. *Geobiology*, 1:37–58, 2003.

- [9] J. P. Amend and E. L. Shock. Energetics of overall metabolic reactions of thermophilic and hyperthermophilic Archaea and Bacteria. *FEMS Microbiology Reviews*, 25:175–243, 2001.
- [10] P. Amico, G. Arena, P. Daniele, G. Ostacoli, E. Rizzarelli, and S. Sammartano. Mixed-metal complexes in solution. 3. thermodynamic study of heterobinuclear copper(ii)-l-histidine and -histamine complexes in aqueous solution. *Inorganic Chemistry*, 20(3):772–777, 1981.
- [11] K. Apel and H. Hirt. Reactive Oxygen Species: Metabolism, oxidative stress, and signal transduction. *Annual Review of Plant Biology*, 55(1):373–399, 2004.
- [12] S. J. Ashcroft and C. T. Mortimer. *Thermochemistry of transition metal complexes*. Academic Press, London/ New York, 1970.
- [13] H. Babich and G. Stotzky. Sensitivity of various bacteria, including Actinomycetes, and fungi to cadmium and the influence of ph on sensitivity. *Applied and Environmental Microbiology*, 33:681–695, 1977.
- [14] M. R. Badger and E. J. Bek. Multiple Rubisco forms in proteobacteria : their functional significance in relation to  $CO_2$  acquisition by the CBB cycle. *Journal of Experimental Botany*, 59:1525–1541, 2008.
- [15] J. W. Ball, R. B. McMleskey, and D. K. Nordstrom. Water-chemistry data for selected springs, geysers, and streams in yellowstone national park, wyoming, 2006-2008. Technical report, U.S. Geological Survey, 2010. Open-File Report 2010-1192.
- [16] J. W. Ball, K. D. Nordstrom, R. B. McCleskey, M. A. Schoonen, and Y. Xu. Water-chemistry and on-site sulfur-speciation data for selected springs in yellowstone national park, wyoming, 1996-1998. Technical report, U.S. Geological Survey, 2001. Open-File Report 01-49.
- [17] J. L. Barron and D. R. Lueking. Growth and maintenance of *Thiobacillus ferrooxidans* cells. *Applied and Environmental Microbiology*, 56(9), 1990.
- [18] N. Barros and S. Feijóo. A combined mass and energy balance to provide bioindicators of soil microbiological quality. *Biophysical Chemistry*, 104(3):561–572, 2003.
- [19] M. Bastías and J. Gentina. Variables affecting the growth and ferrous oxidation capacity of *L. Ferrooxidans* in continuous culture. *Hydrometallurgy*, 104(3):351–355, 2010.

- [20] E. Battley. A theoretical study of the thermodynamics of microbial growth using *Saccharomyces cerevisiae* and a different free energy equation. *The Quarterly Review of Biology*, 88(2):69–96, 2013.
- [21] M. T. Beck and I. Nagypal. *Chemistry of complex equilibria*. Budapest: Akademiai Kiado, 1990.
- [22] I. A. Berg, D. Kockelkorn, W. Buckel, and G. Fuchs. A 3-Hydroxypropionate / 4-Hydroxybutyrate Autotrophic Carbon Dioxide Assimilation Pathway in Archaea. *Science*, 318(5857):1782–1786, 2007.
- [23] H. C. Bernstein, J. P. Beam, M. A. Kozubal, R. P. Carlson, and W. P. Inskeep. In situ analysis of oxygen consumption and diffusive transport in high-temperature acidic iron-oxide microbial mats. *Environmental Microbiology*, 15:2360–2370, 2013.
- [24] E. S. Boyd, R. A. Jackson, G. Encarnacion, J. A. Zahn, T. Beard, W. D. Leavitt, Y. Pi, C. L. Zhang, A. Pearson, and G. G. Geesey. Isolation, characterization, and ecology of sulfur-respiring Crenarchaea inhabiting acid-sulfate-chloride-containing geothermal springs in Yellowstone National Park. *Applied and Environmental Microbiology*, 73(20):6669–6677, 2007.
- [25] O. Braissant, D. Wirz, B. Göpfert, and A. U. Daniels. Use of isothermal microcalorimetry to monitor microbial activities. *FEMS Microbiology Letters*, 303(1):1–8, 2010.
- [26] T. D. Brock, K. M. Brock, R. T. Belly, and R. L. Weiss. *Sulfolobus*: a new genus of sulfur-oxidizing bacteria living at low pH and high temperature. *Archiv für Mikrobiologie*, 84(1):54–68, 1972.
- [27] G. E. Brown, A. L. Foster, and J. D. Ostergren. Mineral surfaces and bioavailability of heavy metals: A molecular-scale perspective. *Proceedings of the National Academy of Sciences*, 96(7):3388–3395, 1999.
- [28] P. G. G. Burnett, K. Handley, D. Peak, and C. J. Daughney. Divalent metal adsorption by the thermophile *Anoxybacillus flavithermus* in single and multi-metal systems. *Chemical Geology*, 244:493–506, 2007.
- [29] R. Chakravarty and P. C. Banerjee. Mechanism of cadmium binding on the cell wall of an acidophilic bacterium. *Bioresource Technology*, 108:176 – 183, 2012.
- [30] B. Chapman, D. Jones, and R. Jung. Processes controlling metal ion attenuation in acid mine drainage streams. *Geochimica et Cosmochimica Acta*, 47(11):1957 – 1973, 1983.

- [31] M. Clark, J. Batty, C. van Buuren, D. Dew, and M. Eamon. Biotechnology in minerals processing: Technological breakthroughs creating value. *Hydrometallurgy*, 83(1):3–9, 2006. 16th International Biohydrometallurgy Symposium.
- [32] J. D. Cline. Spectrophotometric determination of hydrogen sulfide in natural waters. *Limnology and Oceanography*, 14:454–458, 1969.
- [33] D. R. Colman, J. Feyhl-Buska, K. M. Fecteau, H. Xu, E. L. Shock, and E. S. Boyd. Ecological differentiation in planktonic and sediment-associated chemotrophic microbial populations in Yellowstone hot springs. *FEMS Microbiology Ecology*, 92(9):1–13, 2016.
- [34] J.-L. Cordier, B. M. Butsch, B. Birou, and U. von Stockar. The relationship between elemental composition and heat of combustion of microbial biomass. *Applied Microbiology and Biotechnology*, 25:305–312, 1987.
- [35] K. C. Costa, J. B. Navarro, E. L. Shock, C. L. Zhang, D. Soukup, and B. P. Hedlund. Microbiology and geochemistry of great boiling and mud hot springs in the United States Great Basin. *Extremophiles*, 13(3):447–459, 2009.
- [36] K. C. Costa, S. H. Yoon, M. Pan, J. A. Burn, N. S. Baliga, and J. A. Leigh. Effects of H<sub>2</sub> and formate on growth yield and regulation of methanogenesis in *Methanococcus maripaludis*. *Journal of Bacteriology*, 195(7):1456–1462, 2013.
- [37] P. G. Daniele, O. Zerbinati, R. Aruga, and G. Ostacoli. Thermodynamic and spectrophotometric study of copper(II) and cadmium(II) homo- and hetero-nuclear complexes with L-histidylglycine in an aqueous medium. *Journal of the Chemical Society, Dalton Transactions*, 0(5):1115–1120, 1988.
- [38] C. J. Daughney and J. B. Fein. Sorption of 2,4,6-trichlorophenol by *Bacillus subtilis*. *Environmental Science and Technology*, 32(6):749–752, March 1998.
- [39] M. Dauner, T. Storni, U. Sauer, and U. W. E. Sauer. *Bacillus subtilis* metabolism and energetics in carbon-limited and excess-carbon chemostat culture. *Journal of Bacteriology*, 183(24):7308–7317, 2001.
- [40] M. Dopson, C. Baker-Austin, P. R. Koppineedi, and P. L. Bond. Growth in sulfidic mineral environments: Metal resistance mechanisms in acidophilic micro-organisms. *Microbiology*, 149(8):1959–1970, 2003.
- [41] M. Dopson, F. J. Ossandon, L. Lovgren, and D. S. Holmes. Metal resistance or tolerance? Acidophiles confront high metal loads via both abiotic and biotic mechanisms. *Frontiers in Microbiology*, 5:10–13, 2014.

- [42] J. S. España, E. L. Pamo, E. Santofimia, O. Aduvire, J. Reyes, and D. Baretino. Acid mine drainage in the Iberian Pyrite Belt (Odiel river watershed, Huelva, SW Spain): Geochemistry, mineralogy and environmental implications. *Applied Geochemistry*, 20:1320 – 1356, 2005.
- [43] M. Esparza, B. Bowien, E. Jedlicki, and D. S. Holmes. Gene organization and CO<sub>2</sub>-responsive expression of four *cbb* operons in the biomining bacterium *Acidithiobacillus ferrooxidans*. *Advanced Materials Research*, 71-73:207–210, 2009.
- [44] M. Esparza, J. P. Cárdenas, B. Bowien, E. Jedlicki, and D. S. Holmes. Genes and pathways for CO<sub>2</sub> fixation in the obligate, chemolithoautotrophic acidophile, *Acidithiobacillus ferrooxidans*, carbon fixation in *A. ferrooxidans*. *BMC microbiology*, 10:229, 2010.
- [45] J. B. Fein, J.-F. Boily, N. Yee, D. Gorman-Lewis, and B. F. Turner. Potentiometric titrations of *Bacillus subtilis* cells to low pH and a comparison of modeling approaches. *Geochimica et Cosmochimica Acta*, 69(5):1123–1132, 2005.
- [46] J. B. Fein, C. J. Daughney, N. Yee, and T. A. Davis. A chemical equilibrium model for metal adsorption onto bacterial surfaces. *Geochimica et Cosmochimica Acta*, 61(16):3319–3328, 1997.
- [47] C. B. Fliermans and T. D. Brock. Ecology of sulfur-oxidizing bacteria in hot acid soils. *Journal of Bacteriology*, 111(2):343–350, 1972.
- [48] B. W. Fouke. Hot-spring Systems Geobiology: Abiotic and biotic influences on travertine formation at Mammoth Hot Springs, Yellowstone National Park, USA. *Sedimentology*, 58(1):170–219, 2011.
- [49] I. Fridovich. Fundamental Aspects of Reactive Oxygen Species, or What’s the Matter with Oxygen? *Annals of the New York Academy of Sciences*, 893(1):13–18, 1999.
- [50] C. G. Friedrich, D. Rother, F. Bardischewsky, A. Ouentmeier, and J. Fischer. Oxidation of reduced inorganic sulfur compounds by bacteria: Emergence of a common mechanism? *Applied and Environmental Microbiology*, 67(7):2873–2882, 2001.
- [51] T. Fuchs, H. Huber, S. Burggraf, and K. O. Stetter. 16S rDNA-based phylogeny of the Archaeal order *Sulfolobales* and Reclassification of *Desulfurolobus ambivalens* as *Acidianus ambivalens* comb. nov. *Systematic and Applied Microbiology*, 19(1):56–60, 1996.

- [52] H. P. Fuchslin, C. Schneider, and T. Egli. In glucose-limited continuous culture the minimum substrate concentration for growth,  $s_{min}$ , is crucial in the competition between the enterobacterium *Escherichia coli* and *Chelatobacter heintzii*, an environmentally abundant bacterium. *ISME Journal*, 6(4):777–789, 2012.
- [53] E. Galán, J. Gómez-Ariza, I. González, J. Fernández-Caliani, E. Morales, and I. Giráldez. Heavy metal partitioning in river sediments severely polluted by acid mine drainage in the Iberian Pyrite Belt. *Applied Geochemistry*, 18:409 – 421, 2003.
- [54] A. García-Moyano, E. González-Toril, A. Aguilera, and R. Amils. Prokaryotic community composition and ecology of floating macroscopic filaments from an extreme acidic environment, Río Tinto (SW, Spain). *Systematic and Applied Microbiology*, 30(8):601–614, 2007.
- [55] W. Ghosh and B. Dam. Biochemistry and molecular biology of lithotrophic sulfur oxidation by taxonomically and ecologically diverse bacteria and archaea. *FEMS Microbiology Reviews*, 33(6):999–1043, 2009.
- [56] B. Ginn and J. B. Fein. Temperature dependence of Cd and Pb binding onto bacterial cells. *Chemical Geology*, 259(3):99–106, 2009.
- [57] R. González-Cabaleiro, I. D. Olieru, J. M. Lema, and J. Rodríguez. Microbial catabolic activities are naturally selected by metabolic energy harvest rate. *ISME Journal*, 9:2630–2641, 2015.
- [58] D. Gorman-Lewis. Enthalpies and Entropies of Cd and Zn Adsorption onto *Bacillus licheniformis* and Enthalpies and Entropies of Zn Adsorption onto *Bacillus subtilis* from Isothermal Titration Calorimetry and Surface Complexation Modeling. *Geomicrobiology Journal*, 31(5):383–395, 2014.
- [59] D. Gorman-Lewis, J. B. Fein, and M. P. Jensen. Enthalpies and entropies of proton and cadmium adsorption onto *Bacillus subtilis* bacterial cells from calorimetric measurements. *Geochimica et Cosmochimica Acta*, 70(19):4862–4873, 2006.
- [60] D. Gorman-Lewis, W. Martens-Habbena, and D. A. Stahl. Thermodynamic characterization of proton-ionizable functional groups on the cell surfaces of ammonia-oxidizing bacteria and archaea. *Geobiology*, 12(2):157–171, 2014.
- [61] I. Grenthe, H. Ots, and O. Ginstrup. A calorimetric determination of the enthalpy of ionization of water and the enthalpy of protonation of THAM at 5, 20, 25, 35, and 50 degrees C. *Acta Chemica Scandinavica*, 24:1067–1080, 1970.



- [62] D. W. Grogan. Phenotypic characterization of the archaeobacterial genus *Sulfolobus*: Comparison of five wild-type strains. *Journal of Bacteriology*, 171:6710–6719, 1989.
- [63] T. Gurakan, I. W. Marison, U. von Stockar, L. Gustafsson, and E. Gnaiger. Proposals for a standardized sample handling procedure for the determination of elemental composition and enthalpy of combustion of biological material. *Thermochimica Acta*, 172:251–266, 1990.
- [64] L. Gustafsson. Microbiological calorimetry. *Thermochimica Acta*, 193:145–171, 1991.
- [65] J. R. Haas. Effects of cultivation conditions on acidbase titration properties of *Shewanella putrefaciens*. *Chemical Geology*, 209(1):67–81, 2004.
- [66] C. M. Hansel, C. J. Lentini, Y. Tang, D. T. Johnston, S. D. Wankel, and P. M. Jardine. Dominance of sulfur-fueled iron oxide reduction in low-sulfate freshwater sediments. *ISME Journal*, 9(11):2400–2412, 2015.
- [67] C. Hart and D. Gorman-Lewis. Energetics of *Acidianus ambivalens* growth in response to oxygen availability. *In prep*, 2018.
- [68] J. J. Heijnen and R. Kleerebezem. *Bioenergetics of Microbial Growth in Encyclopedia of Industrial Biotechnology*, pages 1–66. John Wiley & Sons Inc., 2010.
- [69] J. J. Heijnen and J. P. van Dijken. In search of a thermodynamic description of biomass yields for the chemotrophic growth of microorganisms. *Biotechnology and Bioengineering*, 39:833–858, 1992.
- [70] S. Heinhorst, S. H. Baker, D. R. Johnson, P. S. Davies, G. C. Cannon, and J. M. Shively. Two copies of form I RuBisCO genes in *Acidithiobacillus ferrooxidans* ATCC 23270. *Current Microbiology*, 45(2):115–117, 2002.
- [71] H. Helgeson, D. Kirkham, and G. Flowers. Theoretical prediction of the thermodynamic behavior of aqueous electrolytes at high pressures and temperatures: IV. Calculation of activity coefficients, osmotic coefficients, and apparent molal and standard and relative partial molal properties to 600° C and 5 kb. *American Journal of Science*, 281(10):1249–1516, 1981.
- [72] H. C. Helgeson, J. M. Delany, H. Nesbitt, and D. K. Bird. Summary and critique of the thermodynamic properties of rock-forming minerals. *American Journal of Science*, 278, 1978.

- [73] L. Holuigue, L. Herrera, O. Phillips, and M. Young. CO<sub>2</sub> Fixation by mineral-leaching bacteria: Characteristics of the ribulose biphosphate carboxylase-oxygenase of *Thiobacillus ferrooxidans*. *Biotechnology and Applied Biochemistry*, 9(6):497–505, 1987.
- [74] R. Homsher and B. Zak. Spectrophotometric investigation of sensitive complexing agents for the determination of zinc in serum. *Clinical chemistry*, 31:1310–1313, 1985.
- [75] Q. Huang, H. Jiang, B. R. Briggs, S. Wang, W. Hou, G. Li, G. Wu, R. Solis, C. A. Arcilla, T. Abrajano, and H. Dong. Archaeal and bacterial diversity in acidic to circumneutral hot springs in the Philippines. *FEMS Microbiology Ecology*, 85(3):452–464, 2013.
- [76] R. Huber, T. Willharm, D. Huber, A. Trincone, S. Burggraf, H. König, R. Rachel, I. Rockinger, H. Fricke, and K. O. Stetter. Aquifex pyrophilus gen. nov. sp. no., represents a novel group of marine hyperthermophilic hydrogen-oxidizing bacteria. *Systematic and Applied Microbiology*, 15:340–351, 1992.
- [77] M. Hügler, H. Huber, K. O. Stetter, and G. Fuchs. Autotrophic CO<sub>2</sub> fixation pathways in archaea (Crenarchaeota). *Archives of Microbiology*, 179(3):160–173, 2003.
- [78] F. Inagaki, K.-U. Hinrichs, Y. Kubo, M. W. Bowles, V. B. Heuer, W.-L. Hong, T. Hoshino, A. Ijiri, H. Imachi, M. Ito, M. Kaneko, M. A. Lever, Y.-S. Lin, B. A. Methé, S. Morita, Y. Morono, W. Tanikawa, M. Bihan, S. A. Bowden, M. Elvert, C. Glombitza, D. Gross, G. J. Harrington, T. Hori, K. Li, D. Limmer, C.-H. Liu, M. Murayama, N. Ohkouchi, S. Ono, Y.-S. Park, S. C. Phillips, X. Prieto-Mollar, M. Purkey, N. Riedinger, Y. Sanada, J. Sauvage, G. Snyder, R. Susilawati, Y. Takano, E. Tasumi, T. Terada, H. Tomaru, E. Trembath-Reichert, D. T. Wang, and Y. Yamada. Exploring deep microbial life in coal-bearing sediment down to ~2.5 km below the ocean floor. *Science*, 349(6246):420–424, 2015.
- [79] W. P. Inskeep, G. G. Ackerman, W. P. Taylor, M. Kozubal, S. Korf, and R. E. Macur. On the energetics of chemolithotropy in nonequilibrium systems: case studies of geothermal springs in Yellowstone National Park. *Geobiology*, 3(3):297–317, 2005.
- [80] P. Johansson and I. Wadsö. An isothermal microcalorimetric titration/perfusion vessel equipped with electrodes and spectrophotometer. *Thermochimica Acta*, 342(1-2):19–29, 1999.
- [81] D. Johnson. Chemical and microbiological characteristics of mineral spoils and drainage waters at abandoned coal and metal mines. *Water, Air and Soil Pollution: Focus*, 34:47–66, 2003.

- [82] D. B. Johnson and K. B. Hallberg. The microbiology of acidic mine waters. *Research in Microbiology*, 154:466–473, 2003.
- [83] J. W. Johnson, E. H. Oelkers, and H. C. Helgeson. SUPCRT92: A software package for calculating the standard molal thermodynamic properties of minerals, gases, aqueous species, and reactions from 1 to 5000 bar and 0 to 1000C. *Computers & Geosciences*, 18(7):899–947, 1992.
- [84] B. B. Jørgensen. Deep seafloor microbial cells on physiological standby. *Proceedings of the National Academy of Sciences*, 108:18193–18194, 2011.
- [85] D. P. Kelly and A. P. Wood. Reclassification of some species of *Thiobacillus* to the newly designated genera *Acidithiobacillus* gen. nov., *Halothiobacillus* gen. nov. and *Thermithiobacillus* gen. nov. *International Journal of Systematic and Evolutionary Microbiology*, 50(2000):511–516, 2000.
- [86] C. P. Kempes, P. M. V. Bodegom, D. Wolpert, E. Libby, J. Amend, T. Hoehler, P. M. van Bodegom, D. Wolpert, E. Libby, J. Amend, and T. Hoehler. Drivers of bacterial maintenance and minimal energy requirements. *Frontiers in Microbiology*, 8:1–10, 2017.
- [87] E. S. Kempner. Upper temperature limit of life. *American Association for the Advancement of Science*, 142(3597):1318–1319, 1963.
- [88] I. Kim, H. Jang, and J.-U. Lee. Kinetics of Fe<sup>2+</sup> oxidation by *Acidithiobacillus ferrooxidans* using total organic carbon measurement. *Journal of Microbiology and Biotechnology*, 12(2):268–272, 2002.
- [89] R. Kleerebezem and M. C. M. van Loosdrecht. Thermodynamic and kinetic characterization using process dynamics: Acidophilic ferrous iron oxidation by *Leptospirillum ferrooxidans*. *Biotechnology and Bioengineering*, 100(1):49–60, 2007.
- [90] A. Kletzin. Coupled enzymatic production of sulfite, thiosulfate, and hydrogen sulfide from sulfur: purification and properties of a sulfur oxygenase reductase from the facultatively anaerobic archaeobacterium *Desulfurolobus ambivalens*. *Journal of Bacteriology*, 171:1638–1643, 1989.
- [91] A. Kletzin, T. Urich, F. Müller, T. M. Bandejas, and C. M. Gomes. Dissimilatory oxidation and reduction of elemental sulfur in thermophilic archaea. *Journal of bioenergetics and biomembranes*, 36(1):77–91, feb 2004.

- [92] C. Knoblauch and B. B. Jorgensen. Effect of temperature on sulphate reduction, growth rate and growth yield in five psychrophilic sulphate-reducing bacteria from Arctic sediments. *Environmental Microbiology*, 1(5):457–467, 1999.
- [93] M. A. Kozubal, R. E. Macur, Z. J. Jay, J. P. Beam, S. A. Malfatti, S. G. Tringe, B. D. Kocar, T. Borch, and W. P. Inskeep. Microbial iron cycling in acidic geothermal springs of Yellowstone National Park: Integrating molecular surveys, geochemical processes, and isolation of novel Fe-active microorganisms. *Frontiers in Microbiology*, 3:Article 109, 2012.
- [94] C. Larsson, A. Blomberg, and L. Gustafsson. Use of microcalorimetric monitoring in establishing continuous energy balances and in continuous determinations of substrate and product concentrations of batch-grown *Saccharomyces cerevisiae*. *Biotechnology and Bioengineering*, 38:447–458, 1991.
- [95] C. Larsson, U. von Stockar, I. Marison, and L. Gustafsson. Growth and metabolism of *Saccharomyces cerevisiae* in chemostat cultures under carbon-, nitrogen-, or carbon- and nitrogen-limiting conditions. *J Bacteriol*, 175(15):4809–4816, 1993.
- [96] J. S. Liu, N. Schill, W. M. Van Gulik, D. Voisard, I. W. Marison, and U. Von Stockar. The coupling between catabolism and anabolism of *Methanobacterium thermoautotrophicum* in H<sub>2</sub>- and iron-limited continuous cultures. *Enzyme and Microbial Technology*, 25(10):784–794, 1999.
- [97] Y. Liu, L. L. Beer, and W. B. Whitman. Sulfur metabolism in archaea reveals novel processes. *Environmental Microbiology*, 14(10):2632–2644, 2012.
- [98] D. R. Lovley. Dissimilatory metal reduction. *Annual Reviews in Microbiology*, 47:263–290, 1993.
- [99] O. H. Lowry, N. J. Rosebrough, A. L. Farr, and R. J. Randall. Protein measurement with the Folin phenol reagent. *Journal of Biological Chemistry*, 193:265–275, 1951.
- [100] M. Lunau, A. Lemke, K. Walther, W. Martens-Habbena, and M. Simon. An improved method for counting bacteria from sediments and turbid environments by epifluorescence microscopy. *Environmental Microbiology*, 7(7):961–968, 2005.
- [101] W. S. Maaty, B. Wiedenheft, P. Tarlykov, N. Schaff, J. Heinemann, J. Robison-Cox, J. Valenzuela, A. Dougherty, P. Blum, C. M. Lawrence, T. Douglas, M. J. Young, and B. Bothner. Something old, something new, something borrowed; how the thermoacidophilic archaeon *Sulfolobus solfataricus* responds to oxidative stress. *PLoS ONE*, 4(9), 2009.

- [102] R. E. Macur, Z. J. Jay, W. P. Taylor, M. A. Kozubal, B. D. Kocar, and W. P. Inskeep. Microbial community structure and sulfur biogeochemistry in mildly-acidic sulfidic geothermal springs in Yellowstone National Park. *Geobiology*, 11(1):86–99, 2013.
- [103] A. Martell, R. Smith, and R. Motekaitis. Critically selected stability constants of metal complexes Database Version 5.0. *NIST Standard Reference Database*, vol. 46, 1998. NIST Standard Reference Data.
- [104] A. E. Martell and R. D. Hancock. *Metal complexes in aqueous solution*. Plenum Press, New York, 1996.
- [105] R. E. Martinez, D. Smith, E. Kulczycki, and F. Ferris. Determination of intrinsic bacterial surface acidity constants using a Donnan shell model and a continuous  $pK_a$  distribution method. *Journal of Colloid And Interface Science*, 253(1):130–139, 2002.
- [106] J. Mathur, R. W. Bizzoco, D. G. Ellis, D. A. Lipson, A. W. Poole, R. Levine, and S. T. Kelley. Effects of abiotic factors on the phylogenetic diversity of bacterial communities in acidic thermal springs. *Applied and Environmental Microbiology*, 73(8):2612–2623, 2007.
- [107] S. McCarthy, T. Johnson, B. J. Pavlik, S. Payne, W. Schackwitz, J. Martin, A. Lipzen, E. Keffeler, and P. Blum. Expanding the limits of thermoacidophily by adaptive evolution. *Applied and Environmental Microbiology*, 82(3):857–867, 2016.
- [108] T. M. McCollom and J. P. Amend. A thermodynamic assessment of energy requirements for biomass synthesis by chemolithoautotrophic micro-organisms in oxic and anoxic environments. *Geobiology*, 3:135–144, 2005.
- [109] D. R. Meyer-Dombard, E. L. Shock, and J. P. Amend. Archaeal and bacterial communities in geochemically diverse hot springs of Yellowstone National Park, USA. *Geobiology*, 3:211–227, 2005.
- [110] K. W. Miller, S. S. Risanico, and J. Bruno Risatti. Differential tolerance of *Sulfolobus* strains to transition metals. *FEMS Microbiology Letters*, 93(1):69–73, 1992.
- [111] V. S. Mukhanov, L. D. Hansen, and R. B. Kemp. Nanocalorimetry of respiration in micro-organisms in natural waters. *Thermochimica Acta*, 531:66–69, 2012.
- [112] M. D. Mullen, D. C. Wolf, F. G. Ferris, T. J. Beveridge, C. A. Flemming, and G. W. Bailey. Bacterial sorption of heavy metals. *Applied and Environmental Microbiology*, 55:3143–3149, 1989.

- [113] K. H. Nealson and D. A. Stahl. Microorganisms and biogeochemical cycles; what can we learn from layered microbial communities? *Reviews in Mineralogy and Geochemistry*, 35:5, 1997.
- [114] M. Neveu, A. T. Poret-Peterson, A. D. Anbar, and J. J. Elser. Ordinary stoichiometry of extraordinary microorganisms. *Geobiology*, 14(1):33–53, 2016.
- [115] B. T. Ngwenya, I. W. Sutherland, and L. Kennedy. Comparison of the acid-base behaviour and metal adsorption characteristics of a gram-negative bacterium with other strains. *Applied Geochemistry*, 18(4):527–538, 2003.
- [116] D. Nordstrom, R. McCleskey, and J. W. Ball. Sulfur geochemistry of hydrothermal waters in Yellowstone National Park: IV Acidsulfate waters. *Applied Geochemistry*, 24:191–207, 2009.
- [117] D. K. Nordstrom and C. N. Alpers. Negative pH, efflorescent mineralogy, and consequences for environmental restoration at the Iron Mountain Superfund site, California. *Proceedings of the National Academy of Sciences*, 96(7):3455–3462, 1999.
- [118] D. K. Nordstrom and G. Southam. Geomicrobiology of sulfide mineral oxidation. *Reviews in Mineralogy*, 35:361–390, 1997.
- [119] D. L. Parkhurst and C. A. J. Appelo. User’s guide to PHREEQC (Version 2): a computer program for speciation, batch-reaction, one-dimensional transport, and inverse geochemical calculations. Technical report, U.S. Geological Survey: Earth Science Information Center, Open-File Reports 99-4259, 1999.
- [120] R. G. Pearson. Hard and soft acids and bases, HSAB, part I: Fundamental principles. *Journal of Chemical Education*, 45(9):581–587, 1968.
- [121] R. G. Pearson. Hard and soft acids and bases, HSAB, part II: Underlying theories. *Journal of Chemical Education*, 45(10):643–648, 1968.
- [122] L. Pettit and K. Powell. Iupac stability constants database (sc-database) academic software data version. *Academic Software, Otley, West Yorkshire, UK*, 2005.
- [123] B. Planer-Friedrich, J. London, R. B. McCleskey, D. K. Nordstrom, and D. Wallschläger. Thioarsenates in geothermal waters of yellowstone National Park: Determination, preservation, and geochemical importance. *Environmental Science and Technology*, 41(15):5245–5251, 2007.

- [124] B. Planer-Friedrich and B. J. Merkel. Volatile metals and metalloids in hydrothermal gases. *Environmental Science and Technology*, 40(10):3181–3187, 2006.
- [125] A. C. Plette, W. H. van Riemsdijk, M. F. Benedetti, and A. van Der Wal. pH dependent charging behavior of isolated cell walls of a gram-positive soil bacterium. *Journal of Colloid And Interface Science*, 173(2):354–363, 1995.
- [126] P. Ramírez, N. Guiliani, L. Valenzuela, S. Beard, and C. Jerez. Differential protein expression during growth of *Acidithiobacillus ferrooxidans* on ferrous iron, sulfur compounds, or metal sulfides. *Applied and Environmental Microbiology*, 70(8):4491–4498, 2004.
- [127] P. Ranawat and S. Rawat. Stress response physiology of thermophiles. *Archives of Microbiology*, 199(3):391–414, 2017.
- [128] F. Remonsellez, A. Orell, and C. A. Jerez. Copper tolerance of the thermoacidophilic archaeon *Sulfolobus metallicus*: Possible role of polyphosphate metabolism. *Microbiology*, 152(1):59–66, 2006.
- [129] N. P. Revsbech and D. M. Ward. Microelectrode studies of interstitial water chemistry and photosynthetic activity in a hot spring microbial mat. *Applied and environmental microbiology*, 48(2):270–275, 1984.
- [130] A.-L. Reysenbach, M. Ehringer, and K. Hershberger. Microbial diversity at 83°C in Calcite Springs, Yellowstone National Park: another environment where the *Aquificales* and "Korarchaeota" coexist. *Extremophiles*, 4(1):0061–0067, 2000.
- [131] A. Robador, D. E. LaRowe, S. P. Jungbluth, H.-t. Lin, M. S. Rappé, K. H. Nealson, and J. P. Amend. Nanocalorimetric Characterization of Microbial Activity in Deep Subsurface Oceanic Crustal Fluids. *Frontiers in Microbiology*, 7:Article 454, 2016.
- [132] J. B. Russell. The Energy Spilling Reactions of Bacteria and Other Organisms. *J Mol Microbiol Biotechnol*, 13:1–11, 2007.
- [133] J. B. Russell and G. M. Cook. Energetics of bacterial growth: Balance of anabolic and catabolic reactions. *Microbiological Reviews*, 59(1):48–62, 1995.
- [134] I. Sánchez-Andrea, N. Rodríguez, R. Amils, and J. L. Sanz. Microbial diversity in anaerobic sediments at Rio Tinto, a naturally acidic environment with a high heavy metal content. *Applied and Environmental Microbiology*, 77(17):6085–6093, 2011.

- [135] N. Schill, J.-S. Liu, and U. von Stockar. Thermodynamic analysis of growth of *Methanobacterium thermoautotrophicum*. *Biotechnology and Bioengineering*, 64:74–81, 1999.
- [136] A. Schippers and W. Sand. Bacterial leaching of metal sulfides proceeds by two indirect mechanisms via thiosulfate or via polysulfides and sulfur. *Applied and Environmental Microbiology*, 65:319–321, 1999.
- [137] P. Schönheit and T. Schäfer. Metabolism of hyperthermophiles. *World Journal of Microbiology & Biotechnology*, 11:26–57, 1995.
- [138] E. L. Shock. Organic acids in hydrothermal solutions: standard molal thermodynamic properties of carboxylic acids and estimates of dissociation constants at high temperatures and pressures. *American Journal of Science*, 295(5):496–580, 1995.
- [139] E. L. Shock, H. C. Helgeson, and D. A. Sverjensky. Calculation of the thermodynamic and transport properties of aqueous species at high pressures and temperatures: Standard partial molal properties of inorganic neutral species. *Geochimica et Cosmochimica Acta*, 53(9):2157 – 2183, 1989.
- [140] E. L. Shock, M. Holland, D. A. Meyer-dombard, J. P. Amend, G. R. Osburn, and T. P. Fischer. Quantifying inorganic sources of geochemical energy in hydrothermal ecosystems , Yellowstone National Park , USA. *Geochimica et Cosmochimica Acta*, 74(14):4005–4043, 2010.
- [141] E. L. Shock, D. C. Sassani, M. Willis, and D. A. Sverjensky. Inorganic species in geologic fluids: Correlations among standard molal thermodynamic properties of aqueous ions and hydroxide complexes. *Geochimica et Cosmochimica Acta*, 61(5):907–950, 1997.
- [142] M. P. Silverman and D. G. Lundgren. Studies on the chemotrophic iron Bacterium *Ferrobacillus ferrooxidans* II.: Manometric Studies. *Journal of Bacteriology*, 78:326331, 1959.
- [143] G. Simon, J. Walther, N. Zabeti, Y. Combet-Blanc, R. Auria, J. Van Der Oost, and L. Casalot. Effect of O<sub>2</sub> concentrations on *Sulfolobus solfataricus* P2. *FEMS Microbiology Letters*, 299(2):255–260, 2009.
- [144] M. Simon and F. Azam. Protein content and protein synthesis rates of planktonic marine bacteria. *Marine Ecology Progress Series*, 51(3):201–213, 1989.
- [145] S. Sjöberg. Critical evaluation of stability constants of metal-imidazole and metal-histamine systems. *Pure And Applied Chemistry*, 69(7):1549–1570, July 1997.



- [146] S. Skirnisdottir, G. O. Hreggvidsson, S. Hjörleifsdottir, V. T. Marteinson, K. Solveig, O. Holst, and J. K. Kristjansson. Influence of Sulfide and Temperature on Species Composition and Community Structure of Hot Spring Microbial Mats Influence of Sulfide and Temperature on Species Composition and Community Structure of Hot Spring Microbial Mats. *Applied and Environmental Microbiology*, 66:2835–2841, 2000.
- [147] J. N. Smith and E. L. Shock. A thermodynamic analysis of microbial growth experiments. *Astrobiology*, 7(6):891–904, dec 2007.
- [148] J. R. Spear, J. J. Walker, T. M. Mccollom, and N. R. Pace. Hydrogen and bioenergetics in the Yellowstone geothermal ecosystem. *Proceedings of the National Academy of Sciences*, 102:2555–2560, 2004.
- [149] K. O. Stetter. Hyperthermophilic procaryotes. *FEMS Microbiology Reviews*, 18:149–158, 1996.
- [150] U. V. Stockar, J. S. Liu, U. von Stockar, and J. S. Liu. Does microbial growth always feed on negative entropy thermodynamic analysis of microbial growth. *Biochimica et Biophysica Acta*, 1412:191–211, 1999.
- [151] L. M. Stout, R. E. Blake, J. P. Greenwood, A. M. Martini, and E. C. Rose. Microbial diversity of boron-rich volcanic hot springs of St. Lucia, Lesser Antilles. *FEMS Microbiology Ecology*, 70(3):402–412, 2009.
- [152] W. Sun, E. Xiao, V. Krumins, Y. Dong, and T. Xiao. Characterization of the microbial community composition and the distribution of Fe-metabolizing bacteria in a creek contaminated by acid mine drainage. *Applied Microbiology and Biotechnology*, 100:8523–8535, 2016.
- [153] I. Suzuki, T. L. Takeuchi, T. D. Yuthasastrakosol, and J. K. Oh. Ferrous iron and sulfur oxidation and ferric iron reduction activities of *Thiobacillus ferrooxidans* are affected by growth on ferrous iron, sulfur, or a sulfide ore. *Applied and Environmental Microbiology*, 56(6):1620–1626, 1990.
- [154] W. D. Swingley, D. R. Meyer-Dombard, E. L. Shock, E. B. Alsop, H. D. Falenski, J. R. Havig, and J. Raymond. Coordinating environmental genomics and geochemistry reveals metabolic transitions in a hot spring ecosystem. *PLoS ONE*, 7(6), 2012.
- [155] J. Telling, E. S. Boyd, N. Bone, E. L. Jones, M. Tranter, J. W. Macfarlane, P. G. Martin, J. L. Wadham, G. Lamarche-Gagnon, M. L. Skidmore, T. L. Hamilton, E. Hill, M. Jackson, and D. A. Hodgson. Rock comminution as a source of hydrogen for subglacial ecosystems. *Nature Geoscience*, 8(11):851–855, 2015.

- [156] R. K. Thauer, K. Jungermann, and K. Decker. Energy conservation in chemotrophic anaerobic bacteria. *Bacteriological reviews*, 41(1):100–180, 1977.
- [157] J. Tourney, B. T. Ngwenya, J. W. F. Mosselmans, L. Tetley, and G. L. Cowie. The effect of extracellular polymers (EPS) on the proton adsorption characteristics of the thermophile *Bacillus licheniformis* S-86. *Chem. Geol.*, 247(1-2):1–15, 2008.
- [158] A. S. Traore, C. E. Hatchikian, J. le Gall, and J.-P. Belaich. Microcalorimetric studies of the growth of sulfate-reducing bacteria: comparison of the growth parameters of some *Desulfovibrio* species. *Journal of Bacteriology*, 149(2):606–611, 1982.
- [159] O. H. Tuovinen, S. I. Niemelä, and H. G. Gyllenberg. Tolerance of *Thiobacillus ferrooxidans* to some metals. *Antonie van Leeuwenhoek*, 37:489–496, 1971.
- [160] J. Valdés, I. Pedroso, R. Quatrini, R. J. Dodson, H. Tettelin, R. Blake, J. A. Eisen, and D. S. Holmes. *Acidithiobacillus ferrooxidans* metabolism: from genome sequence to industrial applications. *BMC Genomics*, 9(1):597, 2008.
- [161] E. Viollier, P. Inglett, K. Hunter, A. Roychoudhury, and P. V. Cappellen. The ferrozine method revisited: Fe(II)/Fe(III) determination in natural waters. *Applied Geochemistry*, 15(6):785 – 790, 2000.
- [162] U. von Stockar, L. Gustafsson, C. Larsson, I. Marison, P. Tissot, and E. Gnaiger. Thermodynamic considerations in constructing energy balances for cellular growth. *Biochimica et Biophysica Acta*, 1183:221–240, 1993.
- [163] U. von Stockar, C. Larsson, and I. W. Marison. Calorimetry and energetic efficiencies in aerobic and anaerobic microbial growth. *Pure and Applied Chemistry*, 65(9):1889–1892, 1993.
- [164] U. von Stockar, T. Maskow, J. Liu, I. W. Marison, and R. Patiño. Thermodynamics of microbial growth and metabolism: An analysis of the current situation. *Journal of Biotechnology*, 121(4):517–533, 2006.
- [165] I. Wadsö and R. N. Goldberg. Standards in isothermal microcalorimetry (IUPAC Technical Report). *Pure and Applied Chemistry*, 73(10):1625–1639, 2001.
- [166] C. L. Wang, P. C. Michels, S. C. Dawson, S. Kitisakkul, J. Baross, and D. S. Clark. Cadmium removal by a new strain of *Pseudomonas aeruginosa* in aerobic culture. *Applied and Environmental Microbiology*, 63:4075–4078, 1997.

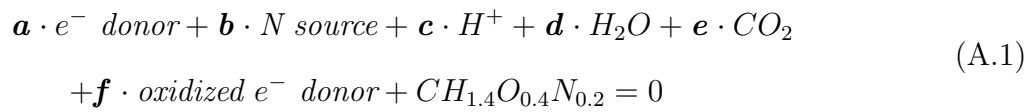
- [167] J. Wang, J. Bai, J. Xu, and B. Liang. Bioleaching of metals from printed wire boards by *Acidithiobacillus ferrooxidans* and *Acidithiobacillus thiooxidans* and their mixture. *Journal of Hazardous Materials*, 172(2-3):1100–1105, 2009.
- [168] Y. S. Wang, Z. Y. Pan, J. M. Lang, J. M. Xu, and Y. G. Zheng. Bioleaching of chromium from tannery sludge by indigenous *Acidithiobacillus thiooxidans*. *Journal of Hazardous Materials*, 147(1-2):319–324, 2007.
- [169] D. M. Ward, M. J. Ferris, S. C. Nold, and M. M. Bateson. A natural view of microbial biodiversity within hot spring cyanobacterial mat communities. *Microbiology and molecular biology reviews : MMBR*, 62(4):1353–1370, 1998.
- [170] L. Warren and F. Ferris. Continuum between sorption and precipitation of fe(iii) on microbial surfaces. *Environmental Science & Technology*, 32:2331–2337, 1998.
- [171] J. C. Westall. Fiteql 2.0, a computer program for determination of chemical equilibrium constants from experimental data. Technical Report Report 82-08, Department of Chemistry, Oregon State University, Corvallis, OR., 1982.
- [172] G. Wheaton, J. Counts, A. Mukherjee, J. Kruh, and R. Kelly. The confluence of heavy metal biooxidation and heavy metal resistance: Implications for bioleaching by extreme thermoacidophiles. *Minerals*, 5(3):397–451, 2015.
- [173] B. Wiedenheft, J. Mosolf, D. Willits, M. Yeager, K. a. Dryden, M. Young, and T. Douglas. An archaeal antioxidant: characterization of a Dps-like protein from *Sulfolobus solfataricus*. *Proceedings of the National Academy of Sciences of the United States of America*, 102(30):10551–6, 2005.
- [174] M. Wikström and M. I. Verkhovsky. Mechanism and energetics of proton translocation by the respiratory heme-copper oxidases. *Biochimica et Biophysica Acta - Bioenergetics*, 1767(10):1200–1214, 2007.
- [175] M. Winkelmann, R. Hüttl, and G. Wolf. Application of batch-calorimetry for the investigation of microbial activity. *Thermochimica Acta*, 415(1-2):75–82, 2004.
- [176] Y. Xu, M. A. A. Schoonen, D. K. Nordstrom, K. M. Cunningham, and J. W. Ball. Sulfur geochemistry of hydrothermal waters in Yellowstone National Park: I. The origin of thiosulfate in hot spring waters. *Geochimica et Cosmochimica Acta*, 62(23-24):3729–3743, 1998.
- [177] N. Yee, L. G. Benning, V. R. Phoenix, and F. G. Ferris. Characterization of metal-cyanobacteria sorption reactions: a combined macroscopic and infrared spectroscopic investigation. *Environmental Science & Technology*, 38:775–782, 2004.

- [178] H. Yin, X. Zhang, X. Li, Z. He, Y. Liang, X. Guo, Q. Hu, Y. Xiao, J. Cong, L. Ma, J. Niu, and X. Liu. Whole-genome sequencing reveals novel insights into sulfur oxidation in the extremophile *Acidithiobacillus thiooxidans*. *BMC Microbiology*, 14(1):1–14, 2014.
- [179] X. Zhang, X. Liu, and Y. Liang. Metabolic diversity and adaptive mechanisms of iron- and / or sulfur-oxidizing autotrophic acidophiles in extremely acidic environments. *Environmental Microbiology Reports*, 8:738–751, 2016.
- [180] W. Zillig, S. Yeats, I. Holz, A. Böck, F. Gropp, M. Rettenberger, and S. Lutz. Plasmid-related anaerobic autotrophy of the novel archaeobacterium *Sulfolobus ambivalens*. *Nature*, 316:789–791, 1985.
- [181] W. Zillig, S. Yeats, I. Holz, A. Böck, M. Rettenberger, F. Gropp, and G. Simon. *Desulfurolobus ambivalens*, gen. nov., sp. nov., an autotrophic archaeobacterium facultatively oxidizing or reducing sulfur. *Systematic and Applied Microbiology*, 8(3):197–203, 1986.

Appendix A  
**SUPPLEMENTARY MATERIALS**

**A.1 Chapter 2**

The anabolism reaction of microbial growth is derived using the following reaction:



Each coefficient, **a-f**, can be solved using the following linear equations to balance mass, charge, and degree of reduction:

$$\begin{aligned} C \text{ conservation} : f + 1 &= 0 \\ H \text{ conservation} : 4 \cdot b + c + 2 \cdot d + 1.8 &= 0 \\ O \text{ conservation} : 2 \cdot f + d + 4 \cdot e + 0.5 &= 0 \\ N \text{ conservation} : b + 0.2 &= 0 \\ S \text{ conservation} : a + e &= 0 \\ Charge \text{ conservation} : f + b + c - 2 \cdot e &= 0 \end{aligned} \quad (\text{A.2})$$

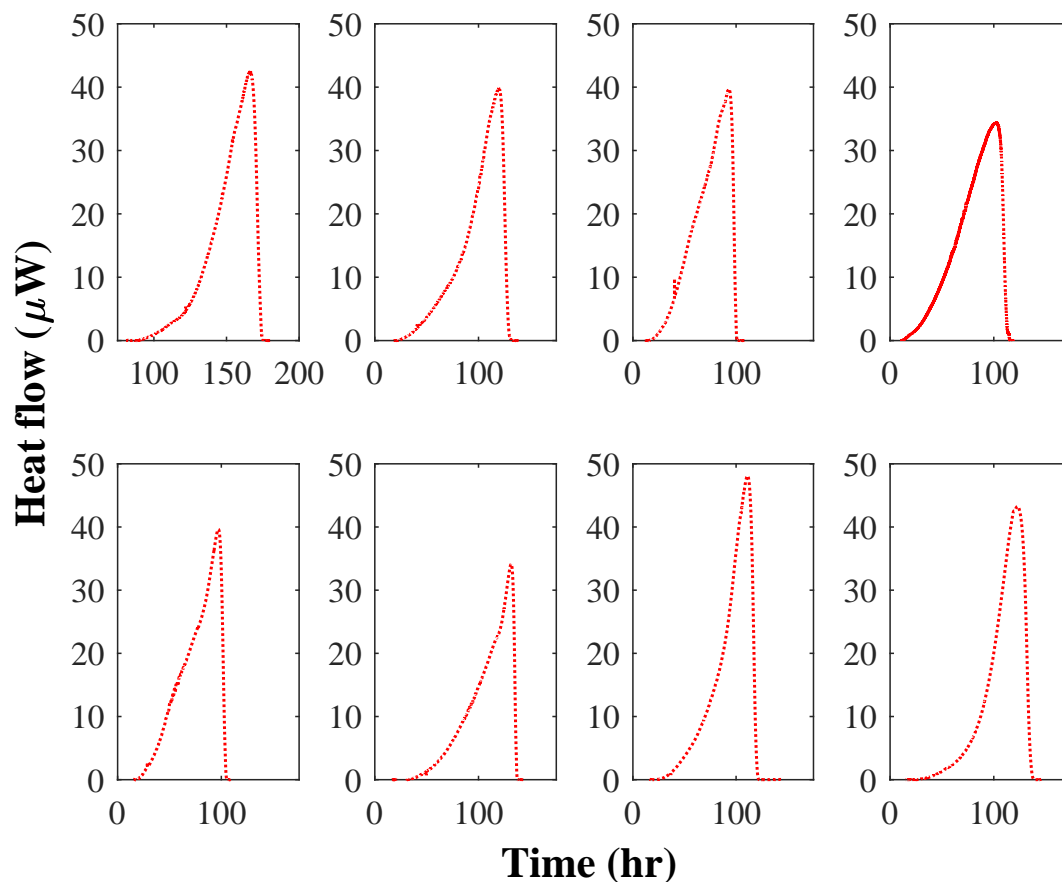


Figure A.1: Summary of heat flow curves produced by *Acidianus ambivalens* during sulfur oxidation under recommended growth conditions.

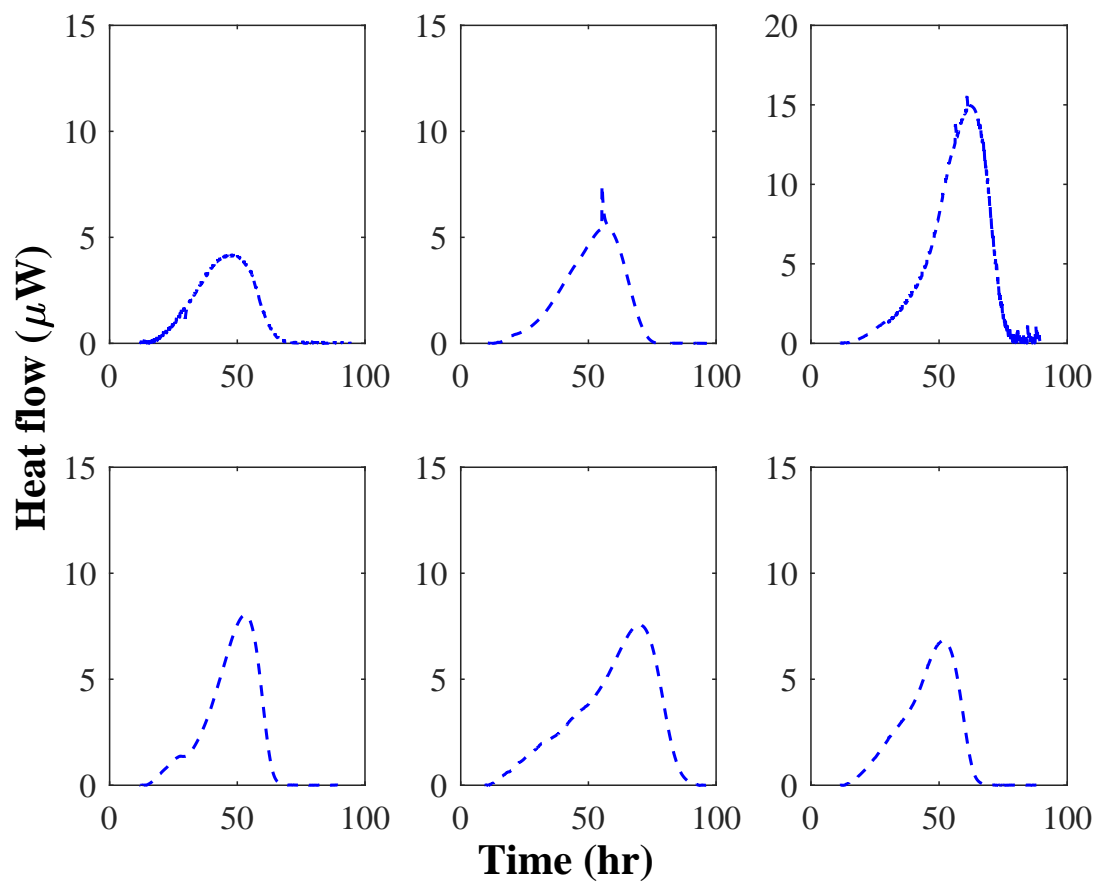


Figure A.2: Summary of heat flow curves produced by *Acidianus ambivalens* during sulfur oxidation under oxygen-limited growth conditions.

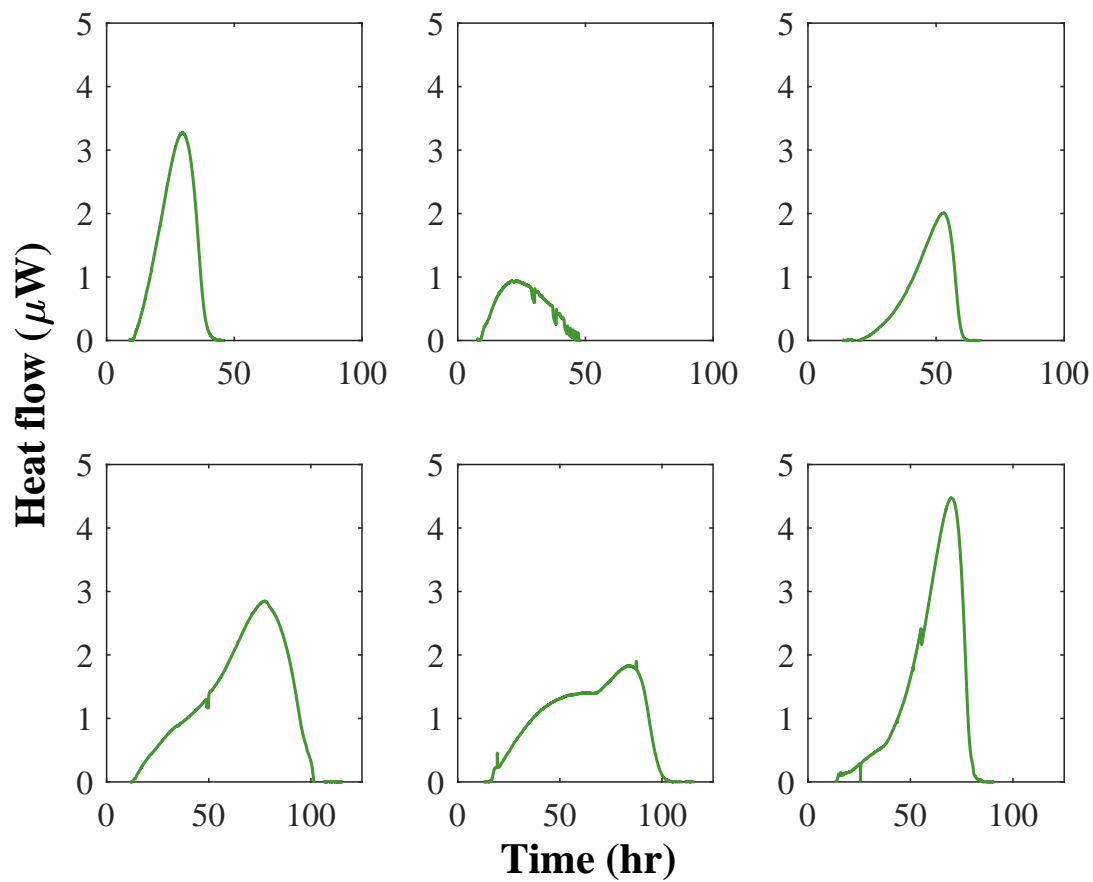


Figure A.3: Summary of heat flow curves produced by *Acidianus ambivalens* during sulfur oxidation under oxygen- and carbon-limited growth conditions.



## A.2 Chapter 4

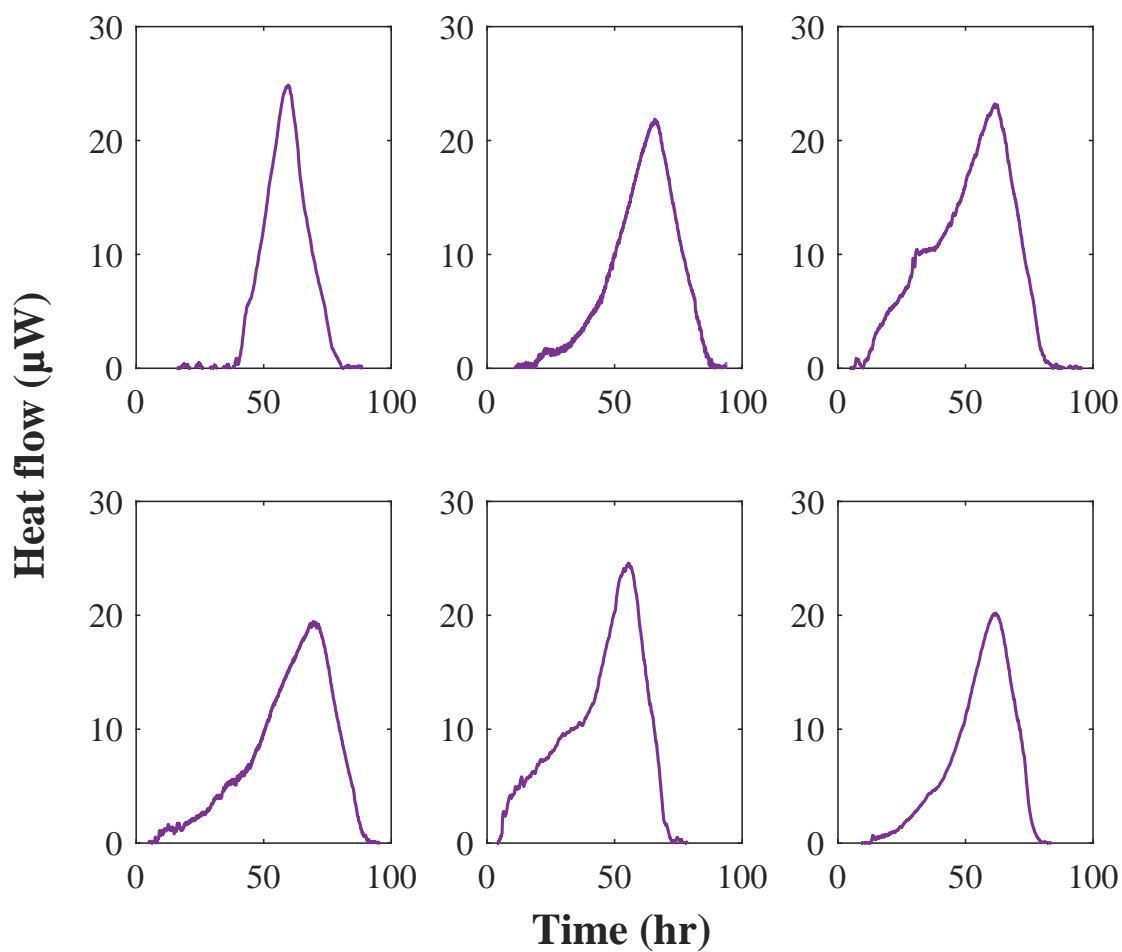


Figure A.4: Summary of heat flows recorded by the nanocalorimeter in  $\mu\text{W}$  versus time in hours produced by *Acidithiobacillus ferrooxidans* during iron oxidation. Average peak heat signal was  $22 \mu\text{W}$  and microbial growth took approximately 83 hours.

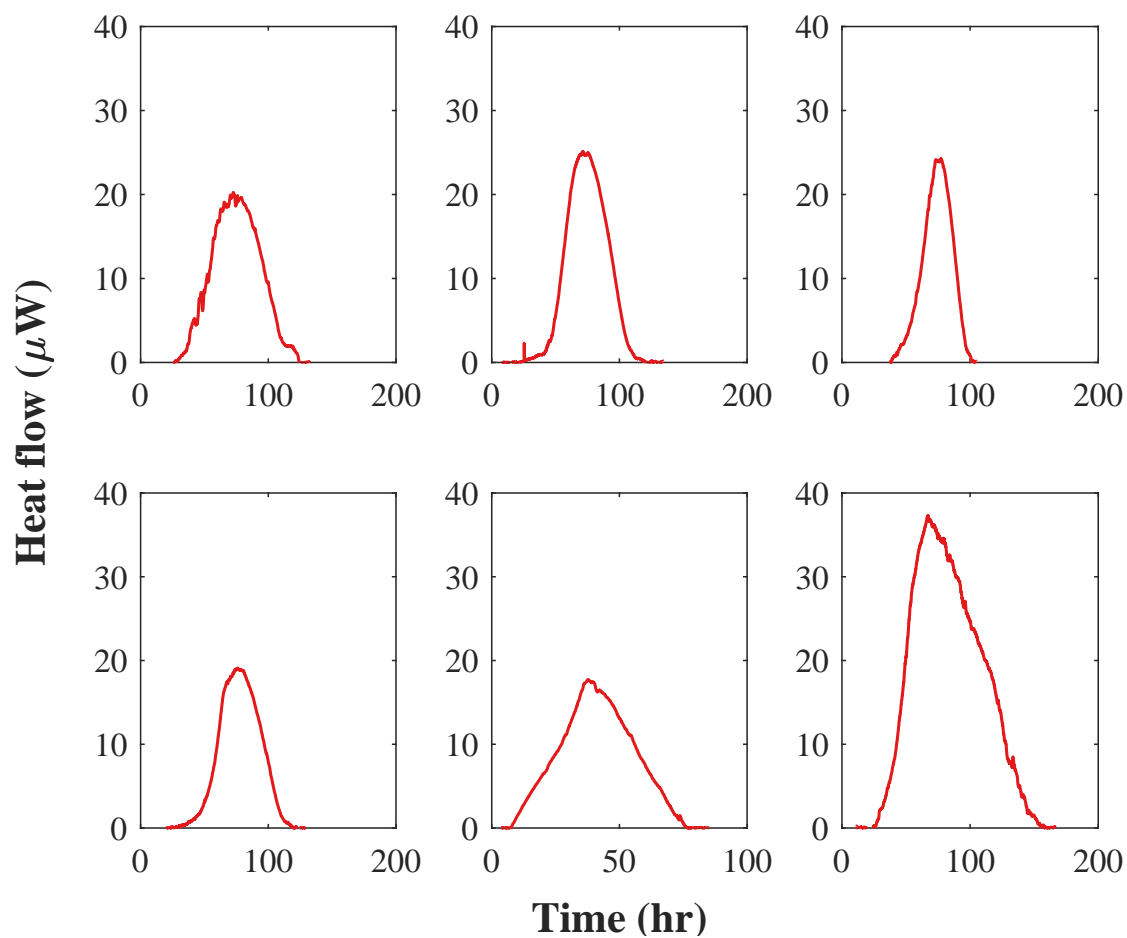


Figure A.5: Calorimetric heat flow, in  $\mu\text{W}$  versus time in hours, for replicates of *Acidithiobacillus ferrooxidans* during sulfur oxidation. The average peak heat signal was  $23 \mu\text{W}$  and growth took approximately 118 hours in the open sytsem experiments.

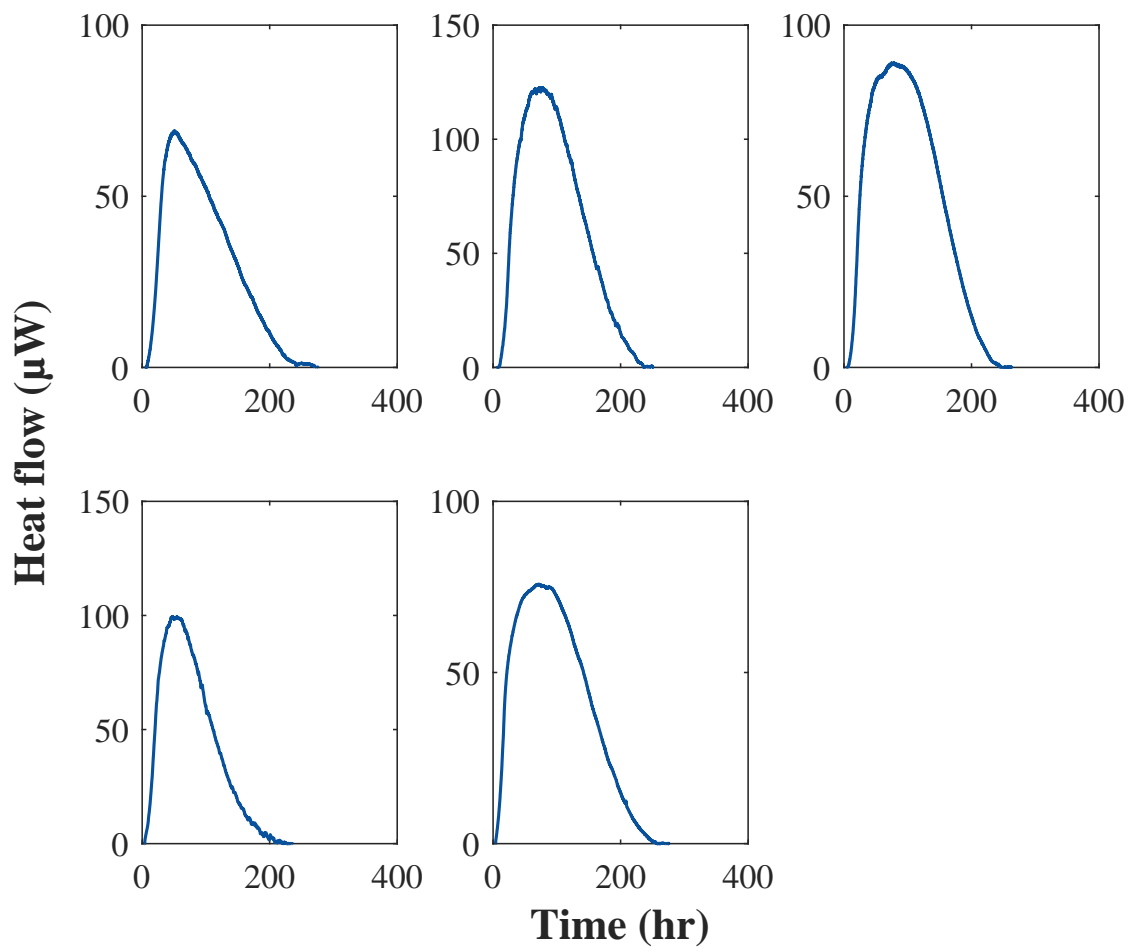


Figure A.6: Heat flow, in  $\mu\text{W}$  versus time in hours, recorded by calorimetry for *Acidithiobacillus thiooxidans* during sulfur oxidation. Peak heat signal in the open design averaged  $91 \mu\text{W}$  and total growth took approximately 234 hours.

## A.3 Chapter 5

Table A.1: 0.18 g/L Biomass

Reaction	log K	$V_Y$
$R - L_1 + Cd^{2+} \leftrightarrow R - L_1 - Cd^+$	3.291	8.455
$R - L_2 + Cd^{2+} \leftrightarrow R - L_2 - Cd^+$	3.341	5.900
$R - L_3 + Cd^{2+} \leftrightarrow R - L_3 - Cd^+$	3.126	4.353
$2R - L_3 + Cd^{2+} \leftrightarrow (R - L_3)_2 - Cd^{\circ}$	7.62	7.62
$R - L_1 + Cd^{2+} \leftrightarrow R - L_1 - Cd^+$		DNC
$R - L_2 + Cd^{2+} \leftrightarrow R - L_2 - Cd^+$		
$R - L_2 + Cd^{2+} \leftrightarrow R - L_2 - Cd^+$	2.973	3.271
$R - L_3 + Cd^{2+} \leftrightarrow R - L_3 - Cd^+$	2.928	
$2R - L_2 + Cd^{2+} \leftrightarrow (R - L_2)_2 - Cd^{\circ}$	7.285	3.103
$R - L_3 + Cd^{2+} \leftrightarrow R - L_3 - Cd^+$	2.874	
$R - L_2 + Cd^{2+} \leftrightarrow R - L_2 - Cd^+$	3.135	3.446
$2R - L_3 + Cd^{2+} \leftrightarrow (R - L_3)_2 - Cd^{\circ}$	6.598	
$2R - L_2 + Cd^{2+} \leftrightarrow (R - L_2)_2 - Cd^{\circ}$	7.436	3.083
$2R - L_3 + Cd^{2+} \leftrightarrow (R - L_3)_2 - Cd^{\circ}$	6.539	
$R - L_1 + Cd^{2+} \leftrightarrow R - L_1 - Cd^+$	2.832	3.592
$R - L_3 + Cd^{2+} \leftrightarrow R - L_3 - Cd^+$	2.996	
$2R - L_1 + Cd^{2+} \leftrightarrow (R - L_1)_2 - Cd^{\circ}$	7.097	3.538
$R - L_3 + Cd^{2+} \leftrightarrow R - L_3 - Cd^+$	2.983	
$R - L_1 + Cd^{2+} \leftrightarrow R - L_1 - Cd^+$	3.036	4.294

Continued on next page

Table A.1 – continued from previous page

Reaction	log K	$V_Y$
$2R - L_3 + Cd^{2+} \leftrightarrow (R - L_3)_2 - Cd^\circ$	6.68	
$R - L_1 + Cd^{2+} \leftrightarrow R - L_1 - Cd^+$	7.315	4.122
$2R - L_3 + Cd^{2+} \leftrightarrow (R - L_3)_2 - Cd^\circ$	6.668	
$2R - L_1 + Cd^{2+} \leftrightarrow (R - L_1)_2 - Cd^\circ$		DNC
$R - L_2 + Cd^{2+} \leftrightarrow R - L_2 - Cd^+$		
$R - L_3 + Cd^{2+} \leftrightarrow R - L_3 - Cd^+$		
$2R - L_1 + Cd^{2+} \leftrightarrow (R - L_1)_2 - Cd^\circ$		DNC
$R - L_2 + Cd^{2+} \leftrightarrow R - L_2 - Cd^+$		
$R - L_3 + Cd^{2+} \leftrightarrow R - L_3 - Cd^+$		
$R - L_1 + Cd^{2+} \leftrightarrow R - L_1 - Cd^+$		DNC
$2R - L_2 + Cd^{2+} \leftrightarrow (R - L_2)_2 - Cd^\circ$		
$R - L_3 + Cd^{2+} \leftrightarrow R - L_3 - Cd^+$		
$R - L_1 + Cd^{2+} \leftrightarrow R - L_1 - Cd^+$		DNC
$R - L_2 + Cd^{2+} \leftrightarrow R - L_2 - Cd^+$		
$2R - L_3 + Cd^{2+} \leftrightarrow (R - L_3)_2 - Cd^\circ$		
$2R - L_1 + Cd^{2+} \leftrightarrow (R - L_1)_2 - Cd^\circ$		DNC
$2R - L_2 + Cd^{2+} \leftrightarrow (R - L_2)_2 - Cd^\circ$		
$2R - L_3 + Cd^{2+} \leftrightarrow (R - L_3)_2 - Cd^\circ$		

Table A.2: 0.61g/L Biomass

Reaction	log K	V <sub>Y</sub>
$R - L_1 + Cd^{2+} \leftrightarrow R - L_1 - Cd^+$	3.375	38.54
$R - L_2 + Cd^{2+} \leftrightarrow R - L_2 - Cd^+$	3.514	19.2
$R - L_3 + Cd^{2+} \leftrightarrow R - L_3 - Cd^+$	3.806	25.12
$2R - L_3 + Cd^{2+} \leftrightarrow (R - L_3)_2 - Cd^{\circ}$	7.389	55.44
$R - L_1 + Cd^{2+} \leftrightarrow R - L_1 - Cd^+$		DNC
$R - L_2 + Cd^{2+} \leftrightarrow R - L_2 - Cd^+$		
$R - L_2 + Cd^{2+} \leftrightarrow R - L_2 - Cd^+$	3.268	8.267
$R - L_3 + Cd^{2+} \leftrightarrow R - L_3 - Cd^+$	3.429	
$2R - L_2 + Cd^{2+} \leftrightarrow (R - L_2)_2 - Cd^{\circ}$	7.136	10.36
$R - L_3 + Cd^{2+} \leftrightarrow R - L_3 - Cd^+$	3.297	
$R - L_2 + Cd^{2+} \leftrightarrow R - L_2 - Cd^+$	3.357	7.897
$2R - L_3 + Cd^{2+} \leftrightarrow (R - L_3)_2 - Cd^{\circ}$	6.943	
$2R - L_2 + Cd^{2+} \leftrightarrow (R - L_2)_2 - Cd^{\circ}$	7.209	9.38
$2R - L_3 + Cd^{2+} \leftrightarrow (R - L_3)_2 - Cd^{\circ}$	6.794	
$R - L_1 + Cd^{2+} \leftrightarrow R - L_1 - Cd^+$	2.943	8.539
$R - L_3 + Cd^{2+} \leftrightarrow R - L_3 - Cd^+$	3.449	
$2R - L_1 + Cd^{2+} \leftrightarrow (R - L_1)_2 - Cd^{\circ}$	6.623	8.444
$R - L_3 + Cd^{2+} \leftrightarrow R - L_3 - Cd^+$	3.416	
$R - L_1 + Cd^{2+} \leftrightarrow R - L_1 - Cd^+$	3.067	11.62
$2R - L_3 + Cd^{2+} \leftrightarrow (R - L_3)_2 - Cd^{\circ}$	6.892	

Continued on next page

Table A.2 – continued from previous page

Reaction	log K	$V_Y$
$2R - L_1 + Cd^{2+} \leftrightarrow (R - L_1)_2 - Cd^\circ$	6.751	10.29
$2R - L_3 + Cd^{2+} \leftrightarrow (R - L_3)_2 - Cd^\circ$	6.851	
$R - L_1 + Cd^{2+} \leftrightarrow R - L_1 - Cd^+$	2.706	8.581
$R - L_2 + Cd^{2+} \leftrightarrow R - L_2 - Cd^+$	3.007	
$R - L_3 + Cd^{2+} \leftrightarrow R - L_3 - Cd^+$	3.482	
$2R - L_1 + Cd^{2+} \leftrightarrow (R - L_1)_2 - Cd^\circ$	6.236	8.976
$R - L_2 + Cd^{2+} \leftrightarrow R - L_2 - Cd^+$	2.922	
$R - L_3 + Cd^{2+} \leftrightarrow R - L_3 - Cd^+$	3.359	
$R - L_1 + Cd^{2+} \leftrightarrow R - L_1 - Cd^+$	2.862	8.258
$2R - L_2 + Cd^{2+} \leftrightarrow (R - L_2)_2 - Cd^\circ$	6.703	
$R - L_3 + Cd^{2+} \leftrightarrow R - L_3 - Cd^+$	3.438	
$R - L_1 + Cd^{2+} \leftrightarrow R - L_1 - Cd^+$	2.218	8.654
$R - L_2 + Cd^{2+} \leftrightarrow R - L_2 - Cd^+$	3.193	
$2R - L_3 + Cd^{2+} \leftrightarrow (R - L_3)_2 - Cd^\circ$	6.759	
$2R - L_1 + Cd^{2+} \leftrightarrow (R - L_1)_2 - Cd^\circ$	6.411	8.41
$2R - L_2 + Cd^{2+} \leftrightarrow (R - L_2)_2 - Cd^\circ$	6.706	
$2R - L_3 + Cd^{2+} \leftrightarrow (R - L_3)_2 - Cd^\circ$	6.705	

## CURRICULUM VITAE

**Chloe E. Hart**• **EDUCATION** •

- 2013-Present **PhD Candidate**, Dual-title Earth and Space Sciences & Astrobiology,  
*University of Washington, Seattle, WA.*
- 2008-2012 **Bachelor of Science**, Biology major, Geology minor, Magna Cum Laude,  
*Wittenberg University, Springfield, OH.*

• **PROFESSIONAL EXPERIENCE** •

- 2013-Present **Research Assistant**, Geomicrobiology; *University of Washington, Seattle, WA.* PI: Drew Gorman-Lewis, PhD.
- Research topics include energetics of microbial growth, response to energy source availability, and heavy metal toxicity in acidophilic microorganisms.
- 2014-2017 **Undergraduate Research Mentor**, *University of Washington, Seattle, WA.*
- Directed 4 students in safe and successful laboratory research.
- 2014-2017 **Pacific Science Center Summer Research Internship Mentor**, *University of Washington, Seattle, WA.*
- Directed 3 students in safe and successful laboratory research.
- 2016 **NASA International Summer School in Astrobiology**, *Universidad Internacional Menéndez Pelayo, Santander, Spain.*
- Topic: Earth analog environments and the search for life beyond the Earth.
- Jun-Sep 2015 **Astrobiology Research Rotation**, Microbiology and Biochemistry,  
*University of Washington, Seattle, WA.* PI: John Leigh, PhD. Research Scientist and mentor: Thomas Lie, PhD.
- Research topics include anaerobic microbial consortia enrichment and isolation and high-temperature nitrogen fixation in *Methanocaldococcus* FS406.
- 2008-2012 **Undergraduate Research Assistant**, *Wittenberg University, Springfield, OH.*
- Research topics include water retention in fiddler crab species, orchid and dandelion seed studies, sugar preference in red mites, and kingsnake genetics and fitness.

• **TEACHING APPOINTMENTS** •

- 2017 **Teaching Assistant: Geobiology (ESS 313; Fall)**, *University of Washington, Seattle, WA.*
- 2015 **Teaching Assistant: Introduction to Geology (ESS 101; Spring)**,  
*University of Washington, Seattle, WA.*



- 2015 **Teaching Assistant: Dinosaurs (ESS 100; Winter)**, *University of Washington, Seattle, WA.*
- 2014 **Teaching Assistant: Introduction to Astrobiology (AstBio 115; Fall)**, *University of Washington, Seattle, WA.*
- 2013-2014 **Teaching Assistant: Introduction to Geology (ESS 101; Fall '13 - Spring '14)**, *University of Washington, Seattle, WA.*
- 2009-2012 **Biology Lab Peer Mentor: Concepts of Biology (BIO 170 and BIO 180)**, *Wittenberg University, Springfield, OH*
- 2012 **Physics Department Peer Mentor: Astronomy (PHYS 107)**, *Wittenberg University, Springfield, OH.*

• **GRANTS, FELLOWSHIPS, AWARDS** •

- 2018 Dept. of Earth and Space Sciences Research Gala Best Session Presentation (Session: Life, the Universe, and Everything)
- 2017 Stephen G. Warren Endowed Fund for Graduate Students in ESS & ESS Distinguished Graduate Student Research Support
- 2016 Stephen G. Warren Endowed Fund for Graduate Students in Earth and Space Sciences
- 2015 Dept. of Earth and Space Sciences Dorothy G. Stephens Fellowship
- 2014 Dept. of Earth and Space Sciences Robert and Jenny Winglee Grad Support Fund & Misch Fellowship
- 2012 Semester University Research Grant, Wittenberg University
- 2009 Biology Department Summer Research Grant, Wittenberg University

• **OUTREACH** •

- Dec 2017 Newton Elementary School (OH), kindergarten class. Topic: Microbiology & How to be a Scientist; microscope activity.
- Jul 2017 UW Summer Youth Microbiology Program (WA). Topic: Microbiology; lab tour and chemistry demonstrations.
- May 2017 Eatonville Elementary School (WA), 6<sup>th</sup> grade science class. Topic: Astrobiology: The Search for Life Elsewhere; exoplanet habitability activity.
- Dec 2016 Local elementary school students (WA). Rockin' Out Activity: Mars Mission Design.
- Aug 2016 UW Summer Youth Microbiology Program (WA). Topic: Microbiology; lab tour and chemistry demonstrations.
- Mar 2015 Wittenberg University's Astronomy Club (OH). Skype talk; Topic: Introduction to Astrobiology and Microbial Energetics.
- Mar 2015 Roosevelt High School (WA), 9<sup>th</sup> grade science classes. Topic: Cosmic

Calendar.

2011 Astronomy Outreach Internship, *Wittenberg University, Springfield, OH.*

• PEER-REVIEWED PUBLICATIONS •

- 2018 **Hart, C. E.** and Gorman-Lewis, D. Energetics of *Acidianus ambivalens* in response to oxygen availability. *In prep.*
- 2018 **Hart, C. E.** and Gorman-Lewis, D. Surface complexation of Cd<sup>2+</sup> by thermoacidophile *Sulfolobus acidocaldarius*. *In prep.*
- 2018 **Hart, C. E.** and Gorman-Lewis, D. *Acidithiobacillus* spp. growth energetics during iron(II) and sulfur oxidation. *In prep.*
- 2018 **Hart, C. E.** and Gorman-Lewis, D. Thermodynamics of anaerobic sulfur reduction by *Acidianus ambivalens*. *In prep.*
- 2010 Hale, A. N., Imfeld, S. M., **Hart, C. E.**, Gribbins, K. M., Yoder, J. A., and M. H. Collier. Reduced seed germination after pappus removal in the North American dandelion (*Taraxacum officinale*; Asteraceae). *Weed Science* 58: 420-425.
- 2010 Yoder, J. A., Bosley, J. W., Chambers, M. J., **Hart, C. E.**, Gribbins, K. M., and M. H. Collier. Reduced cuticular permeability promotes inland habitat expansion and freshwater survival in the fiddler crab *Uca minax* but not in its less terrestrial counterparts *U. pugilator* and *U. pugnax*. *Crustaceana* 83: 481-492.
- 2010 Yoder, J. A., Condon, M. R., **Hart, C. E.**, Collier, M. H., Patrick, K. R., and J. B. Benoit. Use of an alarm pheromone against ants for gaining access to ant/scale prey by the red velvet mite *Balaustium* sp. (Erythraeidae) in a honeydew rich environment. *The Journal of Experimental Biology* 213: 386-392.
- 2010 Yoder, J. A., Imfeld, S. M., Heydinger, D. J., **Hart, C. E.**, Collier, M. H., Gribbins, K. M., and L. W. Zettler. Comparative water balance profiles of Orchidaceae seeds for epiphytic and terrestrial taxa endemic to North America. *Plant Ecology* 211: 7-17.

• ORAL PRESENTATIONS •

- 2018 **Hart, Chloe** and Gorman-Lewis, Drew. Energetics of iron- and sulfur-oxidizing acidophiles. Department of Earth and Space Sciences Research Gala, University of Washington, Seattle, Washington.
- 2017 **Hart, Chloe** and Gorman-Lewis, Drew. Energetics of *Acidianus ambivalens* during aerobic growth on sulfur and varying nutrient availability. Astrobiology Science Conference (AbSciCon), Mesa, Arizona.

- 2017 **Hart, Chloe** and Gorman-Lewis, Drew. Energetics of *Acidianus ambivalens* during aerobic growth on sulfur and varying nutrient availability. Department of Earth and Space Sciences Research Gala, University of Washington, Seattle, Washington.
- 2015 **Hart, Chloe** and Gorman-Lewis, Drew. Thermodynamic analysis of microbial growth during aerobic and anaerobic sulfur metabolisms. Department of Earth and Space Sciences Research Gala, University of Washington, Seattle, Washington.
- POSTER PRESENTATIONS •
- 2017 **Hart, C.** and Gorman-Lewis, D. Energetics of sulfur-oxidizer *Acidianus ambivalens* on varying nutrient availability. Geobiology Conference, Banff, Alberta, Canada.
- 2014 **Hart, C.** and Gorman-Lewis, D. Mineral Surface Mediated Metabolism of *Sulfolobus acidocaldarius*. Department of Earth and Space Sciences Research Gala, University of Washington, Seattle, Washington.
- 2012 Rausch, B., **Hart, C.E.**, Hagen, B., Hurst, S., Metz, D., and Phillips, R. S. Fluctuating asymmetry's effect on fitness indicators at varying incubation temperatures in the variable. Butler University Undergraduate Research Conference, Indianapolis, Indiana.
- 2010 **Hart, C. E.**, Collier, M. H., and J. A. Yoder. Release of neryl formate prevents detection of red velvet mites by ants when feeding on aphid/scale prey in honeydew-laden habitats. Annual Meeting of The Association of Southeastern Biologists, University of North Carolina, Asheville, Asheville, North Carolina. Online Abstract (P1.73)
- 2010 Imfeld, S. M., Heydinger, D. J., **Hart, C. E.**, Collier, M. H., Gribbins, K. M., Yoder, J. A., and L. W. Zettler. Water relations of terrestrial and epiphytic orchid seeds of North America with special reference to species endemic to Hawaii and an only known truly aquatic. Annual Meeting of The Association of Southeastern Biologists, University of North Carolina, Asheville, Asheville, North Carolina. Online Abstract (P1.48).
- 2010 Stueber, S. E., Winters, K. A., Heffelfinger, M. E., Wollaeger, H. M., Almdale, K. M., Imfeld, S. M., **Hart, C. E.**, Yoder, J. A., and M. H. Collier. Upper thermal limitations of the sand fiddler crab, *Uca pugilator*. Butler University Undergraduate Research Conference, Indianapolis, Indiana. Abstract p. 131.
- 2010 Stueber, S. E., Bosley, J. W., **Hart, C. E.**, Collier, M. H., Gribbins, K. M., and J. A. Yoder. Differences in habitat preference and suitability based on

water balance profiles of *Uca minax*, *U. pugilator*, and *U. pugnax*. Annual Meeting of the Association of Southeastern Biologists, University of North Carolina, Asheville, North Carolina. Online Abstract (P1.69).